385
11/3/80 T.S.

Lh. 1985

MASTER

DOE/NOAA/OTEC-1

# THE EFFECTS OF SHEAR AND ROUGHNESS ON VORTEX SHEDDING PATTERNS BEHIND A CIRCULAR CYLINDER AT CRITICAL REYNOLDS NUMBERS

A Report to the National Oceanic and Atmospheric Administration

By
David M. Rooney
Rodney D. Peltzer

October 1979

Work Performed Under Contract No. EG-77-A-29-1078

Virginia Polytechnic Institute
and State University
Blacksburg, Virginia

U.S. Department of Energy

Solar Energy

DISTRIBUTION OF THIS DOCUMENT IS UNLIMITED

**DISCLAIMER**

**This report was prepared as an account of work sponsored by an agency of the United States Government. Neither the United States Government nor any agency Thereof, nor any of their employees, makes any warranty, express or implied, or assumes any legal liability or responsibility for the accuracy, completeness, or usefulness of any information, apparatus, product, or process disclosed, or represents that its use would not infringe privately owned rights. Reference herein to any specific commercial product, process, or service by trade name, trademark, manufacturer, or otherwise does not necessarily constitute or imply its endorsement, recommendation, or favoring by the United States Government or any agency thereof. The views and opinions of authors expressed herein do not necessarily state or reflect those of the United States Government or any agency thereof.**

## DISCLAIMER

**Portions of this document may be illegible in electronic image products. Images are produced from the best available original document.**

## DISCLAIMER

"This book was prepared as an account of work sponsored by an agency of the United States Government. Neither the United States Government nor any agency thereof, nor any of their employees, makes any warranty, express or implied, or assumes any legal liability or responsibility for the accuracy, completeness, or usefulness of any information, apparatus, product, or process disclosed, or represents that its use would not infringe privately owned rights. Reference herein to any specific commercial product, process, or service by trade name, trademark, manufacturer, or otherwise, does not necessarily constitute or imply its endorsement, recommendation, or favoring by the United States Government or any agency thereof. The views and opinions of authors expressed herein do not necessarily state or reflect those of the United States Government or any agency thereof."

This report has been reproduced directly from the best available copy.

Available from the National Technical Information Service, U. S. Department of Commerce, Springfield, Virginia 22161.

Price: Paper Copy $9.00
Microfiche $3.50

DOE/NOAA/OTEC-1
Distribution Category UC-64

# The Effects of Shear and Roughness on Vortex Shedding Patterns Behind a Circular Cylinder at Critical Reynolds Numbers

A Report to the National Oceanic and Atmospheric Administration

by

David M. Rooney
Rodney D. Peltzer

Virginia Polytechnic Institute
and State University

October 1979

DISTRIBUTION OF THIS DOCUMENT IS UNLIMITED

Table of Contents


| | | Page No. |
|---|---|---|
| I. | Background and Objectives | 1 |
| II. | Experimental Set-Up | 4 |
| III. | Test Procedures | 11 |
| | A. Velocity and Turbulence Profiles | 11 |
| | B. Surface Pressure Measurements | 12 |
| | C. Eddy Shedding Characteristics | 19 |
| | D. List of Test Runs | 20 |
| IV. | Results and Discussion | 22 |
| | A. Surface Pressure Distributions for Uniform Flow Cases | 22 |
| | B. Surface Pressure Distributions for Sheared Flow Cases | 26 |
| | C. Vortex Shedding Patterns for Smooth and Rough Cylinders in Uniform Flow | 33 |
| | D. Vortex Shedding Patterns for Smooth and Rough Cylinders in Sheared Flow | 45 |
| | (i) Shear parameter, $\beta$ = .007 | 47 |
| | (ii) Shear parameter, $\beta$ = .016 | 58 |
| | (iii) Shear parameter, $\beta$ = .021 | 68 |
| | (iv) Shear parameter, $\beta$ = .033 | 75 |
| | (v) Shear parameter, $\beta$ = .041 | 86 |
| | E. Effect of Shear on Cell Length | 97 |
| V. | Conclusions | 100 |
| VI. | Recommendations | 102 |
| VII. | References | 103 |
| | Appendix | 104 |
| | A. General Experimental Set-Up | 104 |
| | B. Accuracy of Velocity Profile Measurements | 104 |
| | C. Accuracy of Turbulent Intensity Profiles | 105 |
| | D. Accuracy of Pressure Transducer Output | 107 |
| | E. Accuracy of Spectral Analysis Methods | 112 |

# The Effects of Shear and Roughness on Vortex Shedding Patterns Behind a Circular Cylinder at Critical Reynolds Numbers

## I. BACKGROUND AND OBJECTIVES

The purpose of the test program undertaken at VPI&SU under a grant from the National Oceanic and Atmospheric Administration was to further the understanding of vortex shedding patterns to be experienced by the OTEC Cold Water Pipe.

Previous studies devoted to determining the effects of shear on shedding frequency begin with the work of Maull and Young,[5] who first verified the existence of coherent cells for one value of upstream shear by examining the power spectral density of the velocity fluctuations behind a bluff body with a long trailing edge. They explained the presence of four distinct cells by maintaining "that the coherence of the shed vortices requires a constant frequency over certain lengths." They theorized that the cell divisions are marked by longitudinal vortices created by the rolling up of the freestream vorticity of the shear flow. Mair and Stansby[4] determined an optimum length for endplate size to minimize interference with coherent vortex shedding behind a cylinder. They noted, however, that to produce appreciable values of shear, the cylinder aspect ratio must be low enough such that end effects cause a variation in base pressure coefficient ($C_{pb}$) across the entire length of the cylinder. They attributed the lack of a measured cellular shedding structure in some results (particularly in runs with no endplates) to fluctuations in cell boundaries which registered on successive time-averaged spectra as a continuous change in peak frequency. Stansby[7] investigated lock-on effects between mechanically produced cylinder vibrations and periodic vortex shedding at Reynolds numbers less than $10^4$. His studies of stationary cylinders included two shear levels

(corresponding to aspect ratios of 8 and 16) so no comprehensive evaluation of the relationship of shear to cell structure was possible. The turbulence levels in the experiments of Maull and Young, Mair and Stansby, and Stansby, who all used the same 28" x 20" wind tunnel, were about 0.5%. Davies[3] approached the problem by analyzing the variation in $C_{pb}$ for a highly sheared, highly turbulent (4% to 7%) flow about a cylinder of low aspect ratio (L/D = 6) in the critical Reynolds number range. The high turbulence levels reduced the onset of the critical Reynolds number by a factor of ten. He attributed the disappearance of measurable vortex shedding to the variation in spanwise wake patterns at a centerline Reynolds number of $1 \times 10^5$, which decreased spanwise correlations in $C_{pb}$.

In an earlier report by the present investigators[6], test results derived from measurements around a 6 inch diameter cylinder placed in a 6' x 6' wind tunnel were published. Those tests were primarily focused toward determining the surface mean and fluctuating pressures around the cylinder, and seeking to identify a cellular organization of eddy shedding frequencies behind the cylinder in high Reynolds number ( $5 \times 10^5$) flow. Given that the maximum Reynolds number achievable in the tunnel was about $5 \times 10^5$, the cylinder was knurled to a roughness K/D = .001 (where K is the depth of a roughness element, and D is the diameter). The surface roughness was expected to trigger a supercritical wake pattern around the cylinder. The relatively low aspect ratio (L/D = 9.3) permitted only a two cell shedding structure behind the cylinder. Therefore an estimate of the lengths of cells of constant shedding frequency, or "correlation length," could not be made.

The present series of tests was planned to incorporate improvements in design of the test model and data gathering capability in order to achieve certain results which the previous program was unable to arrive at. Specifically, three goals were envisioned:

(a) Determination of eddy shedding correlation lengths as a function of upstream shear. Improved endplate design and larger aspect ratio were the chief steps taken toward attaining this objective.

(b) Determination of minimum shear level producing cellular shedding patterns. A wider range of upstream velocity shears was to be tested than in any previous study.

(c) Detailed analysis of the effect of roughness on shedding patterns. A very smooth cylinder was to be tested under the same conditions as a roughened cylinder, and the two sets of results compared.

Two weeks of wind tunnel testing were scheduled to perform the tests. The first week was allotted to the roughened cylinder, and the second week was devoted to examining the smooth cylinder.

## II. EXPERIMENTAL SET-UP

Experiments were conducted in the 6' x 6' cross section Stability Wind Tunnel located on the VPI&SU campus. An upstream velocity shear was generated in the tunnel by a series of six wire screens, incorporating vertical rods in a non-uniform cross-tunnel distribution. The screens were located approximately 15 feet upstream of the test model and could be arranged in any combination to produce a variety of freestream shear levels. Three diameters of rods (.017", .025", and .040") were used in the screens, with the vast majority being .025" thick.

The OTEC cold water pipe, represented by a 3.5" diameter, 60" long hollow aluminum pipe, spanned the tunnel midway between the floor and the ceiling of the test section. The pipe was rigidly attached to rectangular steel endplates, approximately .05" thick, and 24" high and 52" long. The cylinder axis was 9" behind the leading edge of the plates and midway in height. The downstream parts of the endplates were fastened to the instrumentation traverse to minimize any vibration of the plates induced by the wind. The main features of the experimental set-up (without the traverse) are shown in Fig. 1.

A significant parametric limitation was imposed by the dimensions of the cylinder. The advantage gained in increasing the aspect ratio was offset to a degree by the decrease in Reynolds number attainable because of the smaller cylinder diameter employed. One technique which has been advocated (by Szechenyi[8] among others) to simulate higher Reynolds number flow is to roughen the cylinder surface. The roughness tends to promote transition from a laminar to a turbulent boundary layer characteristic of supercritical flow, at a lower Reynolds number. The conditions under which, according to Szechenyi, transition to supercritical flow occurs are that $Re \geq 1 \times 10^5$ and the roughness Reynolds number ($Re_\delta = U_c\delta/\nu$, where $\delta$ is the roughness element thickness)

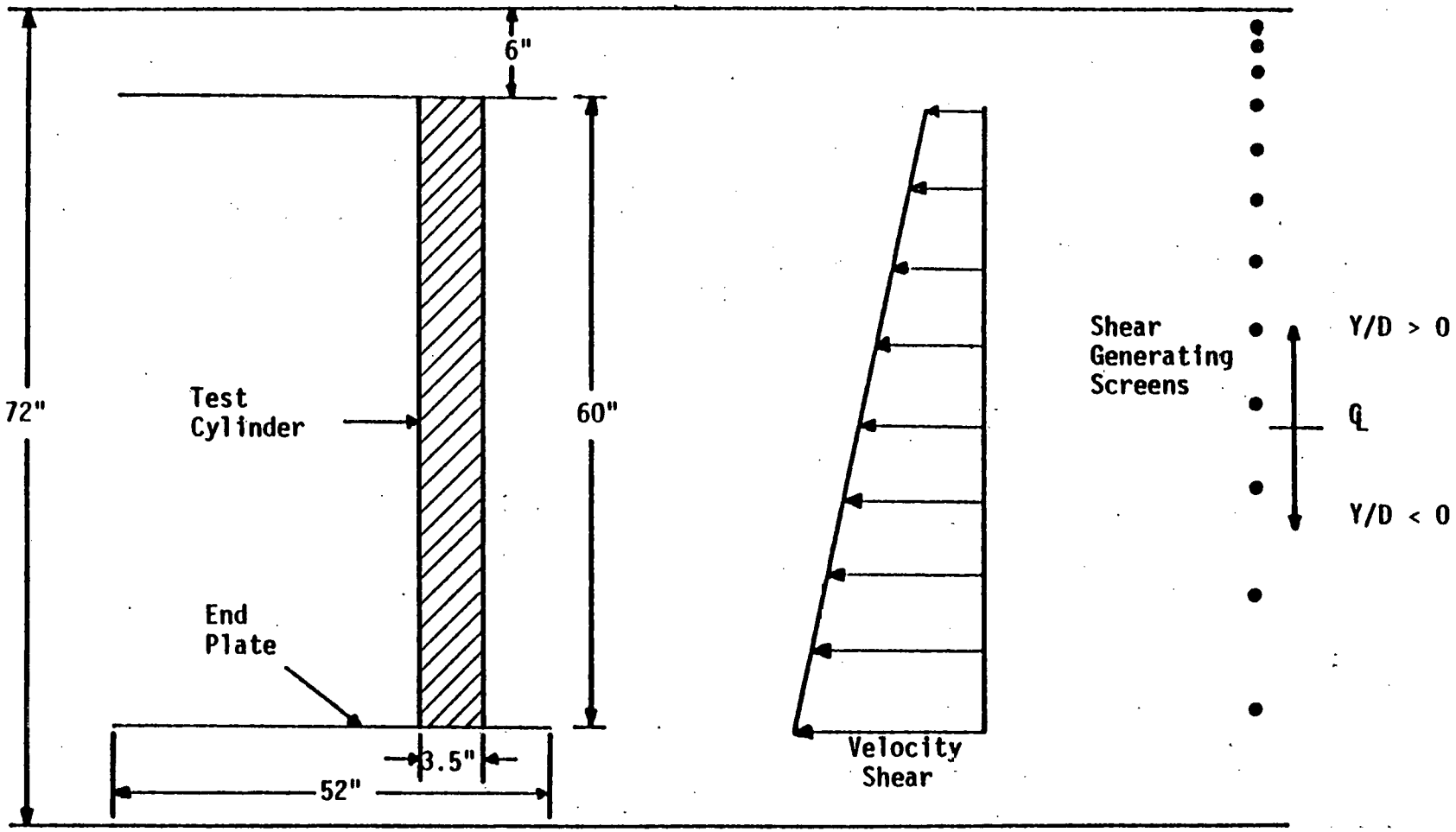


Fig. 1 Wind Tunnel Test Configuration

exceeds 200, which implies $\delta/D < 2.2 \times 10^{-3}$. Accordingly, two models of identical dimensions were constructed to determine whether roughening the surface negated the Reynolds number decrease. One cylinder had a roughness $\delta/D = 1 \times 10^{-3}$, while the other was smoothed to as uniform a surface as machine shop turning can produce.

Both cylinders were drilled with four circumferential series of 1/16" diameter ports at spanwise distances of 11, 23, 35, and 47 inches from the high velocity end of the cylinder. Each circumferential series contained 24 ports spaced 15° apart, so that complete coverage of the pressure distribution around the cylinder was provided at the four locations. In addition, two ports at the front center of the cylinder 2 inches apart measured the centerline stagnation pressure. In all, 98 ports were drilled in each cylinder, and 1/16" diameter plastic tubing connected them to a scanivalve pressure transducer unit. The scanivalve unit successively sampled the pressure readings at each port, with the output in volts being fed to a Hewlett-Packard Model 7100B strip chart recorder. By analyzing the data in terms of a pressure coefficient (i.e., as a ratio of a given port voltage reading to the local stagnation port voltage reading) a tedious conversion of voltage readings to pressures was avoided. Output from the two centerline ports was channeled to a Hewlett-Packard Model 3476 B Multimeter which gave a d.c. digital readout, which was used to set the centerline velocity.

Prior to placing the cylinder in the tunnel, an electronically controlled traverse was situated about 3 feet downstream of the position to be occupied by the test model. The traverse controls permitted positioning of a probe mount to within any .04" increment along the 60 inch span of the cylinder. In addition, vertical adjustment was possible within a limited height range. The traverse mount held a hot-wire anemometer probe, which was positioned approximately 3 diameters (10 inches) behind the base of the cylinder. Since the

main traverse structure was responsible for some tunnel blockage and flow channeling, its effect on cylinder readings was examined. Tests were performed to see if the probe mount (which included a large vertical rod and various smaller rods supporting the probe) altered the flow conditions when it was moved from one side of the tunnel to the other. This was done by monitoring the pressure at a given cylinder stagnation port during the entire traversing process. The change in pressure observed was negligible, so sufficient assurance was obtained that the measuring apparatus was not contaminating the results.

Hot-wire equipment performed two functions: a) it measured freestream turbulence levels without the cylinder in place, and b) it measured the flow field behind the cylinder, from which eddy shedding characteristics could be extracted.

For the freestream turbulence readings, a single hot-wire probe was connected to a Thermo-Systems, Inc. Model 1051-6 constant temperature anemometer. The output from the anemometer was not linearized (d.c. voltage vs. mean velocity) as in the previous test program because a linearizer introduces some distortion (i.e., electronic noise) into the resulting values of turbulent intensities. Instead the d.c. output was fed into a Hewlett-Packard Data Acquisition System, which digitized it and directed it to a computer terminal. A program then calculated the voltage-velocity relationship, given the operating temperature and pressure. The turbulent intensities were then calculated when output from a Disa Type 55 D 35 RMS voltmeter (which had been received from the anemometer via a Tektronix TM 503 amplifier which filtered the signal to eliminate frequencies above 300 Hz) was fed into the program. This procedural modification eliminated the visual averaging of an RMS signal inherent in reading the voltmeter output by eye. A block diagram of the steps involved in the pressure and turbulence measurements is shown in Fig. 2.

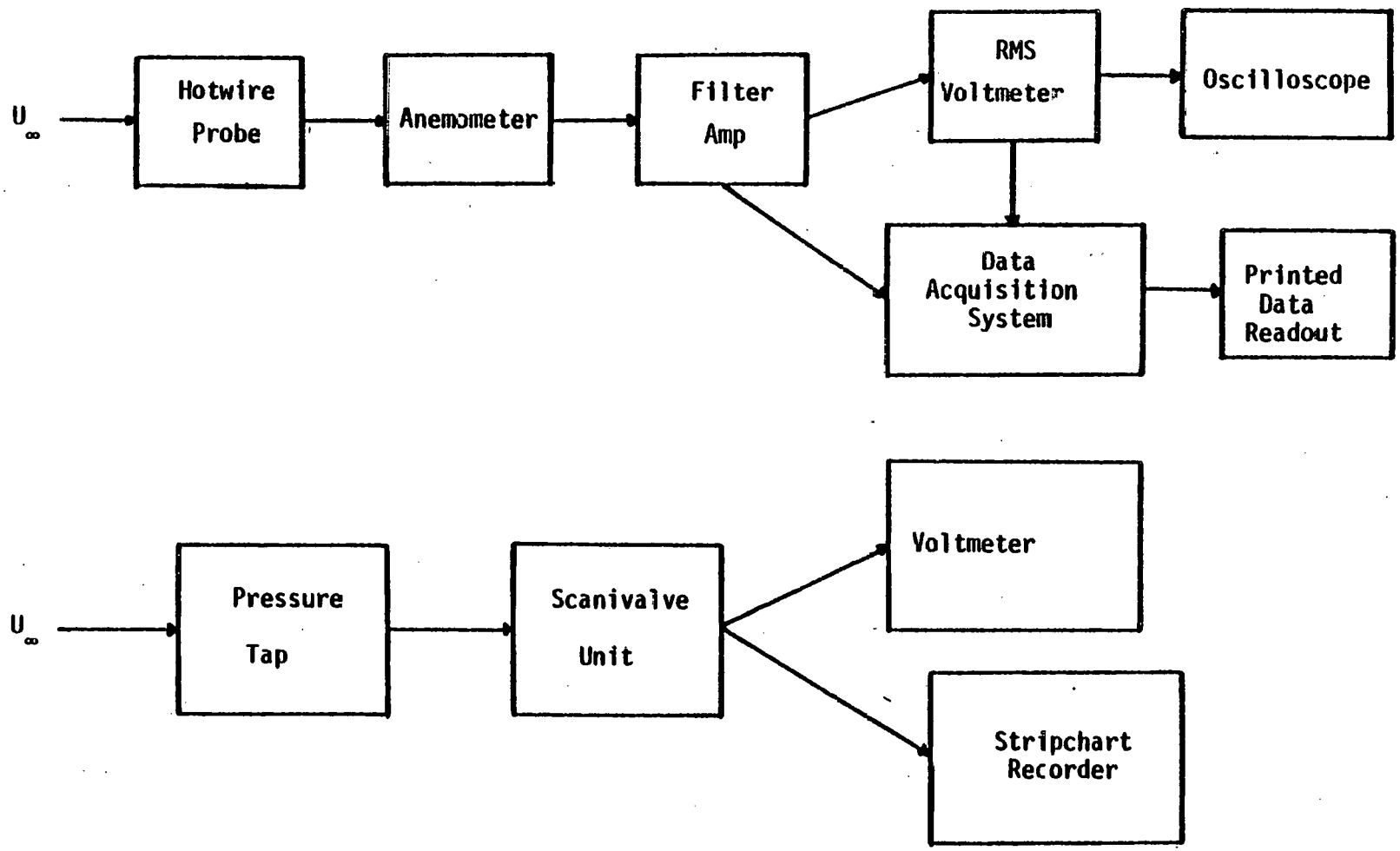


Fig. 2 Turbulence, Circumferential Pressure, Shear Centerline Velocity Measurements

To examine the spectral characteristics of the shear layer between the wake and the freestream flow behind the cylinder, the filtered anemometer signal was transmitted to a Zonic Technical Laboratories, Inc. Multichannel FFT Processor. Real-time visual inspection of the signal was available through simultaneous monitoring on a Tektronix Type 561A Oscilloscope. A two-channel Data Memory System received and quantitized the incoming data and a DMS 5003 Computer performed the spectral analysis. The output, in the form of a power density spectrum (log amplitude vs. frequency), was plotted on a Tektronix Model 4010 Graphics Display Terminal. Through keyboard commands, variables such as sampling rate, number of spectral averages, and frequency range of the displayed spectrum could be specified. A hard copy of the results was obtained by photographing the terminal screen with high speed Type 5710 Polaroid black and white film loaded in a Graflex camera mounted on a tripod. This set-up is displayed in Fig. 3.

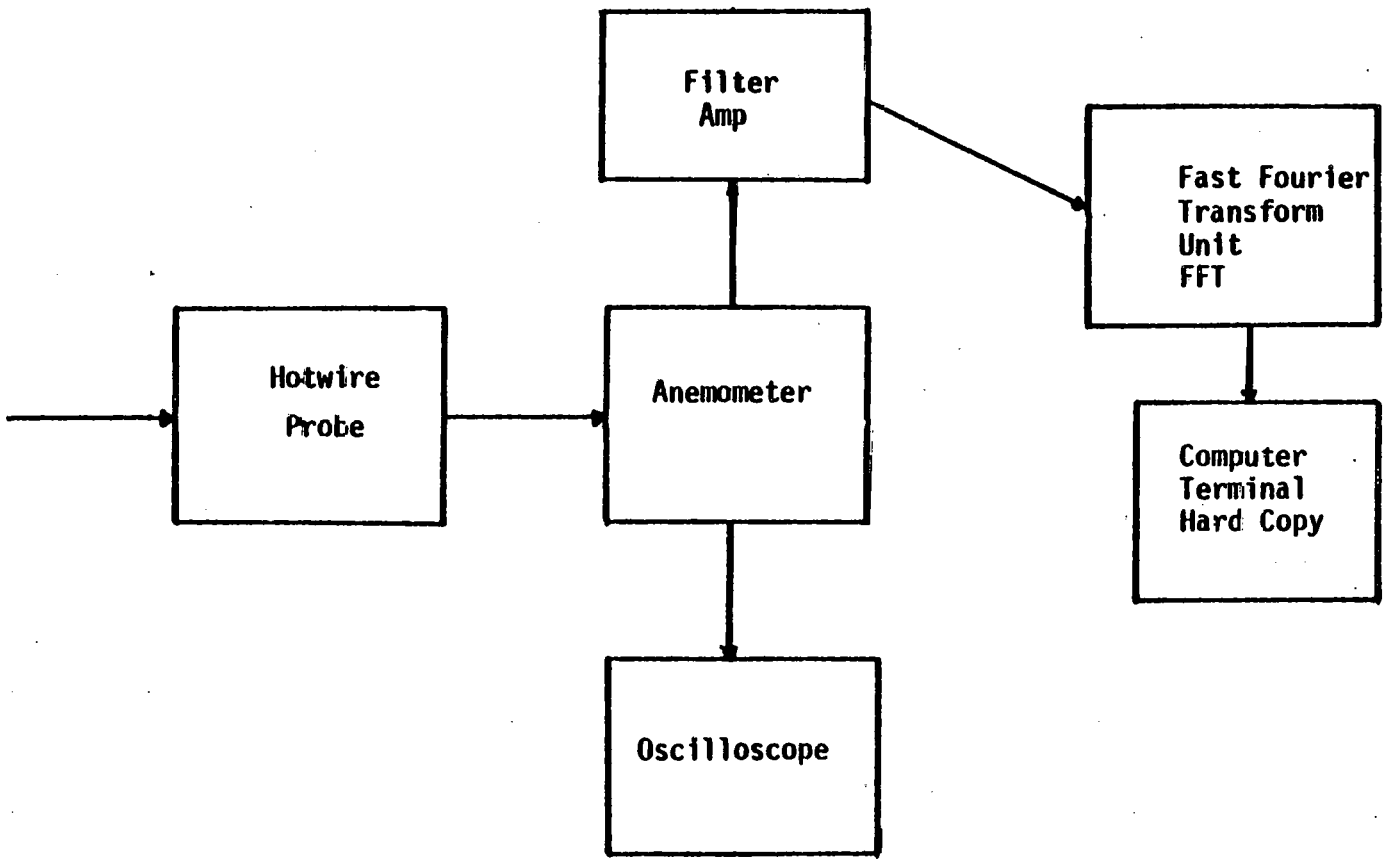


Fig. 3 Eddy Shedding Frequency Measurements

## III. TEST PROCEDURES

### A. Velocity and Turbulence Profiles

The first stage of the test program involved measuring the pertinent wind tunnel flow parameters: cross-tunnel velocity profiles and turbulence levels. In order to insure minimal interference with test results, the cross-tunnel shear was desired to be as nearly linear as possible, and turbulence levels to be below 1.0% (where turbulent intensities were measured as $\sqrt{\overline{u'^2}}/U$). The turbulence levels also were to vary as little as possible from one shear configuration (i.e., number of upstream screens) to the next.

Upstream velocity profiles were determined from total head tube readings at 25 stations across the tunnel. The readings were fed into the turbulence profile computer program which converted the stagnation pressures to velocities. The values obtained correlated well with readings of the stagnation pressure at a series of 28 ports along the front of the roughened cylinder. Each profile corresponded to a given set of screens placed in slots 15 feet upstream from the cylinder. Each screen configuration also produced a different turbulence level, and in Figs. 4 through 9, mean velocities and turbulence levels are plotted on the same graph for each of six shear cases studied. The free-stream velocity is plotted as a dimensionless ratio $U/U_c$ (where $U_c$ is the centerline velocity and U is the local velocity) as a function of dimensionless spanwise distance Y/D (where Y is the actual distance from the center and D is the cylinder diameter). Negative values of Y/D correspond to positions on the high velocity side of the center (where Y/D = 0). On the right hand vertical axis the turbulent intensities in percentages are graphed, again as a function of Y/D.

It is immediately obvious that an increase in shear levels was ordinarily

accompanied by some growth in turbulence levels. Fig. 4 shows that the intensities produced by a uniform flow (one screen, with wires of uniform spanwise distribution) was approximately 0.2% across the tunnel.

Shear levels are characterized by a dimensionless parameter $\beta$, defined as $D/U_c \; dU/dy$, where all the symbols are as previously defined. With $\beta = .007$, which corresponds to a weakly sheared flow profile, the turbulent intensities varied between 0.2% and 0.6% across the tunnel, as shown in Fig. 5. No significant change occurred in raising the shear level to $\beta = .016$ (see Fig. 6), but for $\beta = .021$, graphed in Fig. 7, mid-tunnel intensities were registered around 0.7%, and the spanwise distribution became more non-uniform. A sharp increase in turbulence was noted when the screen configuration producing $\beta = .033$, and the points in Fig. 8, was placed in the tunnel. This was the result, in large part, of the additional blockage occurring at the low velocity end, where $U/U_c = 0.64$, compared to a value of 0.83 for $\beta = .021$. The turbulent intensities reached magnitudes of about 1.1% at two points on the low velocity end, whereas the highest value recorded for $\beta = .021$ was 0.75%.

The increased shear generated by adding the final two screens to produce $\beta = .041$, shown in Fig. 9, was actually accompanied by a decrease in peak turbulent intensities except for the final point at $Y/D = 8.1$. Apparently, the additional screens tended to dampen out small scale irregularities in the sheared profile.

## B. Surface Pressure Measurements

The standard approach used to determine whether the flow conditions around a circular cylinder are subcritical or otherwise is to examine the surface pressure distribution around the cylinder circumference. A supercritical condition, characteristic of high Reynolds number or very turbulent upstream flow, is marked by a highly negative value of the pressure coefficient

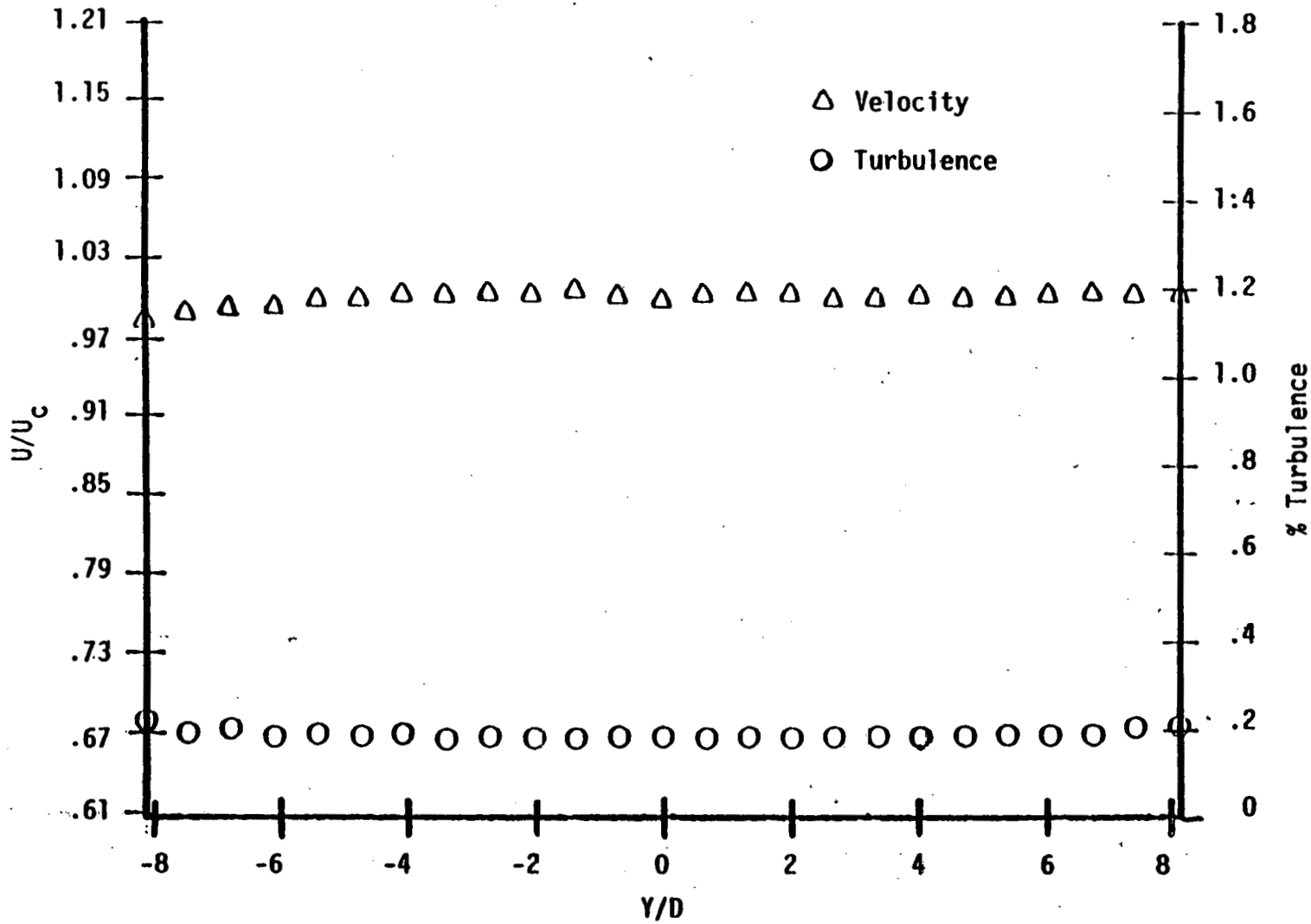


Fig. 4 Spanwise Velocity and Turbulence Profiles ($\beta$ = 0)

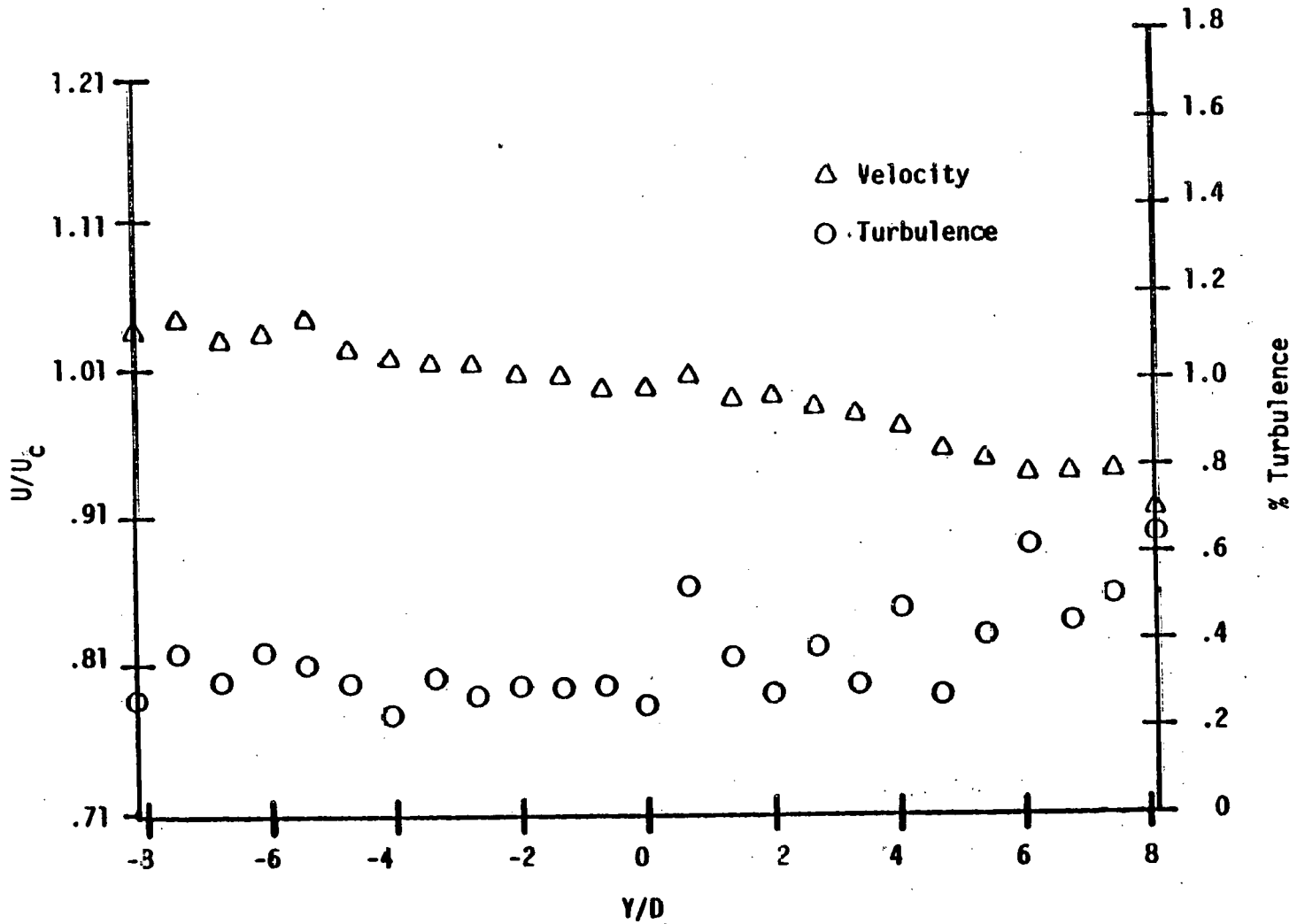


Fig. 5 Spanwise Velocity and Turbulence Profiles ( $\beta$ = .007)

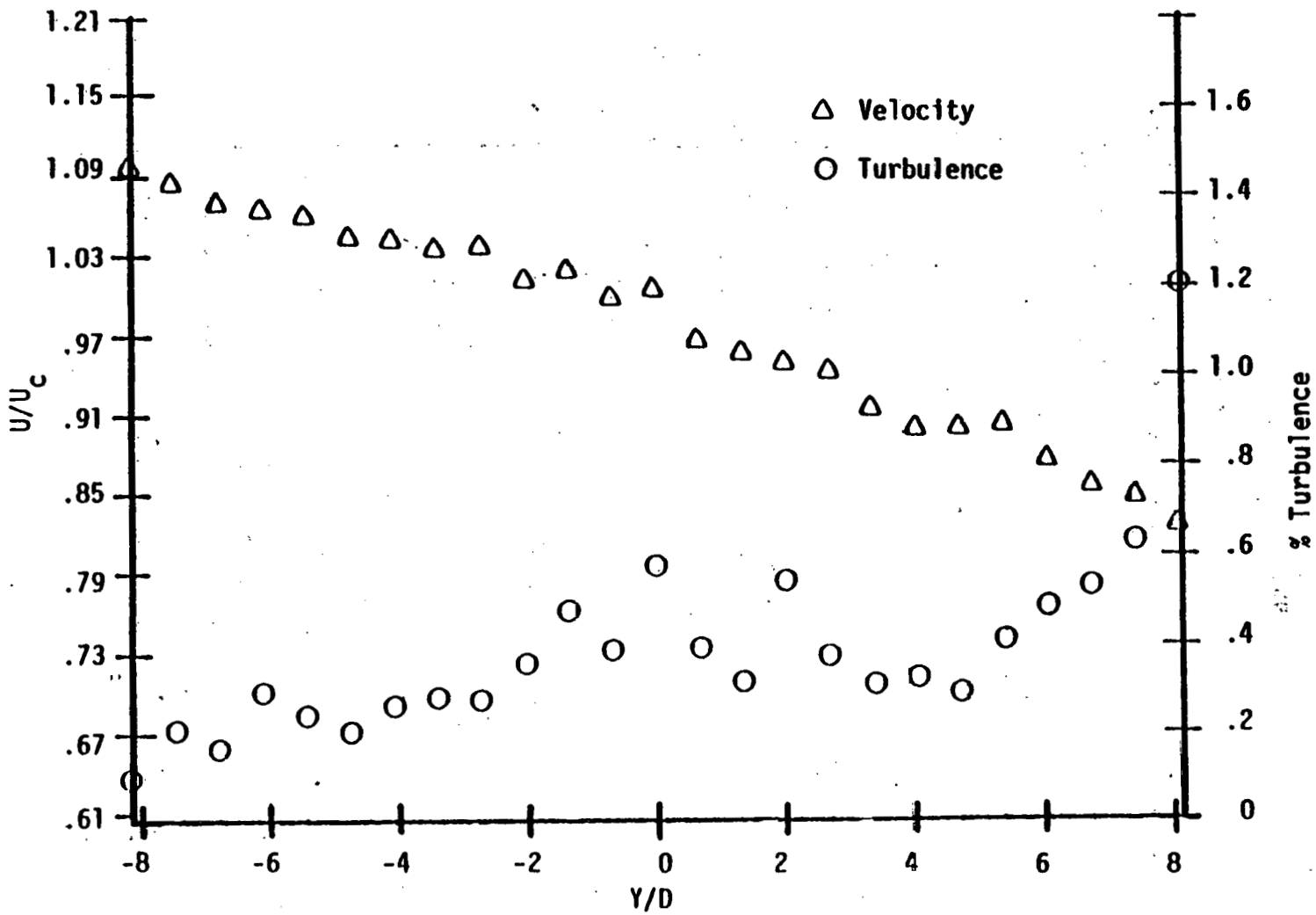


Fig. 6 Spanwise Velocity and Turbulence Profiles ($\beta$ = .016)

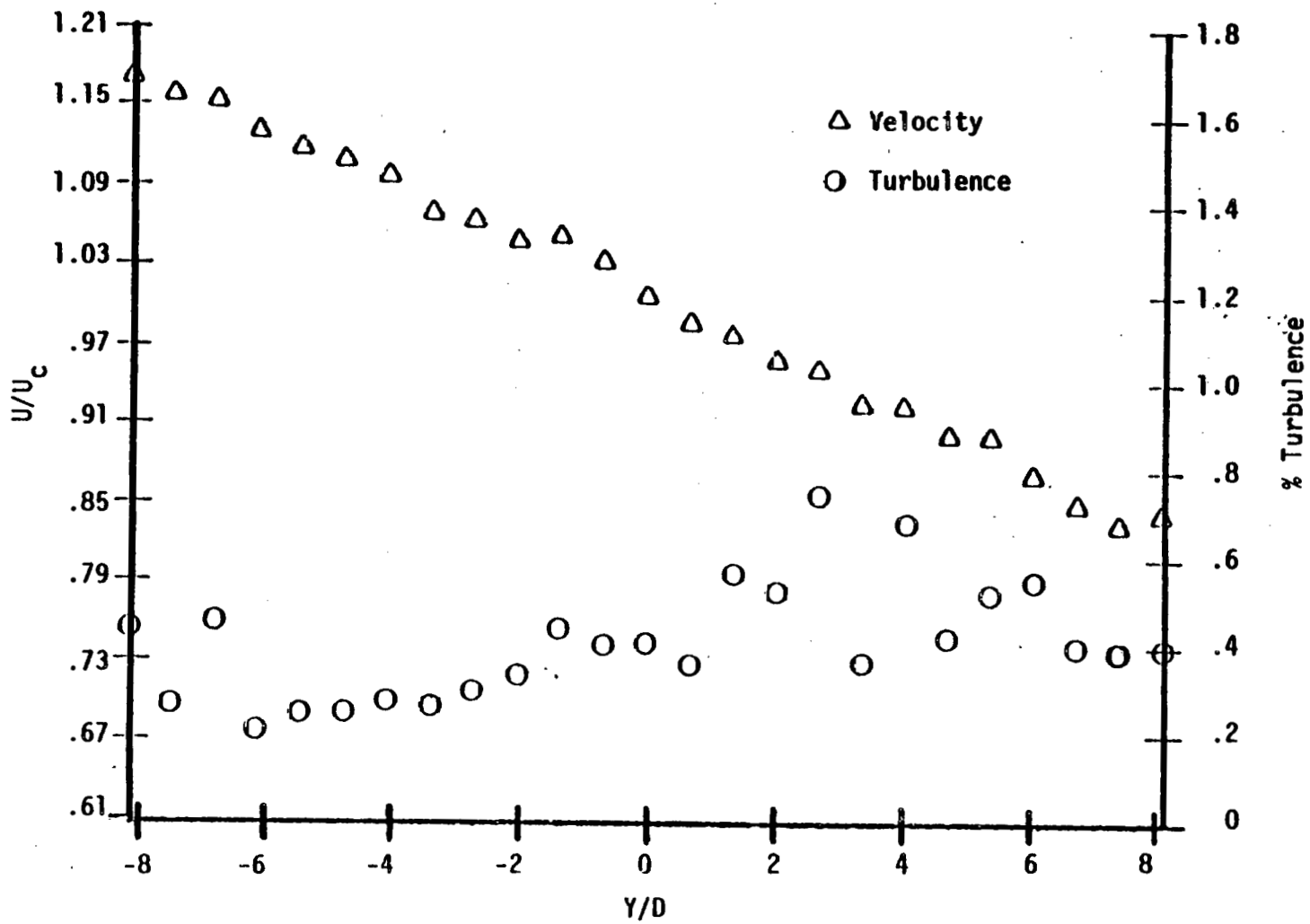


Fig. 7 Spanwise Velocity and Turbulence Profiles ($\beta$ = .021)

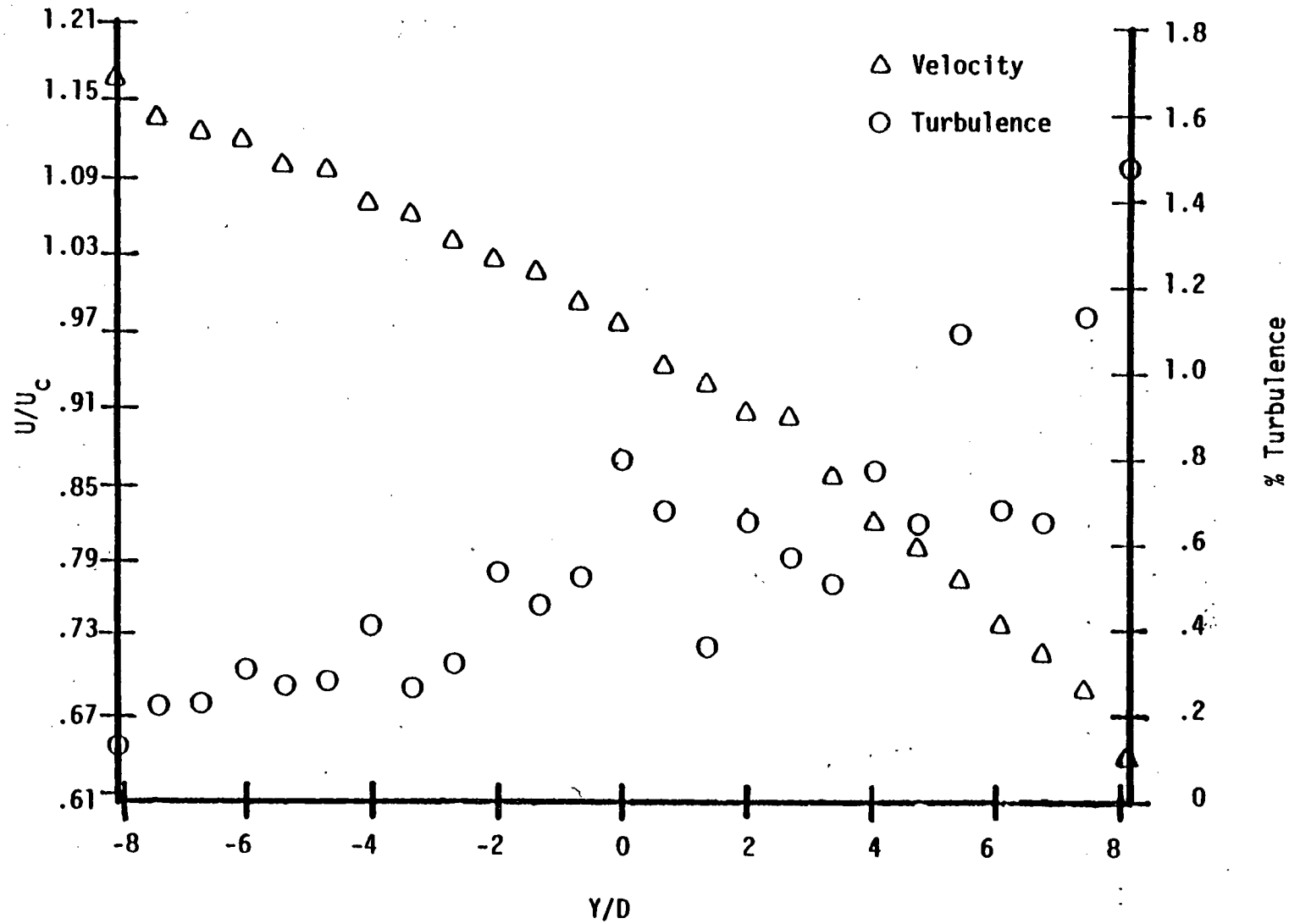


Fig. 8 Spanwise Velocity and Turbulence Profile ($\beta$ = .033)

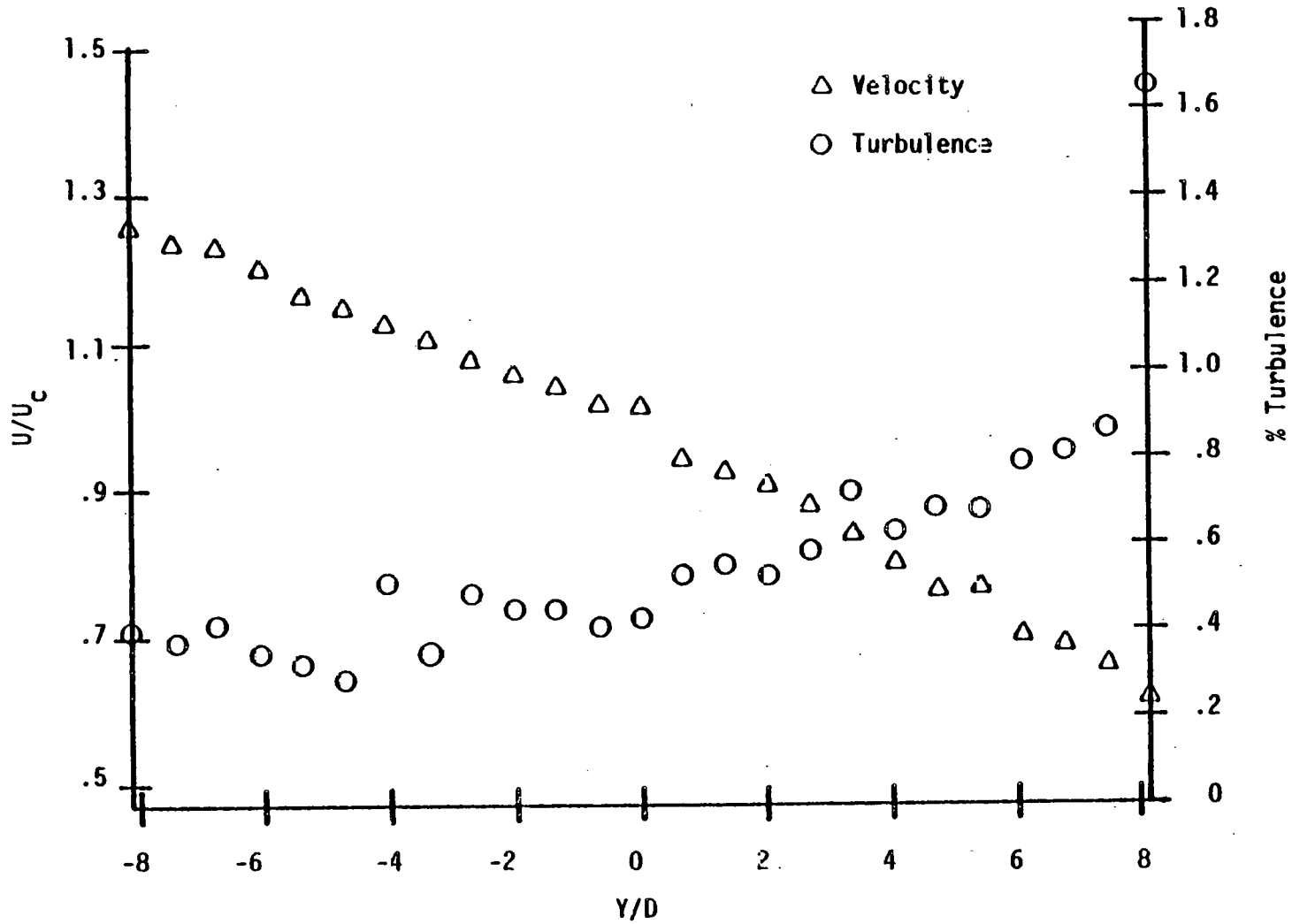


Fig. 9 Spanwise Velocity and Turbulence Profiles ($\beta$ = .041)

$C_p$ (defined as $P/(\rho U^2/2)$ where p is the pressure at a point and $\rho U^2/2$ is the stagnation pressure) around $\theta = 90°$ and 270° on the cylinder surface (where $\theta = 0°$ is the stagnation point). In subcritical flow, only mildly negative values ($C_p \approx -1.0$) occur all along the rear side.

One of the goals of the present study was to determine the effect of roughness on the shedding characteristics in a shear flow. In addition, it was hoped that further light would be shed on the ability of roughness to place a flow regime in a super-critical state despite centerline Reynolds numbers around $2 \times 10^5$, as Szechenyi has demonstrated can be done in two dimensional (uniform upstream flow) cases. Consequently, a plot of the pressure coefficient for both the rough and smooth cylinder cases should resolve the issue for three-dimensional flow regimes. All the surface pressure plots, discussed in Sections IV A and B, represent the pressure coefficient $C_p$ ($\theta$), at a single spanwise point, Y/D = -2.0, except for one graph demonstrating a transition across the span of the cylinder.

## C. Eddy Shedding Characteristics

The traverse mechanism supporting the hot-wire probe was positioned to take readings along the shear layer behind the cylinder in increments of 9 cm (approximately 1 cylinder diameter). At each setting, a spectral analysis of the signal was performed, usually consisting of 25 averages of individual spectra, with the dominant energy level yielding the shedding frequency. A complete set of readings consisted of 17 points along the cylinder, although for a number of cases where the shedding pattern was non-existent or relatively uniform, fewer readings were taken.

The very large quantity of spectra taken during the course of the test program required that a trade-off between amount of wind tunnel time available and resolution of the averaged spectra be made.

When the maximum spanwise shedding frequency was expected to occur at less than 100 Hz (as was the case for all test runs at Re = $1.6 \times 10^5$) the output was plotted on the 0 to 100 Hz frequency scale. This necessitated a sampling rate of 5 msec. With 1024 samples per spectrum, the time required to average 25 spectra was approximately two minutes. A general guideline for averaging random data spectra is that at least 100 averages be taken in order to eliminate the fluctuations noticeable in the spectral plots (particularly away from the peaks) reproduced later in the report. Such a procedure would have quadrupled the tunning time for a single test, with only a modest increase in resolution of the results. The fact that a narrow band frequency, often nearly sinusoidal, high energy level signal was being measured at most stations was regarded as sufficient reason to opt for a lower number of averages. Only a few spectra (occurring around cell boundaries) might have yielded more precise information with one hundred averages instead of twenty-five.

D. List of Test Runs

A complete listing of all test runs is given in the table below. All cases for which pressure distributions alone were taken are marked by an asterisk. The remainder of the cases were analyzed for both pressure and eddy shedding characteristics. For $\beta = 0$, a range of Reynolds numbers is shown, since only one point was required to determine the shedding frequency, and therefore a large number of Reynolds numbers were investigated.

Table of Test Runs

| Shear Parameter ($\beta = D/U_c \, dU/dy$) | Reynolds Number ($Re = U_c D/\nu$) Smooth | Rough |
|---|---|---|
| .000 | $1.6\times10^5$-$3.2\times10^5$ | $1.6\times10^5$-$3.3\times10^5$ |
| | | $1.6\times10^5$-$3.6\times10^5$† |
| .007 | $1.6\times10^5$ | $1.6\times10^5$ |
| | $2.2\times10^5$ | $2.2\times10^5$* |
| | $2.6\times10^5$ | $2.6\times10^5$ |
| | $3.0\times10^5$ | $3.0\times10^5$ |
| .016 | $1.6\times10^5$ | $1.6\times10^5$ |
| | $2.2\times10^5$* | $2.2\times10^5$* |
| | $2.6\times10^5$ | $2.6\times10^5$ |
| | $3.0\times10^5$ | $3.0\times10^5$ |
| .021 | $1.6\times10^5$ | $1.6\times10^5$ |
| | $2.2\times10^5$* | $2.2\times10^5$* |
| | $2.6\times10^5$ | $2.6\times10^5$ |
| .033 | $1.6\times10^5$ | $1.6\times10^5$ |
| | $2.2\times10^5$* | $2.2\times10^5$* |
| | $2.6\times10^5$ | $2.6\times10^5$ |
| .041 | $1.6\times10^5$ | $1.6\times10^5$ |
| | $2.2\times10^5$ | $2.2\times10^5$ |

†A second set of rough cylinder measurements at $\beta = .000$ was performed at a much lower freestream turbulence level.

## IV. RESULTS AND DISCUSSION

### A. Surface Pressure Distributions for Uniform Flow Cases

All pressure distributions discussed in the following section were obtained at the set of circumferential pressure taps located at Y/D = -2, except when otherwise indicated.

Figs. 10 to 12 show a plot of $C_p$ as a function of $\theta$ for the three cases of unsheared flow examined. From Fig. 10, it is seen that even for Re = $3.2 \times 10^5$, the pressure distribution (with a maximum negative $C_p \approx 1.6$) did not reach the typical supercritical profile, recognizable by peak suction values of $C_p \approx -2.5$. Nevertheless, since for Re = $1.6 \times 10^5$, $C_p$ was only -1.2 at $\theta = 90°$, the highest Reynolds number case was very close to the transition regime. Fig. 11 is the identical plot for the rough cylinder in uniform flow with freestream turbulent intensities of 0.2%. At the lowest speed, with Re = $1.6 \times 10^5$, a subcritical profile was produced. At Re = $2.2 \times 10^5$, one side of the cylinder revealed a peak suction $C_p = -2.0$, while on the other side $C_p = -1.3$. This asymmetry in pressure distribution appears to correspond to the condition noted by Bearman[2] regarding the separation bubble phenomenon in flow over a smooth cylinder at Re = $3.4 \times 10^5$. On the smooth cylinder it preceded entry into the critical regime. Beyond Re = $2.6 \times 10^5$, the rough cylinder pattern assumed the expected symmetrical supercritical shape.

With an order of magnitude decrease in freestream turbulence to about .03%, the pressure distribution over the rough cylinder was as shown in Fig. 12. Again, a subcritical profile existed at Re= $1.6 \times 10^5$, but at Re= $2.2 \times 10^5$ the flow, as demonstrated by the maximum $C_p = -1.5$, was not as fully critical as in the previous case. The highest Reynolds number examined, Re = $3.0 \times 10^5$, was correspondingly slightly less supercritical than at the same Reynolds number at the higher turbulence level. Therefore, an increase in freestream

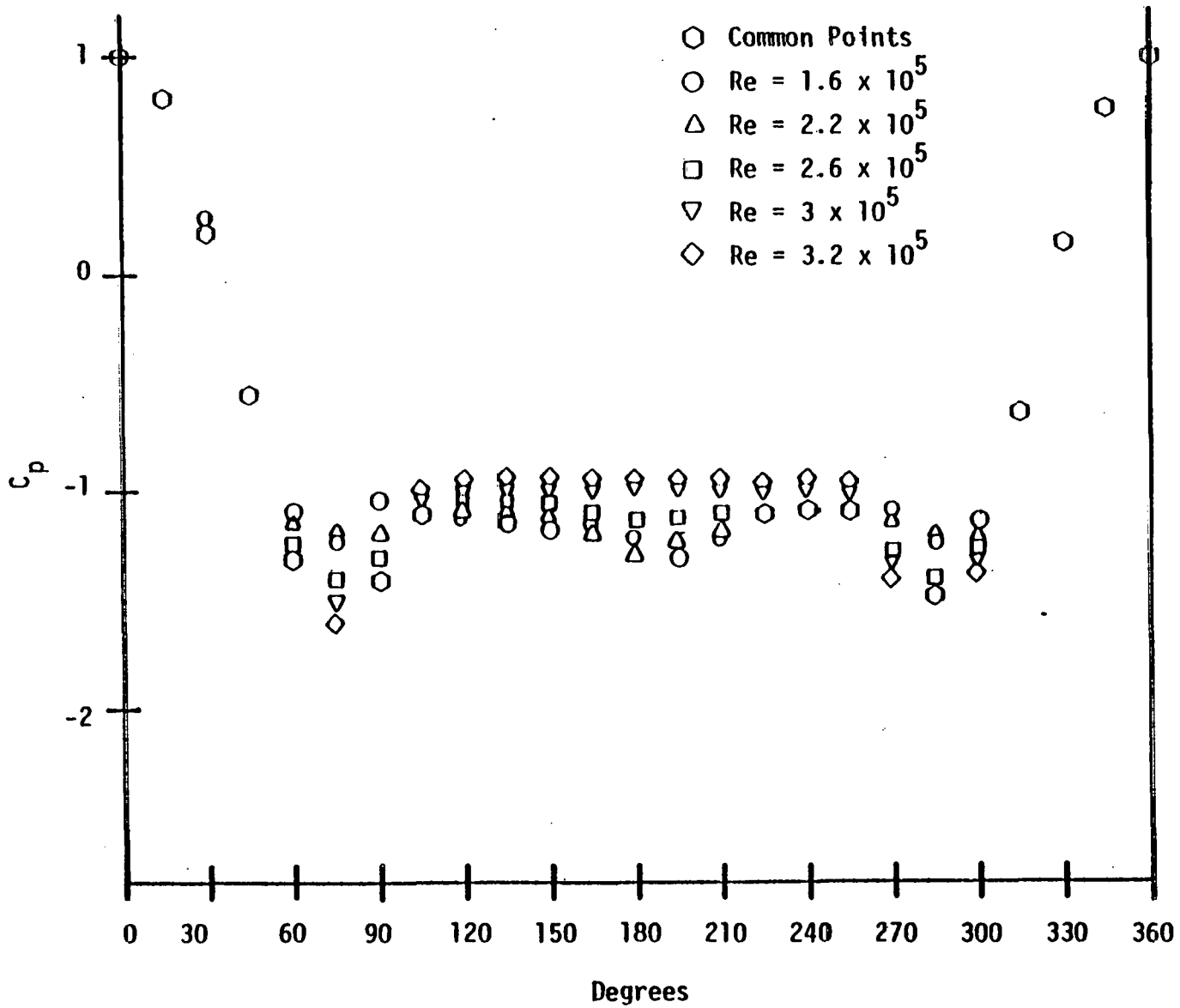


Fig. 10 Circumferential Pressure Distribution ($\beta$ = 0, Smooth Cylinder)

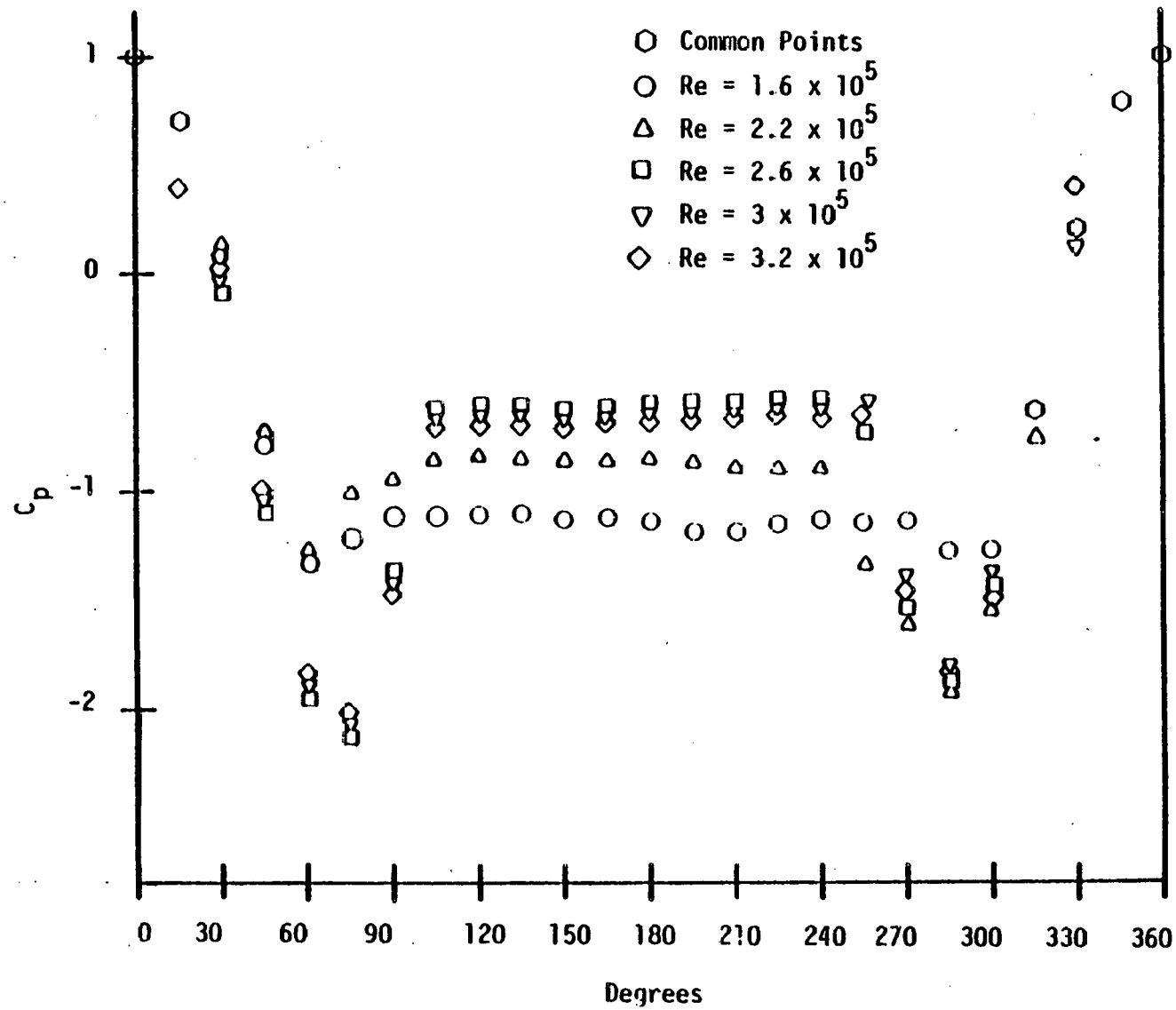


Fig. 11 Circumferential Pressure Distribution ($\beta$ = 0, Rough Cylinder)

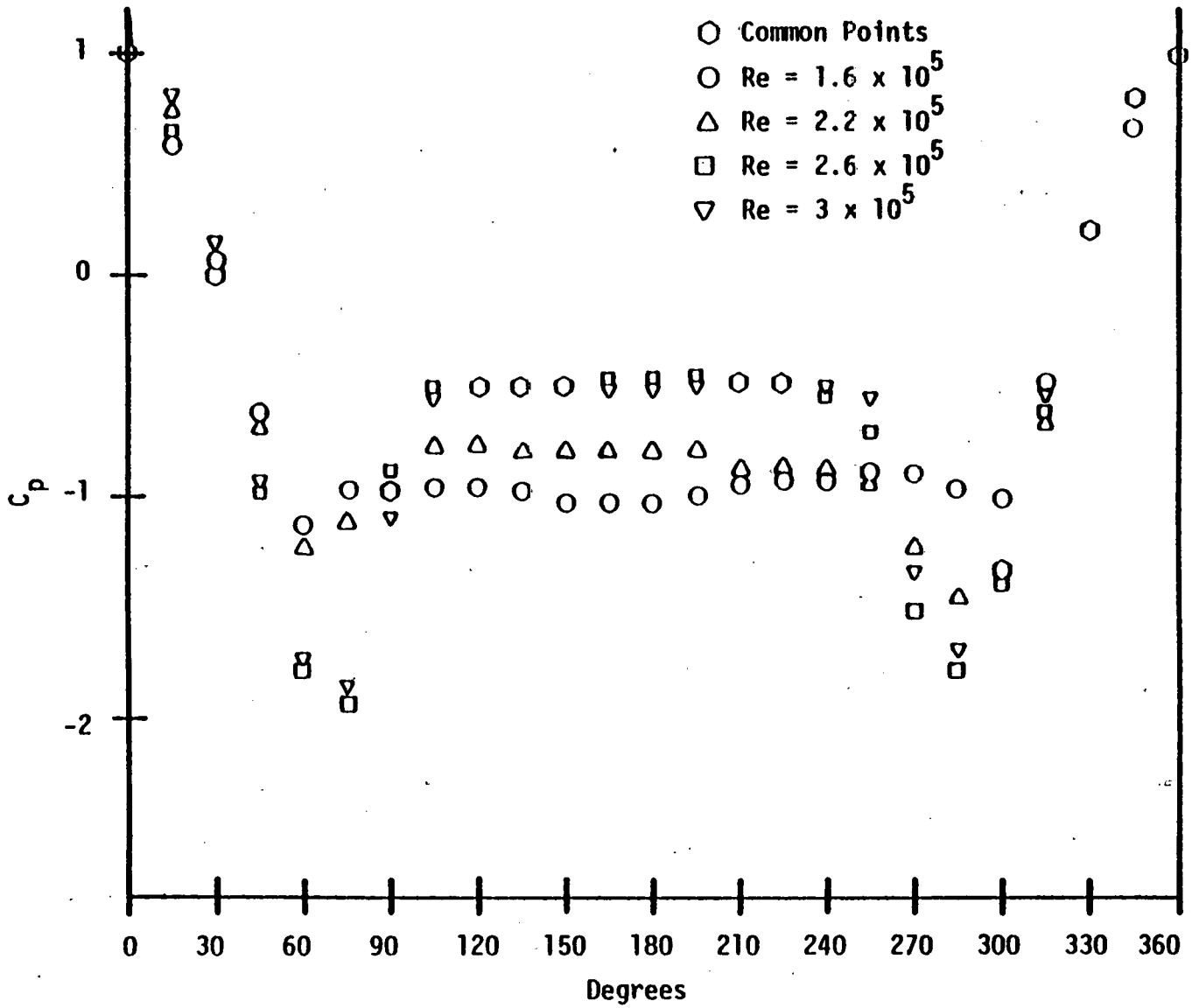


Fig. 12 Circumferential Pressure Distribution ($\beta$ = 0, Rough Cylinder, Turbulence = .03%)

from a negligible amount (.03%) to a small amount (.20%) had a measurable effect in transforming the flow regime to supercritical at a lower Reynolds number. This phenomenon will be brought out again when shedding frequencies are examined later in the report.

A similar conclusion was reached by Batham[1], who noted that increased turbulence "promoted earlier transition in the shear layers and this effect was more pronounced than the effect of roughness" at Re = $1.1 \times 10^5$. At a higher Reynolds number, surface roughness effects superseded those of freestream turbulence. In general, he concluded that "the critical range of Reynolds number is narrower for high roughness and wider for high turbulence." Since no tests were performed on the smooth cylinder with turbulence levels of .03%, a more complete qualitative comparison with Batham's results is not possible. However, a cursory comparison of Figs. 10 and 11 amply testifies to Batham's other observation "that cylinders in uniform streams which exhibit critical mean pressure distributions are highly sensitive to surface roughness."

B. Surface Pressure Distributions for Sheared Flow Cases

Figs. 13 to 15 represent the circumferential pressure distribution at Y/D = -2.0 for a shear level $\beta$ = .007. From Fig. 13, it is evident that the profile remained subcritical throughout the centerline Reynolds number range tested. However, the roughened cylinder results of Fig. 14 show again that even as low as at Re = $2.2 \times 10^5$, a highly critical profile emerged. At higher Reynolds numbers the profile remained essentially the same, except for a slight decrease in the peak suction.

An interesting spanwise variation in the $C_p$ profile occurred at Re = $3.0 \times 10^5$ for the smooth cylinder, as shown in Fig. 15. The profile at Y/D = -5.4 showed the greatest peak suction at about 75° from the stagnation point, while at Y/D = -2, Y/D = 1.4, and Y/D = 4.9, the profile was in a transitional stage.

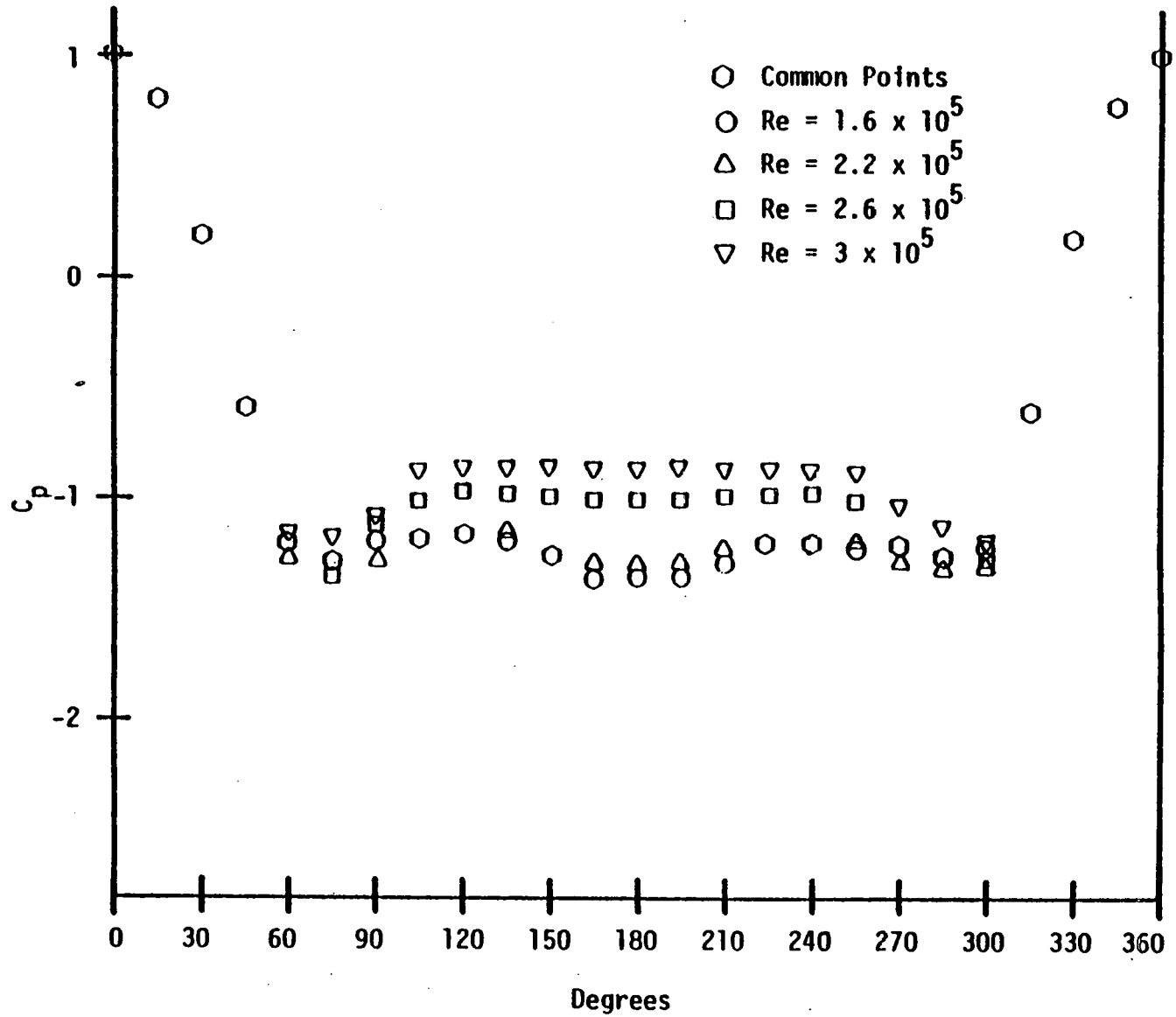


Fig. 13 Circumferential Pressure Distribution ($\beta$ = .007, Smooth Cylinder)

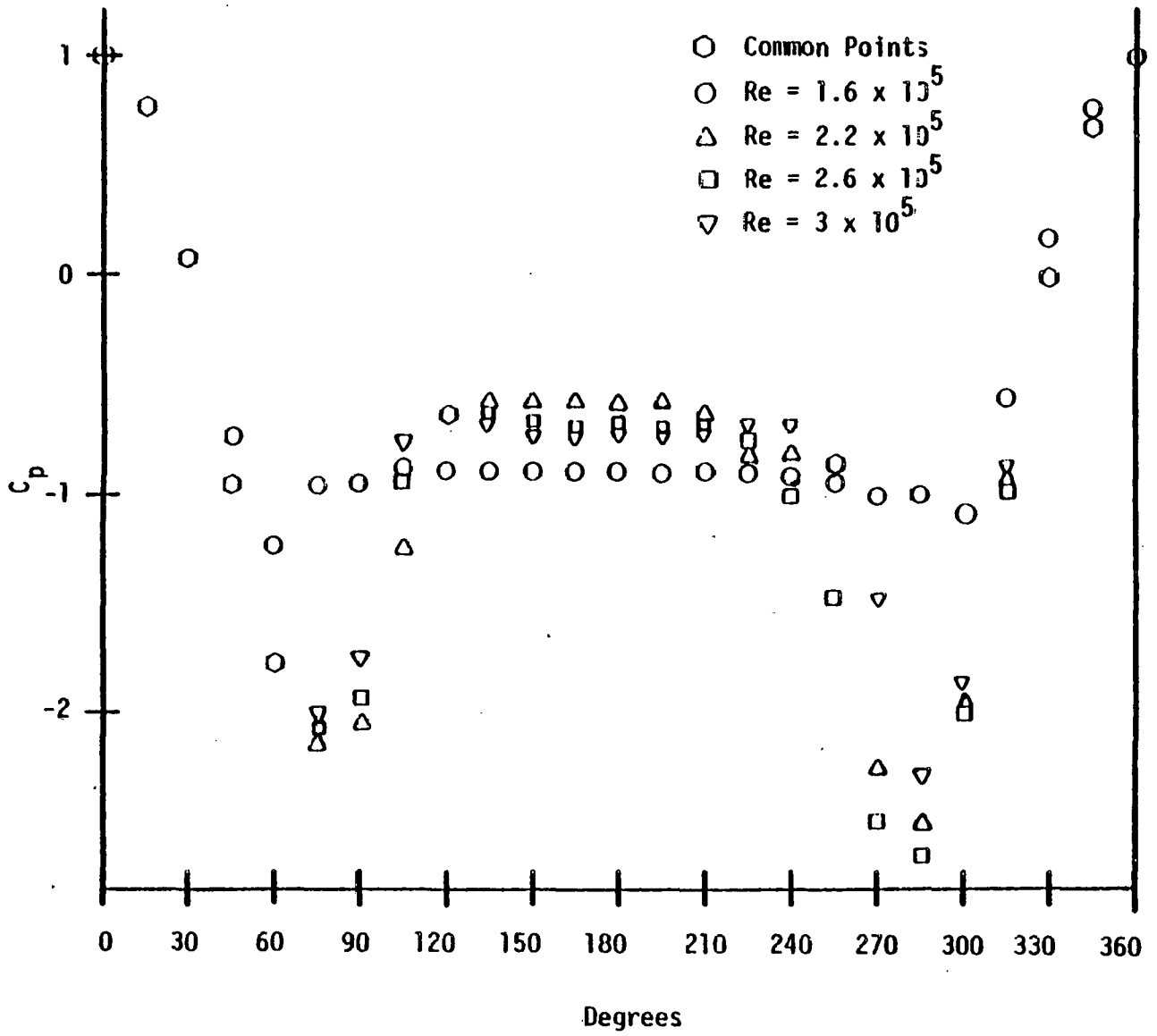


Fig. 14 Circumferential Pressure Distribution ($\beta$ = .007, Rough Cylinder)

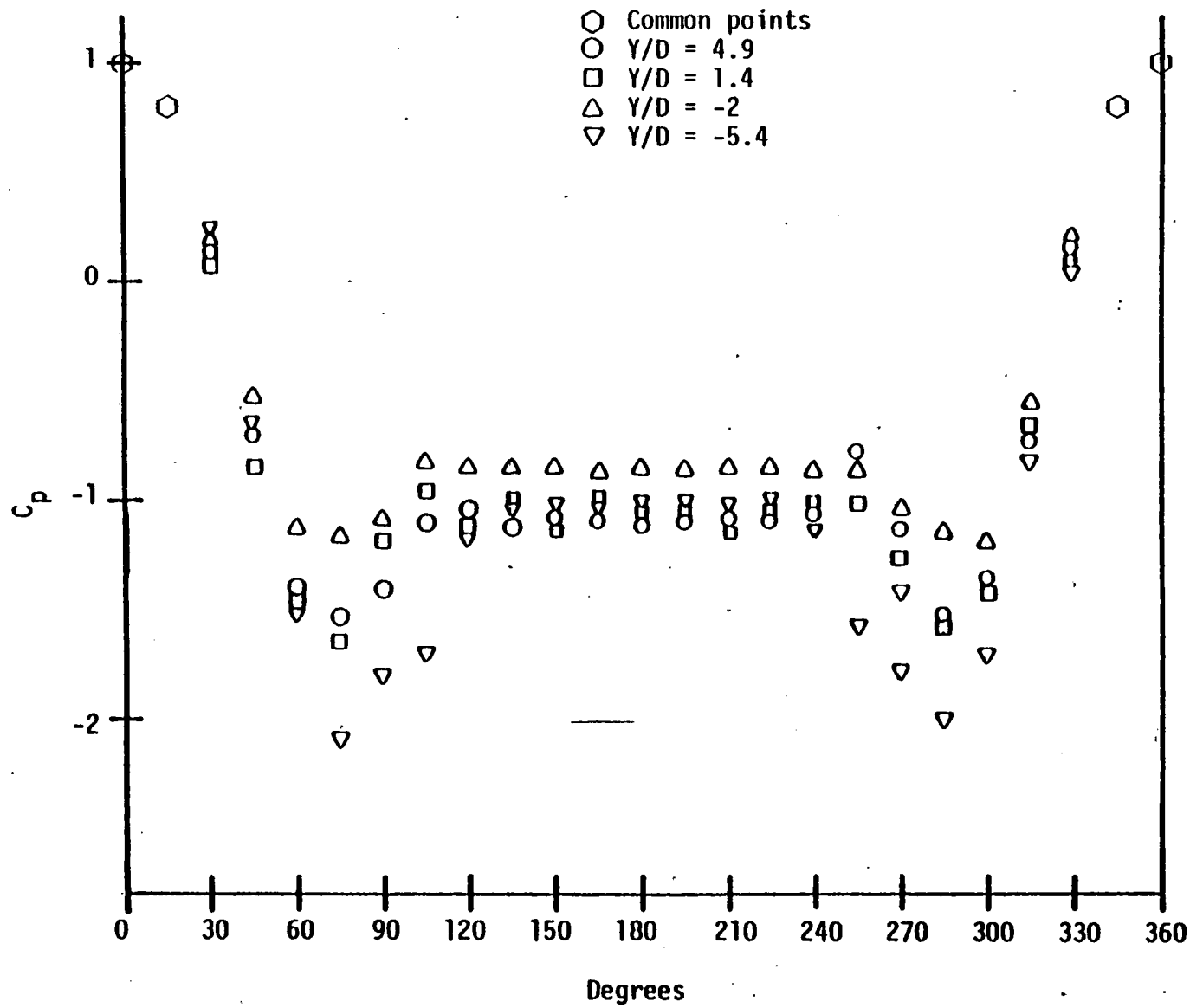


Fig. 15 Spanwise Variation of Circumferential Pressure Distribution
($Re = 3x10^5$, $\beta = .007$, Smooth Cylinder)

Referring back to Fig. 5, the nondimensional velocity profile for this case, one observes that the difference in mean velocity was unlikely to be the source of the variation in the pressure distribution. Also the magnitude of the peak suction did not decrease uniformly toward the low velocity side. It is very possible that the apparent supercritical pressure state was brought on by small discontinuities in the freestream profile which introduced locally significant three dimensionality in the flow field. Supporting that hypothesis is the observation that the greatest deviation from the subcritical profile occurred at Y/D = 5.4, exactly where a small hump in the velocity profile was located. This spanwise variation in pressure profiles was not observed in any other smooth cylinder case. On the rough cylinder, however, very significant spanwise pressure variations were recorded at a centerline Reynolds number of $2.2 \times 10^5$. For example, with $\beta = .007$, the peak suction at Y/D = 4.8 was $C_p = -1.2$, while at Y/D = -5.4, it had grown to $C_p = -3.2$. Similar dramatic variations occurred for all other shear levels at the same Reynolds number. Therefore further evidence was obtained that $Re = 2.2 \times 10^5$ was very close to the critical value for the rough cylinder.

Figs. 16 and 17 show the respective pressure plots for the smooth and rough cylinders at $\beta = .016$. The smooth cylinder was entirely within the subcritical range. The most noteworthy feature of the rough cylinder case is the extreme asymmetry recorded for $Re = 2.2 \times 10^5$, which again appears to be the result of the separation bubble phenomenon mentioned in the discussion of the uniform flow case. There was only slight difference in freestream turbulence between this and the previous ($\beta = .007$) case. The only discrepancy between the pressure profiles is the absence of the asymmetry for $\beta = .007$ at exactly $Re = 2.2 \times 10^5$. Since this phenomenon may be expected to occur somewhere in a narrow range, the inability to record it at a specific Reynolds number for different cases is not surprising.

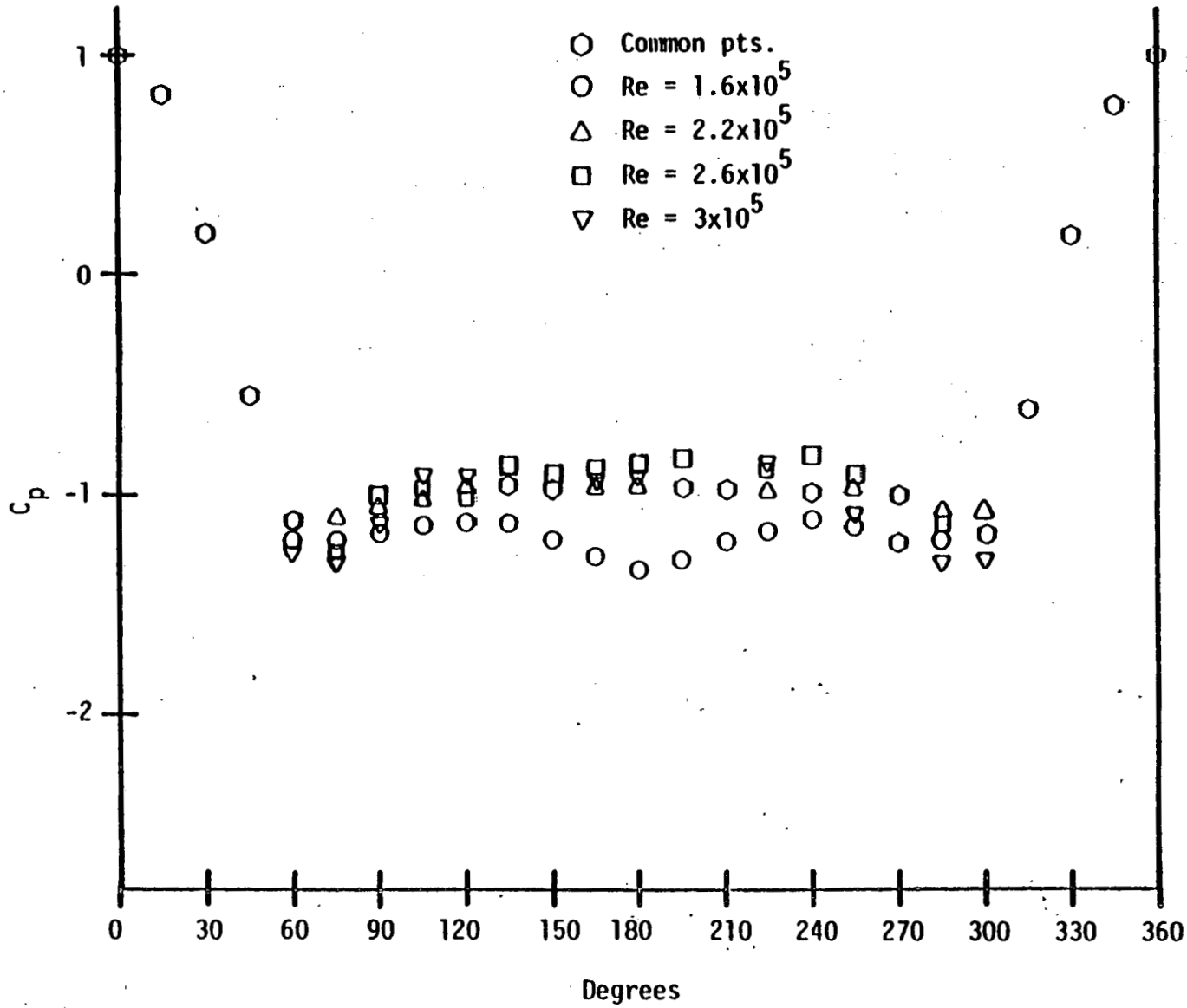


Fig. 16 Circumferential Pressure Distribution
($\beta$ = .016, Smooth Cylinder)

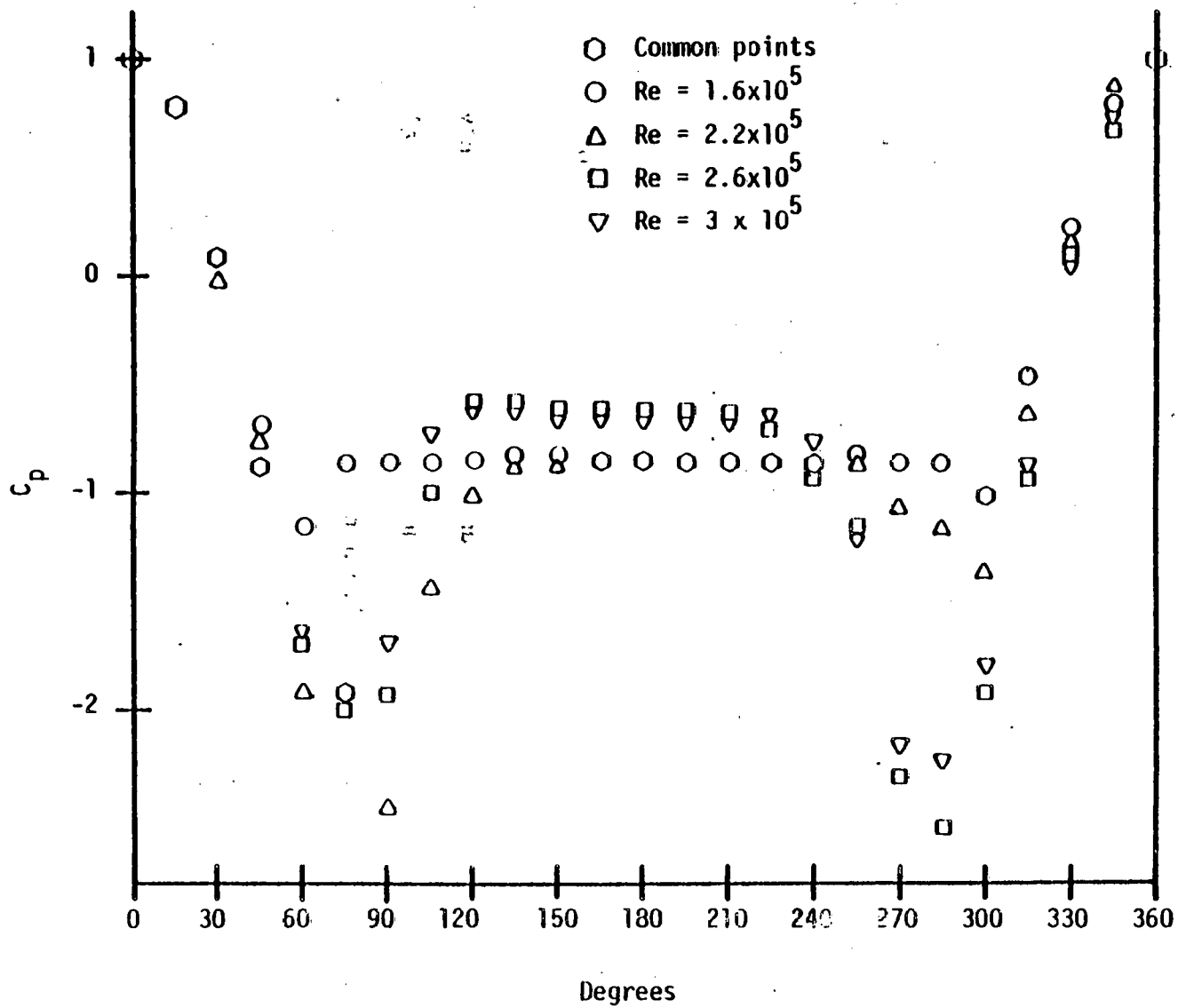


Fig. 17 Circumferential Pressure Distribution
($\beta$ = .016, Rough Cylinder)

As the shear level was increased by inserting more screens in the upstream flow, fewer Reynolds number cases were achievable in the wind tunnel. For $\beta = .021$, results for three flow levels are plotted in Figs. 18 and 19. The smooth cylinder profiles were still completely subcritical, while the rough cylinder again manifested supercritical characteristics for $Re \geq 2.2 \times 10^5$. Another point worth noting is that for virtually every preceding case, and particularly in the present case, the peak suction for the rough cylinder decreased in magnitude beyond $Re = 2.2 \times 10^5$. Batham' has presented a sketch of roughness Reynolds number as a function of peak suction which bears out this result.

For $\beta = .033$, the smooth cylinder profile assumed its usual shape (Fig. 20), but for the rough cylinder (Fig. 21), the asymmetry once again appeared at $Re = 2.2 \times 10^5$. During all test runs where the asymmetry was observed, the more negative $C_p$ value occurred on the $\theta = 90°$ side of the cylinder (facing the tunnel ceiling).

The final shear case, $\beta = .041$, was run for only two values of Reynolds number. Both profiles for the smooth cylinder were virtually identical to previous runs, as can be seen in Fig. 22, and the rough cylinder (Fig. 23), showed full growth of the two suction lobes.

The effect of freestream turbulence on the profiles appeared to be quite small, since for $Y/D = -2$, the intensity increased from 0.2% only to 0.5%, which was not a significant enough difference to affect the location of a separation point or alter the transition Reynolds number for either cylinder.

## C. Vortex Shedding Patterns for Smooth and Rough Cylinders in Uniform Flow

Three cases were examined. First the smooth cylinder was placed in the unsheared flow generated by a single screen. Fig. 24 shows the progression of the shedding frequency with Reynolds number. The energy in the peaks remained

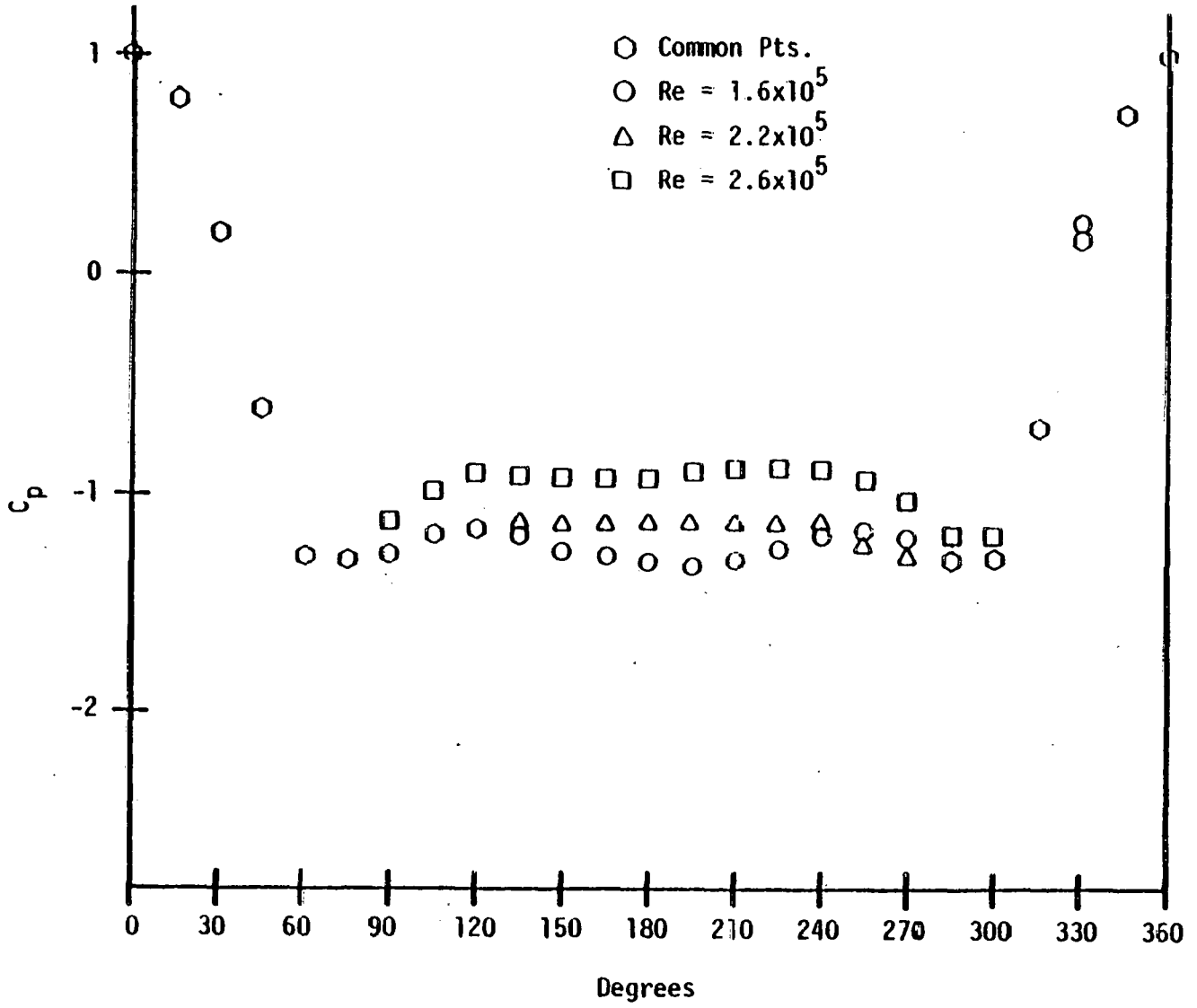


Fig. 18 Circumferential Pressure Distribution
($\beta$ = .021, Smooth Cylinder)

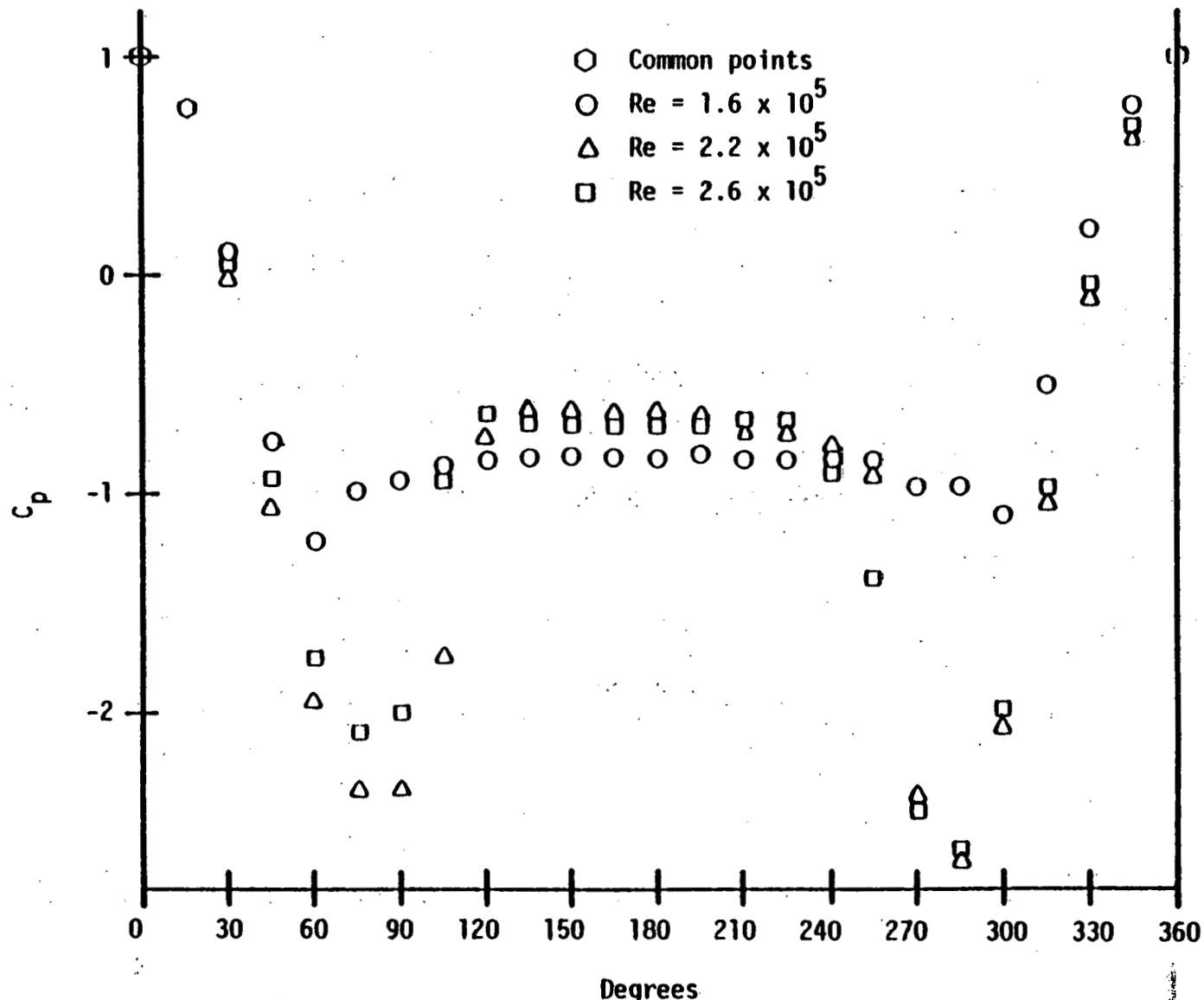


Fig. 19 Circumferential Pressure Distribution
($\beta$ = .021, Rough Cylinder)

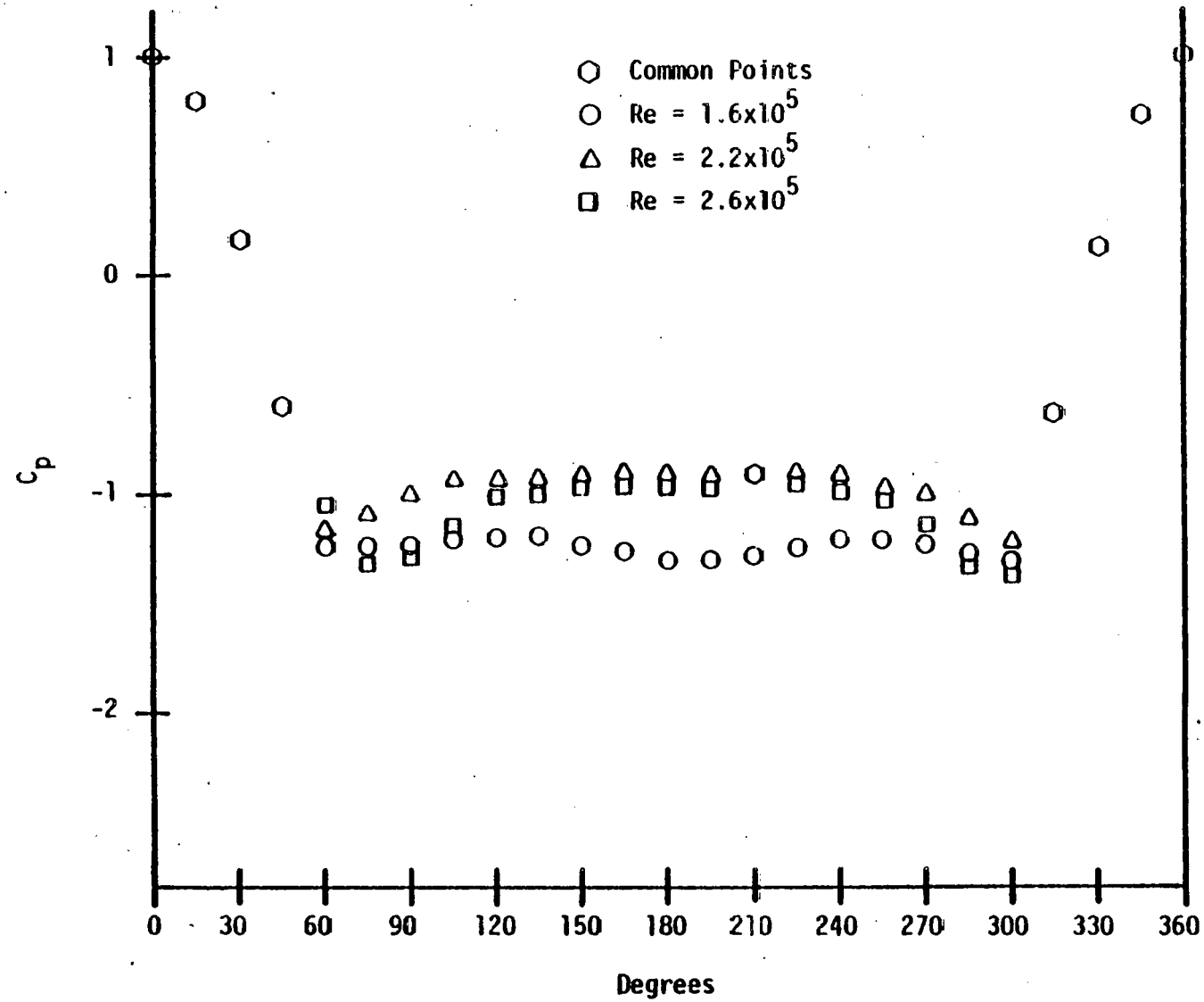


Fig. 20 Circumferential Pressure Distribution
($\beta$ = .033, Smooth Cylinder)

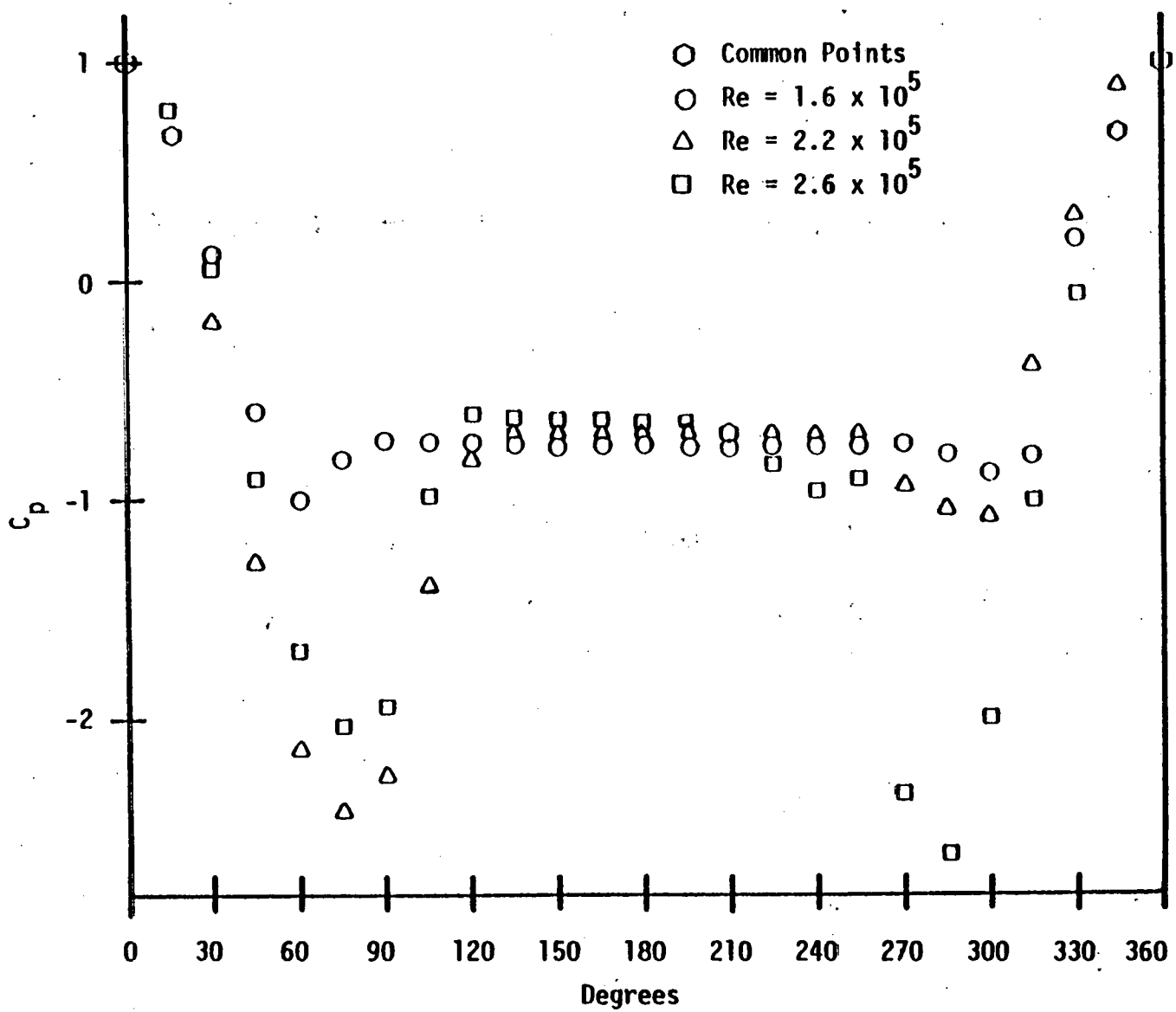


Fig. 21 Circumferential Pressure Distribution ($\beta$ = .033, Rough Cylinder)

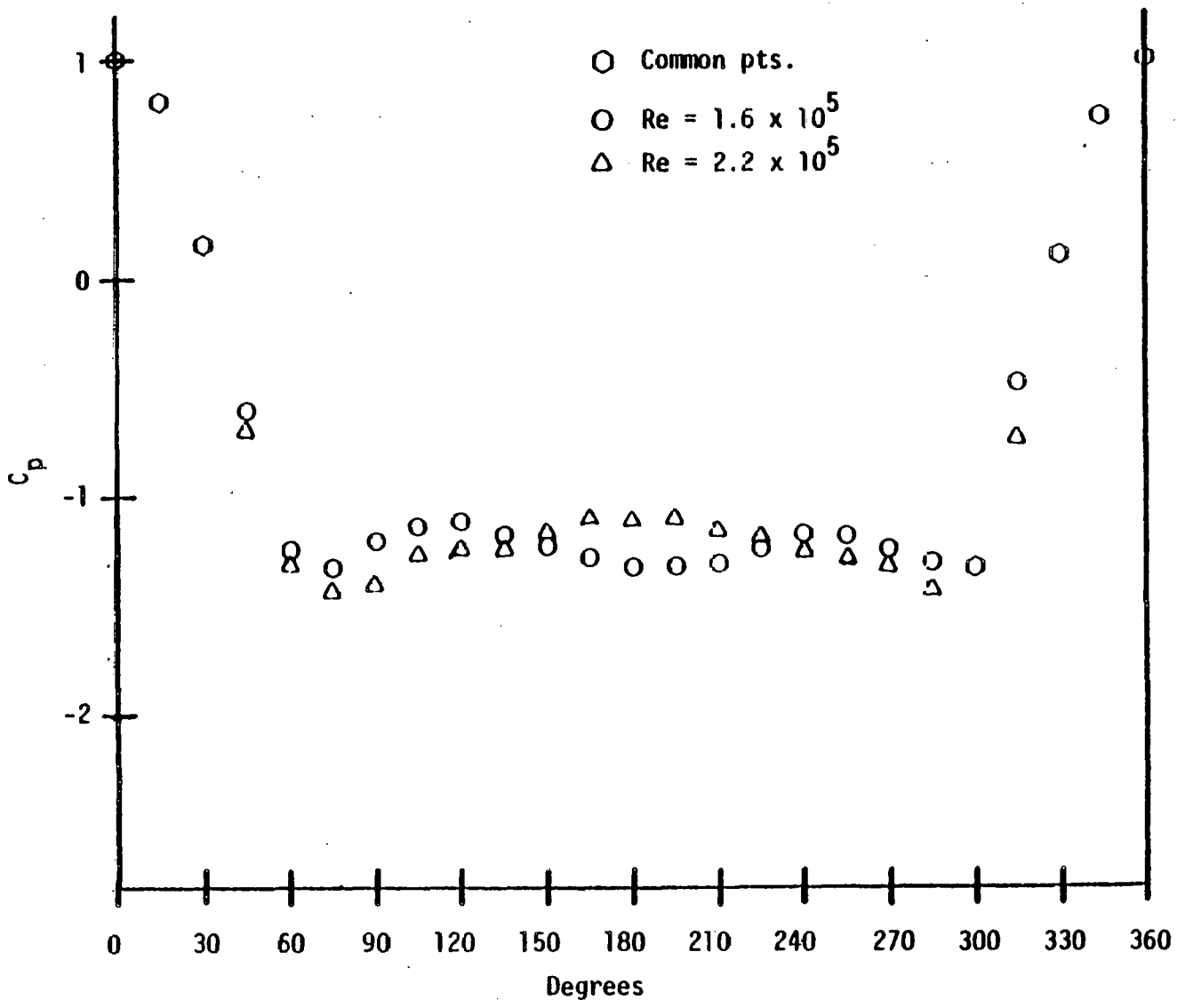


Fig. 22 Circumferential Pressure Distribution ($\beta$ = .041, Smooth Cylinder)

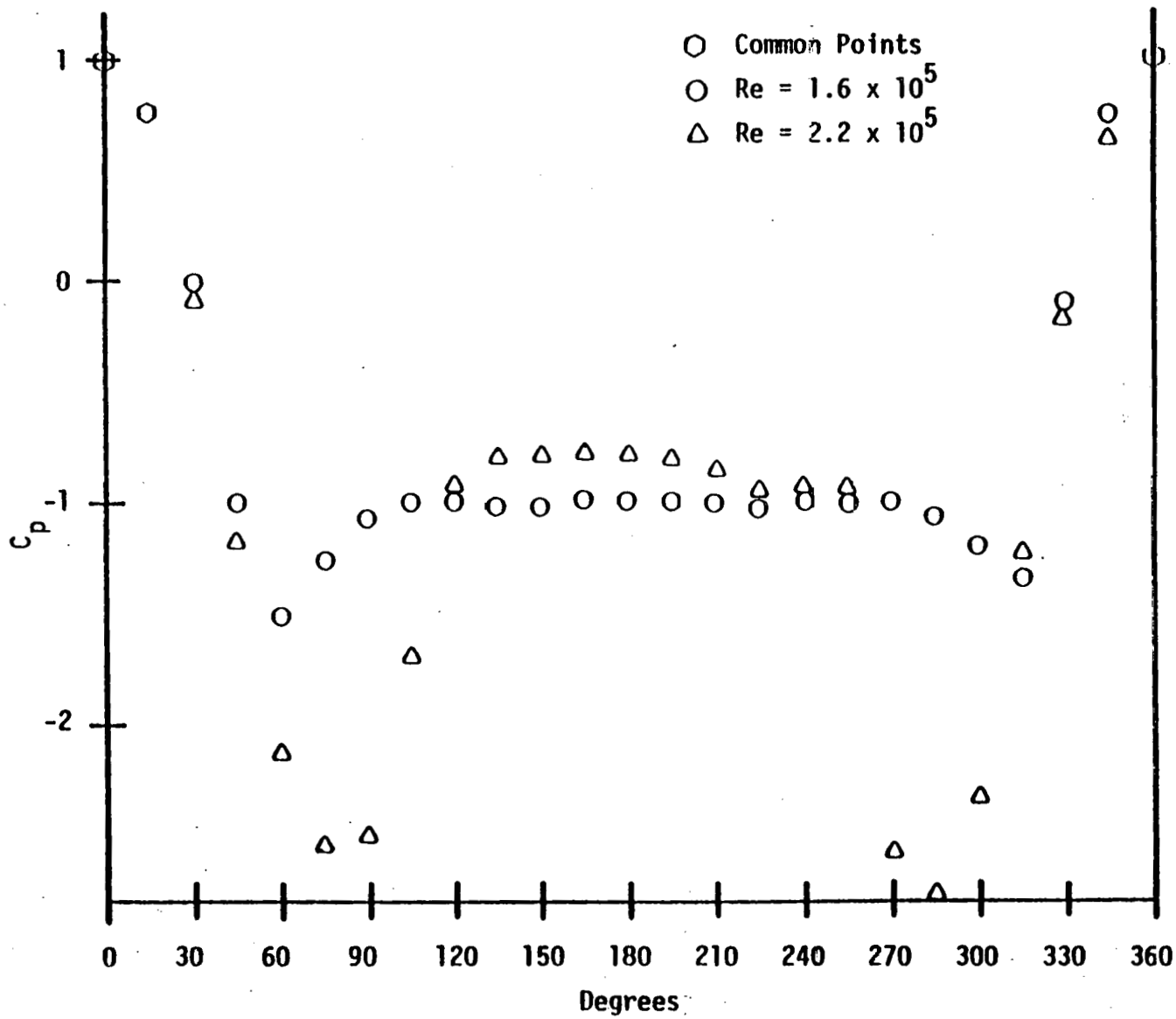


Fig. 23 Circumferential Pressure Distribution ($\beta$ = .041, Rough Cylinder)

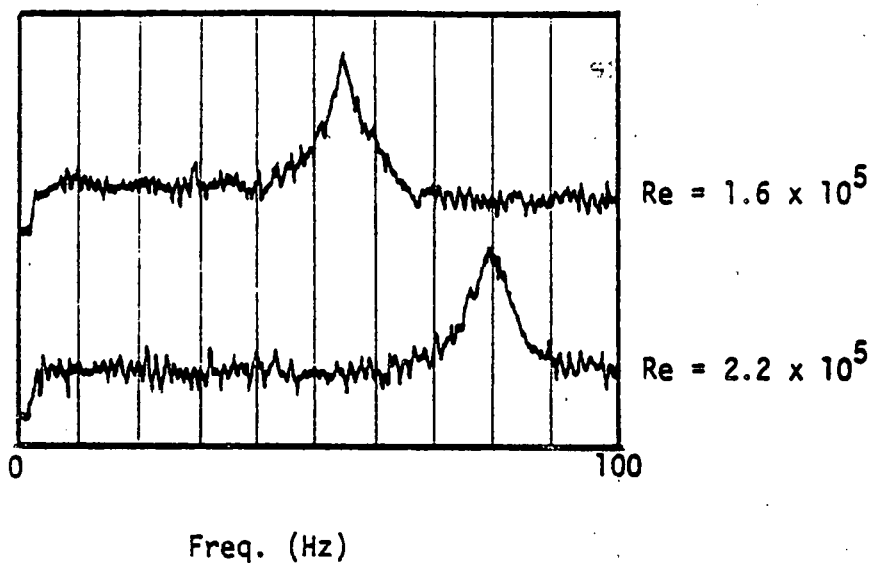


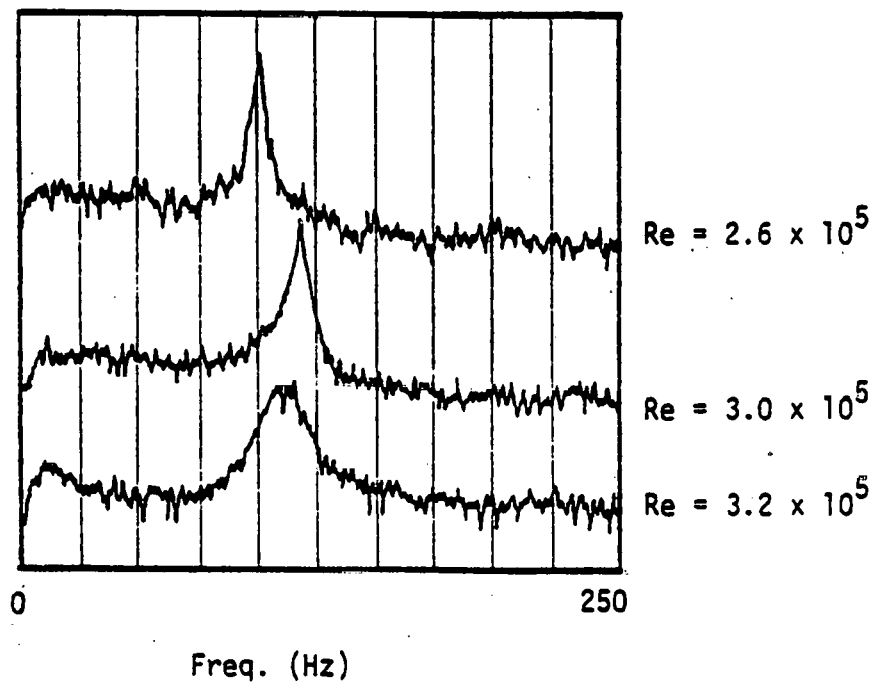


Fig. 24 Power Spectral Density of Eddy Shedding Frequency
(Y/D = 0, $\beta$= 0, Smooth Cylinder)

concentrated around a narrow frequency band as the Reynolds number increased. The final point at Re = $3.2 \times 10^5$ was not indicative of the dominant shedding frequency, as subsequent tests revealed. The measurements for the case shown were taken behind the center of the cylinder, at Y/D = 0. It was discovered that a small region near the center showed a more confused shedding pattern in the unsheared flow than did other points further from the center when the Reynolds number approached the critical range, which of course depended on the cylinder roughness. This was attributed to the fact that the cylinder was fashioned from two 30 inch sections, joined at the center. Therefore, a very small seam existed at the center, which may have triggered a prematurely critical wake pattern when the Reynolds number approached the critical value.

Consequently, measurements for the knurled cylinder, the second case, were taken at Y/D = 4.0, as well as at the centerline. The results at Y/D = 4.0 are plotted in Fig. 25. It is evident that organized shedding activity disappeared just above Re = $2.2 \times 10^5$, and began to reappear around Re = $3.2 \times 10^5$. It should be noted that, at the centerline, the final subcritical peak was found to exist at Re = $1.9 \times 10^5$, suggesting enhanced turbulent influence from the cylinder joint. An attempt was then made to estimate the influence of free-stream turbulence on the shedding characteristics by removing the single uniform wire screen from the upstream end of the tunnel. For this third case, with no screens impeding the flow, the tunnel turbulence decreased to about .03%. The resulting spectra (shown in Fig. 26), taken at Y/D = 4.0 on the rough cylinder, showed a pattern very similar to that observed at the higher turbulence level. An additional spectrum (at Re = $2.4 \times 10^5$) is included to indicate a slightly greater persistence of the subcritical peak. However, the super-critical peak at Re = $3.3 \times 10^5$ is weaker than in Fig. 25. The reduced blockage permitted results to be obtained for Reynolds numbers up to $3.6 \times 10^5$, for which

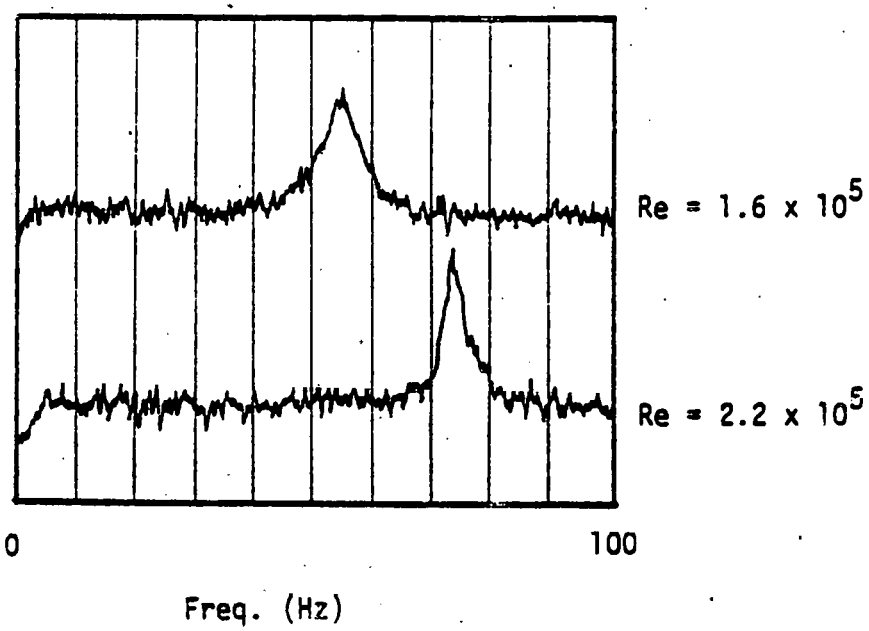


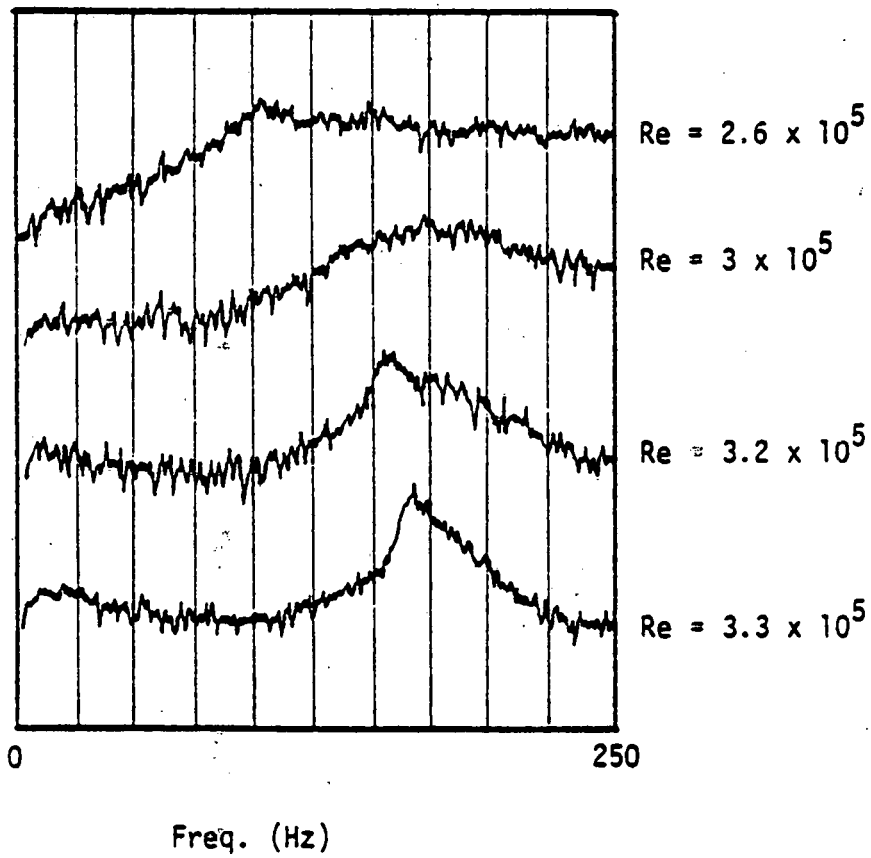


Fig. 25 Power Spectral Density of Eddy Shedding Frequency
($Y/D = 0$, $\beta = 0$, Rough Cylinder)

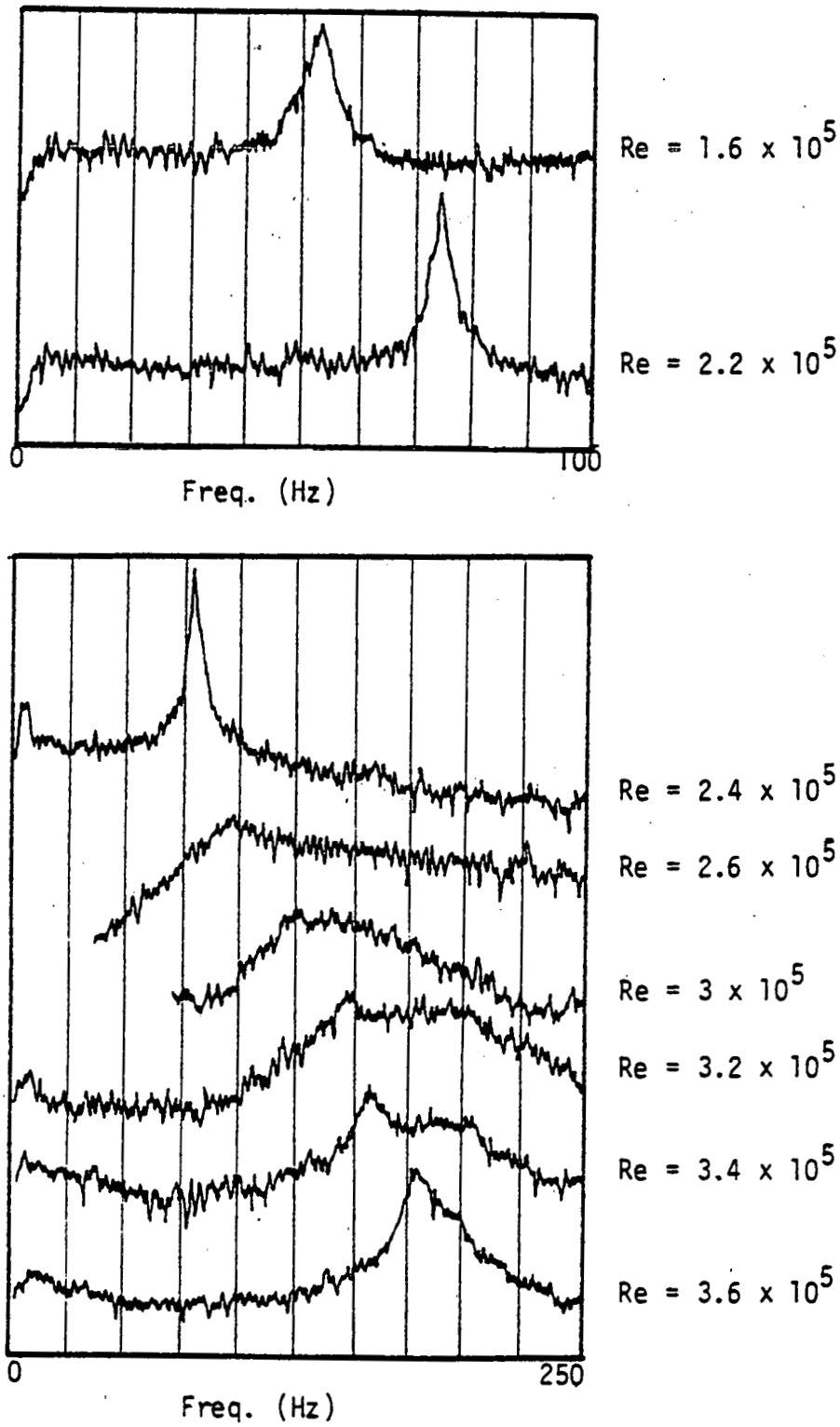


Fig. 26 Power Spectral Density of Eddy Shedding Frequency (Y/D = 0, $\beta$ = 0, Rough Cylinder, Turbulence = .03%)

the power spectral density of the eddies appeared to correspond to those at $Re = 3.3x10^5$ for the higher turbulence knurled case. Therefore the effect of an increase in freestream turbulence is seen to be a shift downward in the Reynolds number range for the transition regime with no discernible eddy structure. Exactly the same conclusion was reached from an analysis of the surface pressure distribution.

No transition regime for the smooth cylinder was reached. Bearman has shown that on a perfectly smooth cylinder in uniform flow, periodic narrow band shedding occurs up to $Re = 5.5x10^5$, which he defined as the end of the critical regime. Around $Re = 3.4x10^5$, the formation of laminar separation bubbles occurs, and a rapid change in Strouhal number, from 0.23 up to 0.46, takes place. The broadband shedding at higher Reynolds numbers is only thinly documented.

One more interesting phenomenon was recorded while examining the uniform flow cases. During the course of the spanwise traversing of the rough cylinder at $Re = 2.2x10^5$ (for which the shedding frequency was 74 Hz) a second strong peak at 69 Hz appeared around $Y/D = -3$. The 69 Hz peak actually replaced the 74 Hz signal during some measurements. An explanation was sought in possible probe mount or traverse vibrations. When the traverse was in motion, vibrations occasionally occurred, particularly at this point in the test program when the traverse had become slightly misaligned. The tunnel was shut off, and with the traverse in motion, a spectrum of the faint probe signal (which appeared on the oscilloscope as a near perfect sinusoid) was taken. The resulting plot showed a sharp peak at 69 Hz, thereby substantiating the speculation about probe vibrations. A subsequent analysis of the rest of the data for sheared cases at $Re = 2.2x10^5$ revealed no instances where contamination by the 69 Hz vibration frequency appeared to have occurred.

Fig. 27 shows a plot of Strouhal number as a function of Reynolds number for the smooth and rough cylinder tests, and vividly depicts the rough model transition regime. For subcritical Reynolds numbers, the Strouhal number was fairly constant around 0.18. When the shedding re-emerged around Re = $3.2 \times 10^5$ (depending on the freestream turbulence level) the Strouhal number was 0.24. For the smooth cylinder, a value between 0.19 and 0.20 was maintained. The smooth cylinder data is entirely consistent with Bearman's results, but the 0.24 value for the rough cylinder suggests that (if it is maintained at even higher Reynolds numbers) roughness causes supercritical shedding to occur at a much lower frequency than on a smooth cylinder.

Further careful tests with larger diameter cylinders, both smooth and rough, are required to clarify the effect of roughness on shedding frequencies in the critical Reynolds number range.

It should be noted that Szechenyi has presented a graph of Strouhal number as a function of roughness Reynolds number (in which the diameter of a roughness element is the length scale) which gives consistently higher values of Strouhal number than either Bearman or the present results. He also locates the critical regime between Re = $1.5 \times 10^5$ and Re = $2.0 \times 10^5$, assuming a perfect equivalence of the effect of a glass bead coated surface and a knurled surface of the same depth.

## D. Vortex Shedding Patterns for Smooth and Rough Cylinders in Sheared Flow

For each of the sheared flow cases examined, two figures are included to present the effect of spanwise shear on vortex shedding frequency. The first figure is a plot of the power spectral density measured at 17 increments of Y/D, each encompassing a length of one cylinder diameter. In some cases, only 9 increments (of Y/D = 2) were employed when the spectra showed little spanwise variation, and measurements at only 3 stations were recorded when no

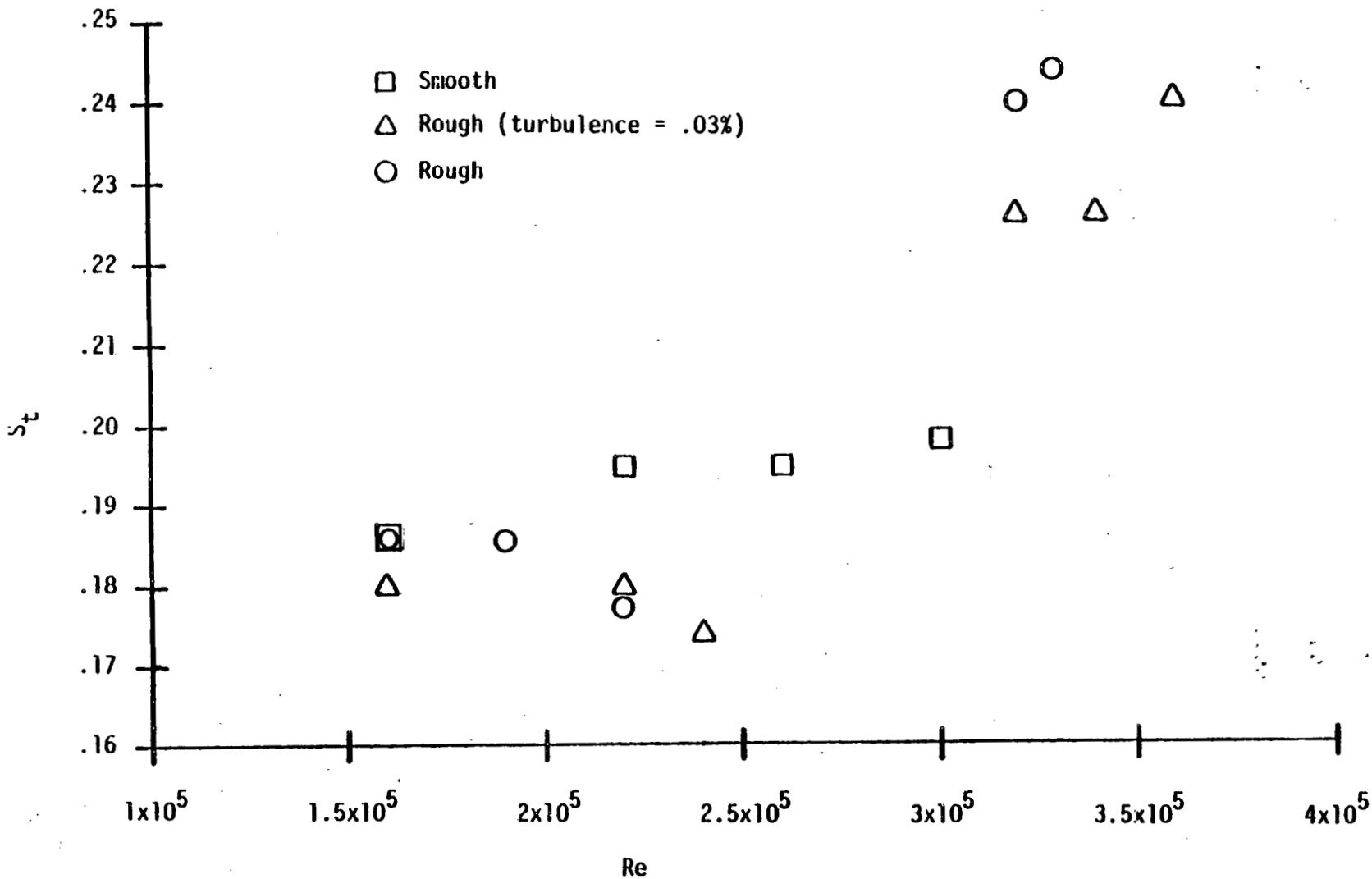


Fig. 27 Strouhal Number vs. Reynolds Number
Smooth and Rough Cylinders

significant shedding was observed. Following this graph is a plot of Strouhal number as a function of Y/D for the given case, where the Strouhal number is, like the Reynolds number, based on the centerline freestream velocity. A spanwise vortex shedding cell is identifiable as a segment of Y/D over which the Strouhal number is constant. A particular station for which the signal had a broad peak is represented by points at the upper and lower limits connected by a bar. A station for which two separate identifiable peaks were measured is represented by two unconnected points, and a very weak, yet still discernible peak is shown as a dotted point.

The following analysis parallels that of the pressure measurements, proceeding from the lowest to the highest shear case, with a comparison of smooth and rough cylinder results for each case.

(i) Shear parameter, $\beta = .007$

Figure 28 shows the frequency distribution along the smooth cylinder for the lowest shear level which can be produced in the wind tunnel. A single peak, rather broad but definitely centered at 56 Hz, persisted from the high velocity end to the center of the cylinder, a length of about eight diameters. The next few peaks appeared to move gradually to a lower frequency, which then stabilized at 49 Hz over the last three diameters of the cylinder. Reference to Fig. 24 shows a uniform flow peak at 55 Hz. Clearly then, a tendency toward an organized cell structure is evident even for very small shear values. The apparent gradual change of the peak near the center of the cylinder (more readily seen in Fig. 29) reflects the unsteadiness of the boundary between the two cells. As noted previously, Mair and Stansby put forward this explanation for some of their results, since they observed "that a vortex that is shed must have some length in the spanwise direction, and the time interval between two successive vortices cannot change continuously

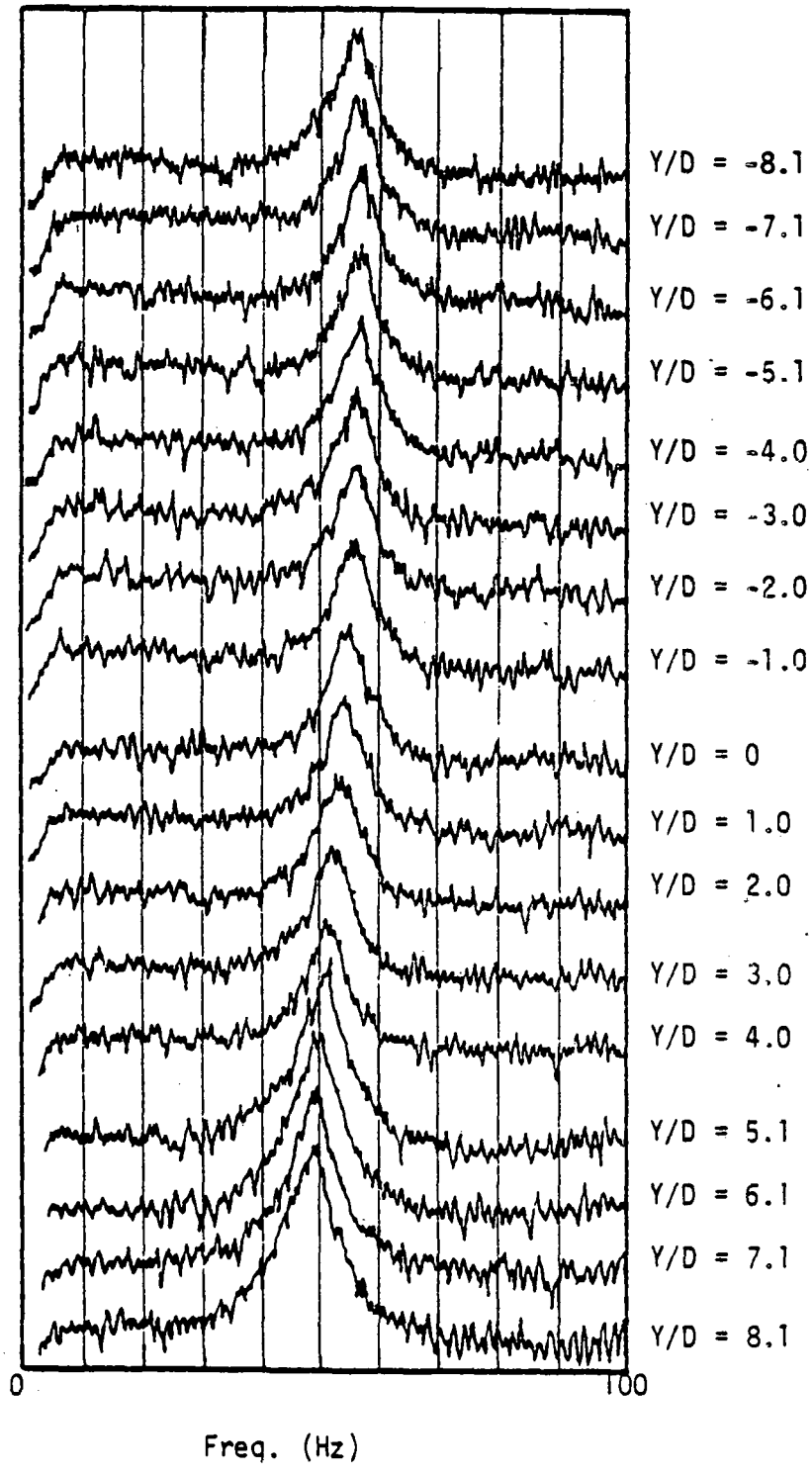


Fig. 28 Power Spectral Density of Eddy Shedding Frequency (Re = $1.6 \times 10^5$, $\beta$ = .007, Smooth Cylinder)

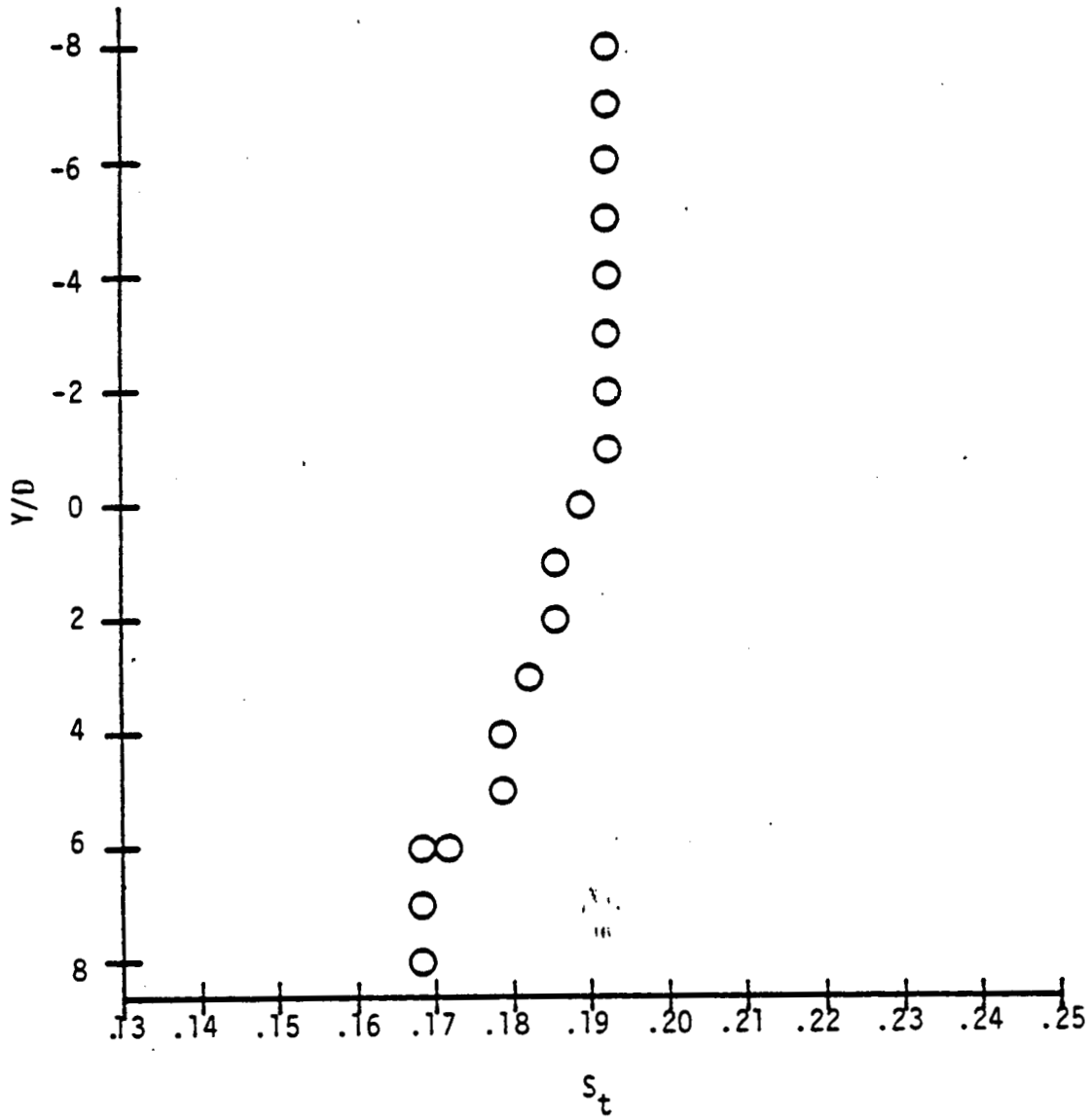


Fig. 29 Spanwise Variation of Centerline Strouhal Number ($Re = 1.6 \times 10^5$, $\beta = .007$, Smooth Cylinder)

along the span." As the present sets of spectra were averaged over a two minute period, there was ample opportunity for contributions from both end peaks to be included in midspan spectral averages. This supposition is strengthened by an examination of Figs. 30 and 31, which represent the same shear conditions over the smooth cylinder at Re = $2.6 \times 10^5$. A sharp division between Y/D = 0 and Y/D = 2 marked the transition from a peak at 105 Hz to a peak at 95 Hz. However, complicating the picture was a third, very distinct peak at about 90 Hz which appeared to coexist with the 95 Hz peak. Actually the double peak was caused by the probe picking up signals from two separate cells with a varying boundary between them, so a total of three cells were present. The apparent growth, decay (at Y/D = 6.1) and regrowth (at Y/D = 8.1) of the 90 Hz peak was occasioned by the change in probe mounting required to give complete coverage of the cylinder length. In one position, the probe covered the distance from Y/D = -8.1 to Y/D = 4.0. Then the tunnel was shut off, the probe relocated from one side to the other of a T-shaped mount, and the test was recommenced after the centerline velocity was re-established. In the few cases where cell boundaries were particularly unstable, this disruption could have produced results similar to that obtained in Fig. 30.

When the Reynolds number was further raised to $3.0 \times 10^5$ (Figs. 32 and 33), the cell boundaries appeared to have stabilized, but at far different locations than in the first two cases. The high frequency cell, now at 120 Hz, extended down only to Y/D = -6, and was then superseded by a cell at 115 Hz with a length of approximately four diameters. The largest cell, extending from Y/D = 0 to the low velocity endplate, was shedding at 105 Hz. The spanwise variation in Strouhal number was virtually identical (.206 down to .176) for the two higher Reynolds number cases, as can be seen by comparing Figs. 31 and 33, but from Fig. 29, it is evident that at Re = $1.6 \times 10^5$, the range was

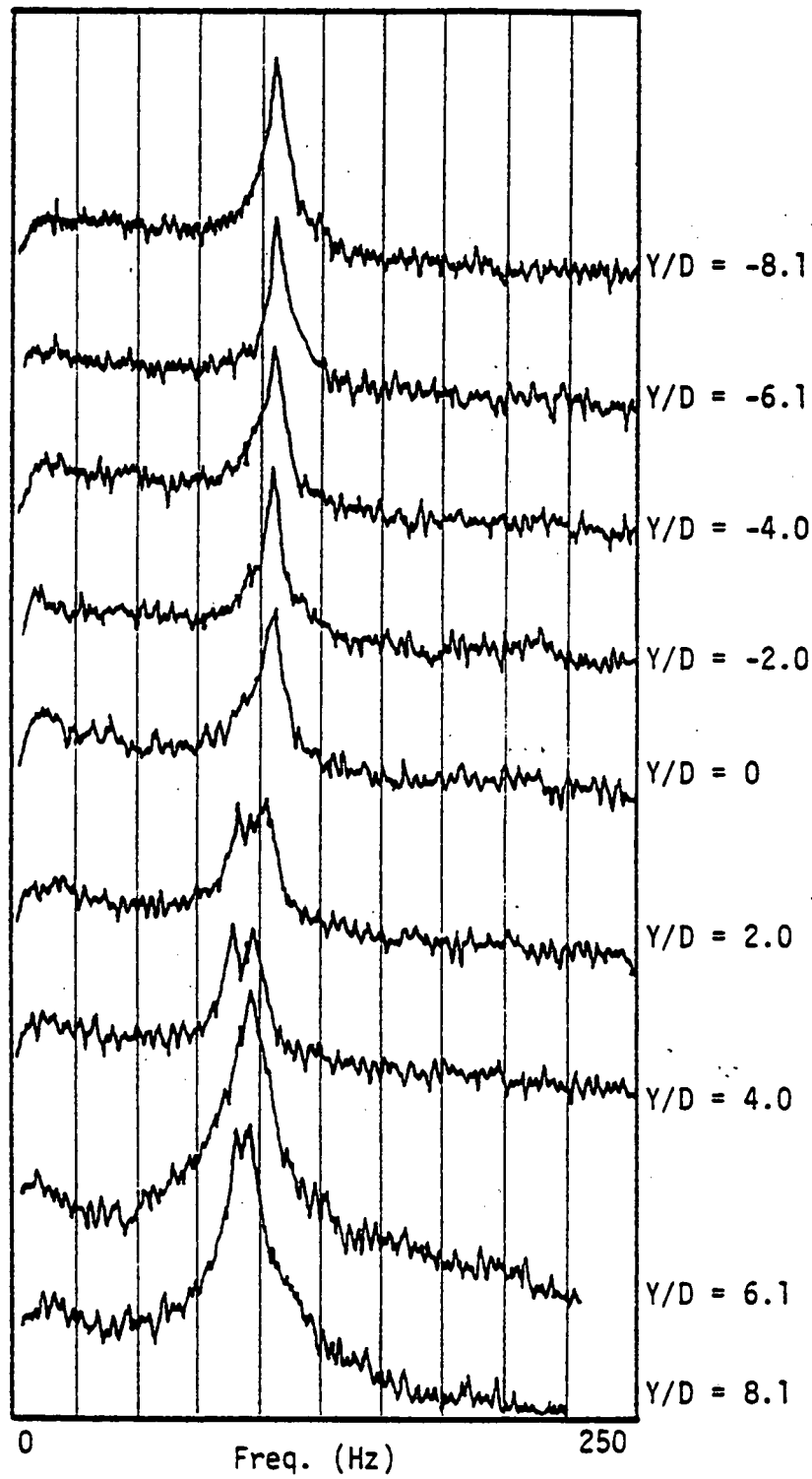


Fig. 30 Power Spectral Density of Eddy Shedding Frequency
($Re = 2.6 \times 10^5$, $\beta = .007$, Smooth Cylinder)

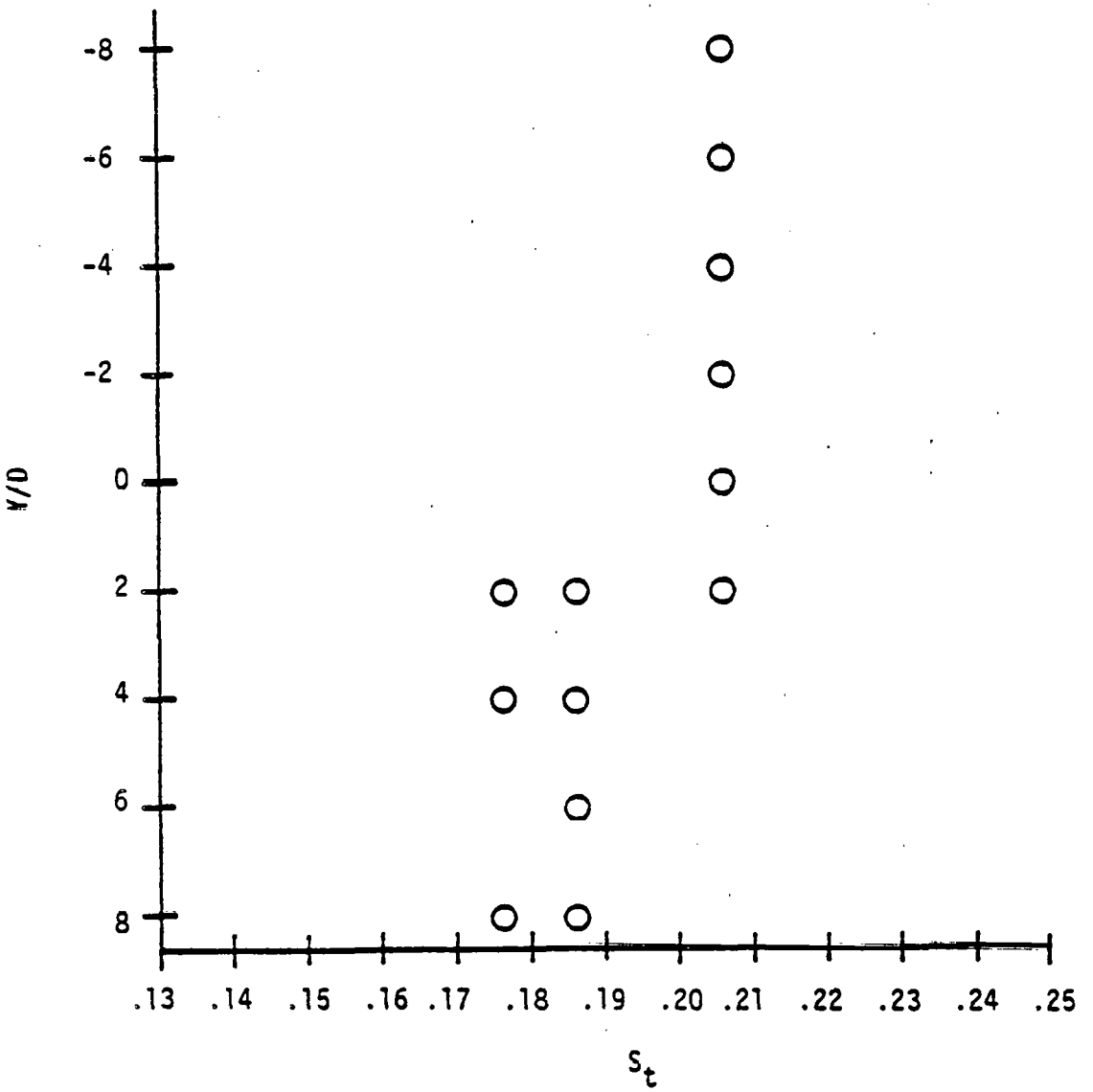


Fig. 31 Spanwise Variation of Centerline Strouhal Number
($Re = 2.6 \times 10^5$, $\beta = .007$, Smooth Cylinder)

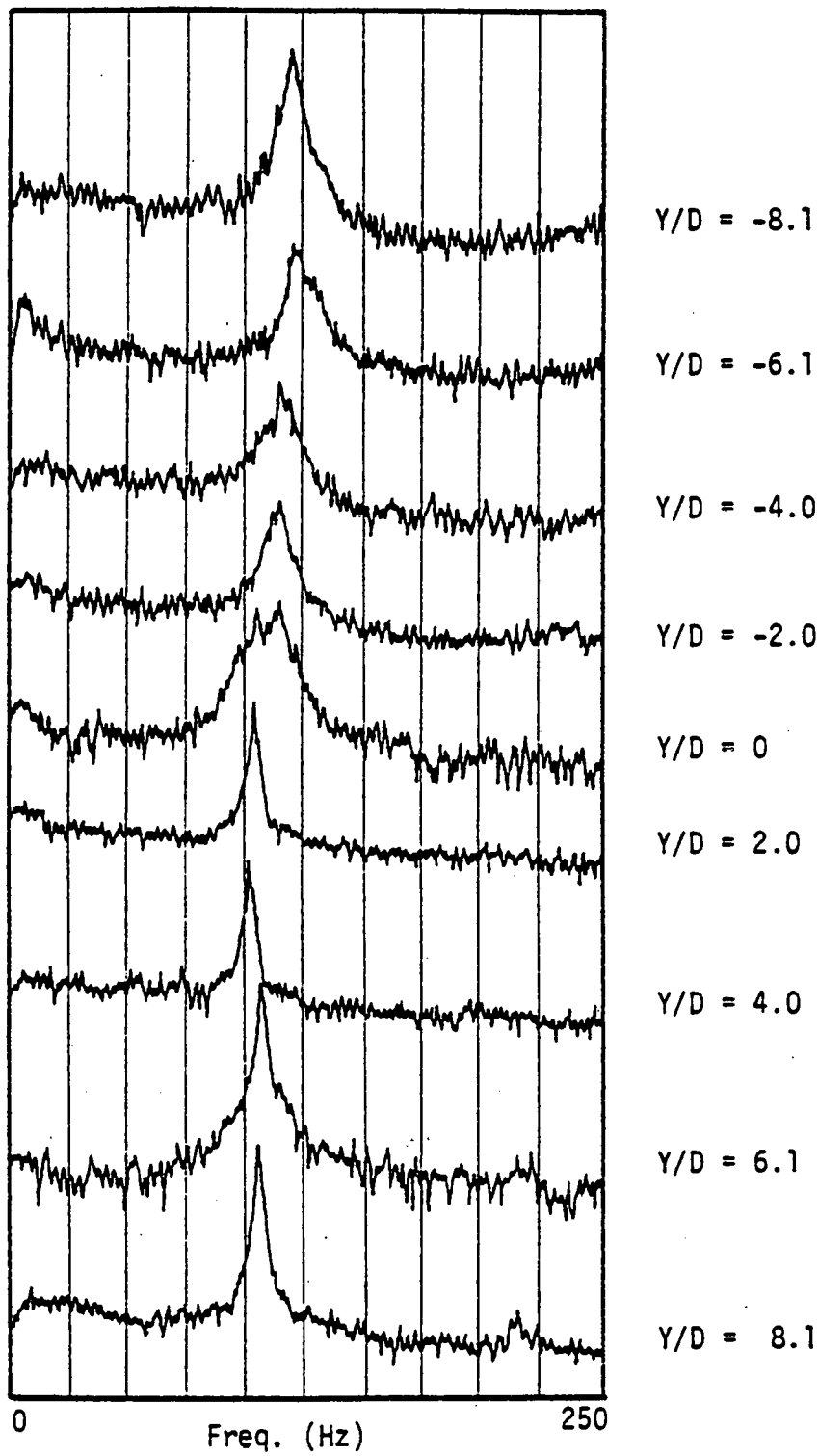


Fig. 32 Power Spectral Density of Eddy Shedding Frequency
($Re = 3x10^5$, $\beta = .007$, Smooth Cylinder)

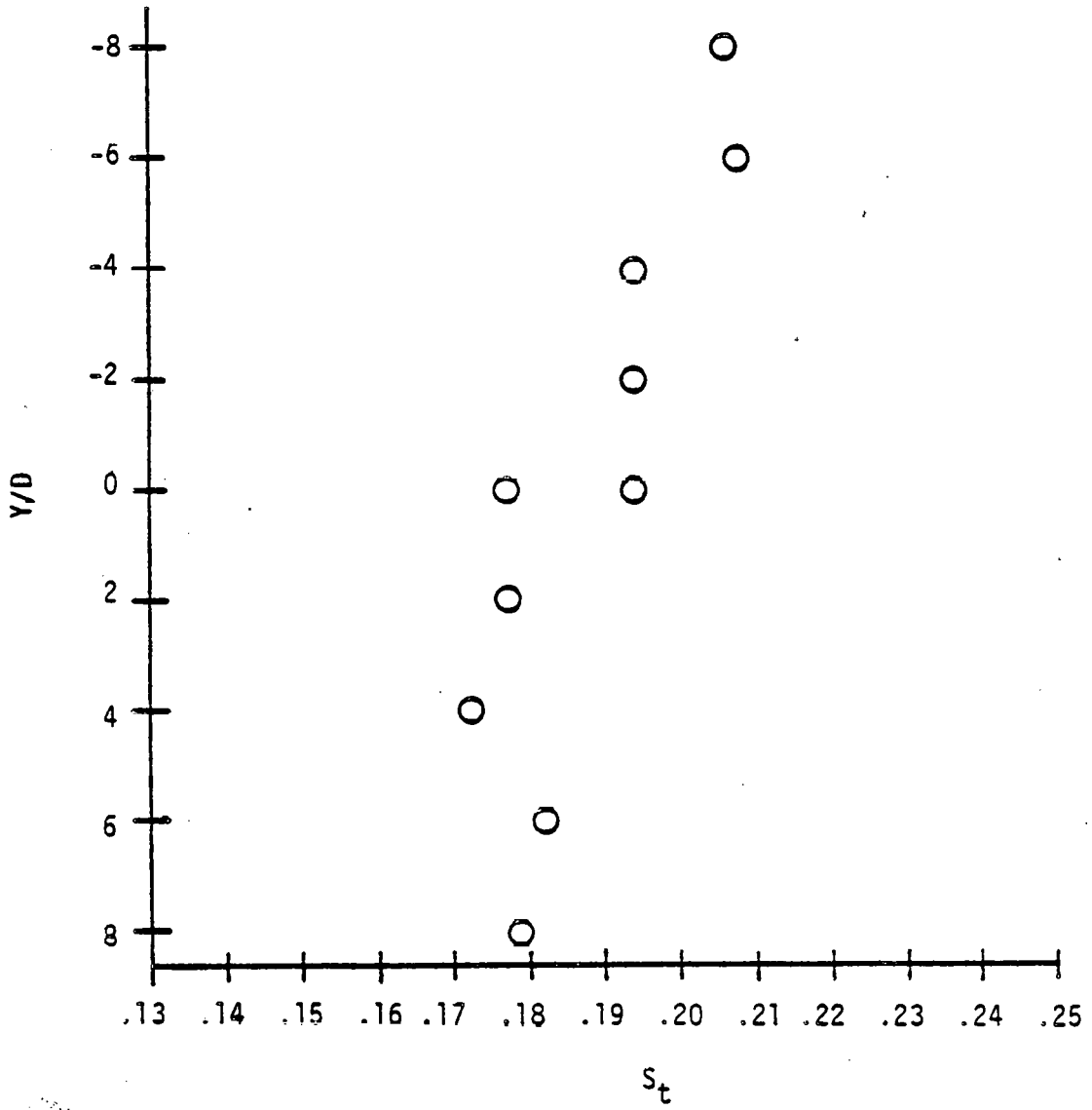


Fig. 33 Spanwise Variation of Centerline Strouhal Number ($Re = 3x10^5$, $\beta = .007$ Smooth Cylinder)

narrower (.192 to .168) as well as being lower. The lower Strouhal numbers correspond to the results graphed in Fig. 27 which show a gradual increase in Strouhal number with Reynolds number for the smooth cylinder over the range tested.

The shedding pattern developed behind the rough cylinder at Re = $1.6 \times 10^5$ (Figs. 34 and 35) was somewhat more confused than in the corresponding smooth cylinder case. For example, between Y/D = -8 and Y/D = -4, a peak at 54 Hz was measured, whereas in the lower velocity region from Y/D = -4 to Y/D = 0, a peak at 57 Hz was measured. The lower value must be the result of endplate effects. The maximum velocity was only 4% greater than the centerline velocity for $\beta$ = .007, so the endplate region may have generated a cell based on a slightly lower boundary velocity. Including the 54 Hz cell, a total of perhaps three separate cells may be discerned, although the final one (from Y/D = 2.0 to Y/D = 8.0) was not very well defined. A significant difference from the smooth cylinder result can be seen in the frequency range from the high to the low velocity ends. Even counting the 57 Hz peak as representative of the high velocity end, the spanwise spread was only 4 Hz, with a Strouhal number range of .196 to .178 (discounting the single point at .171, which from Fig. 34 is seen to be less prominent than the one at .178 in the spectrum for Y/D = 8.1). When the Reynolds number was raised to $2.6 \times 10^5$ and $3.0 \times 10^5$, the flow pattern assumed critical characteristics, unlike the smooth cylinder case, which was still subcritical, as has already been noted in the analysis of the surface pressure distributions. Consequently, no significant amount of energy was concentrated at a Strouhal frequency, except at Y/D = -4.0 at Re = $3.0 \times 10^5$, where a broadband signal with a peak near 150 Hz was noted. That frequency translates into a Strouhal number of about .260, or about 25% higher than the corresponding Strouhal number at the same location on the smooth cylinder at

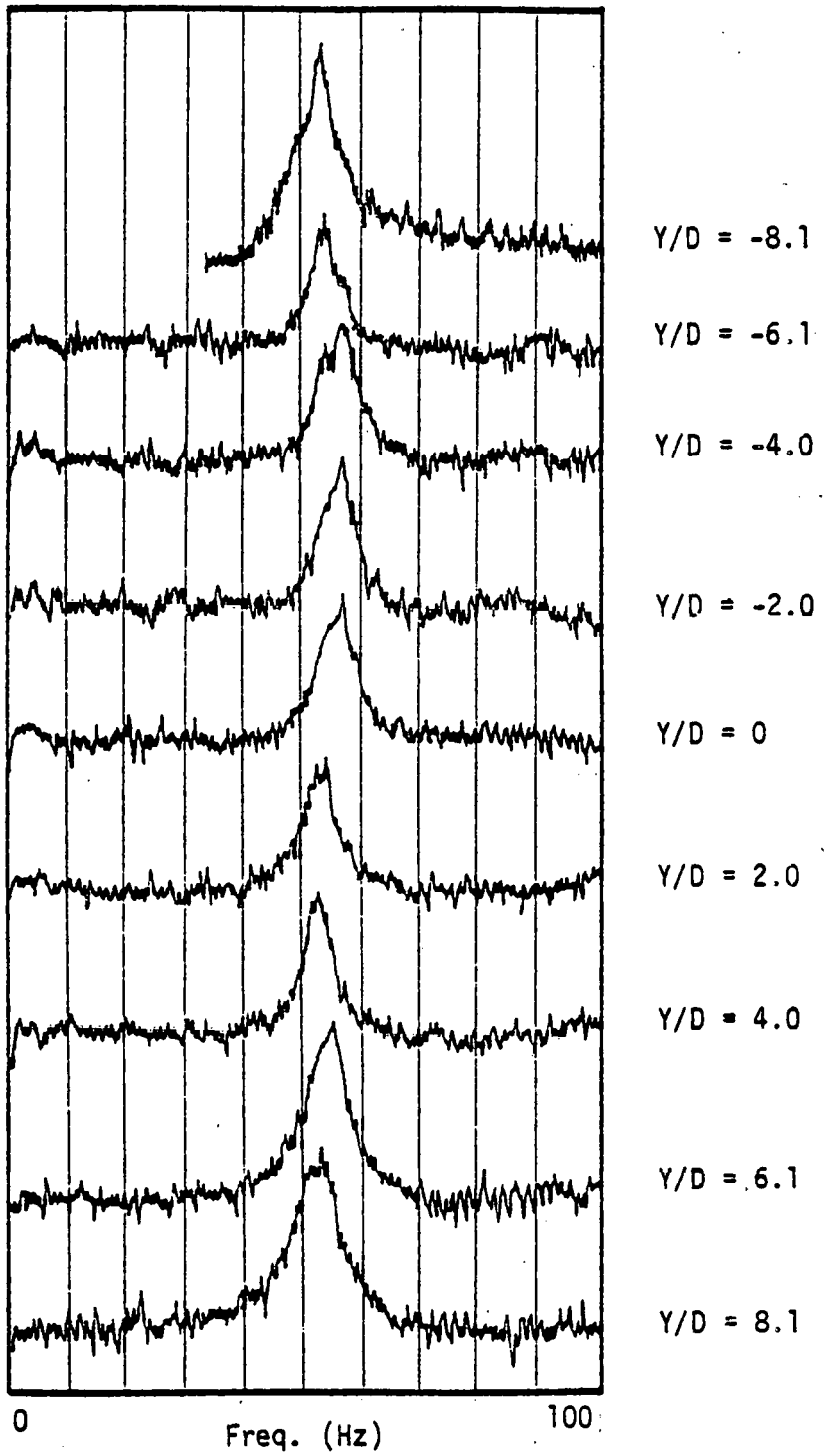


Fig. 34 Power Spectral Density of Eddy Shedding Frequency
($Re = 1.6 \times 10^5$, $\beta = .007$, Rough Cylinder)

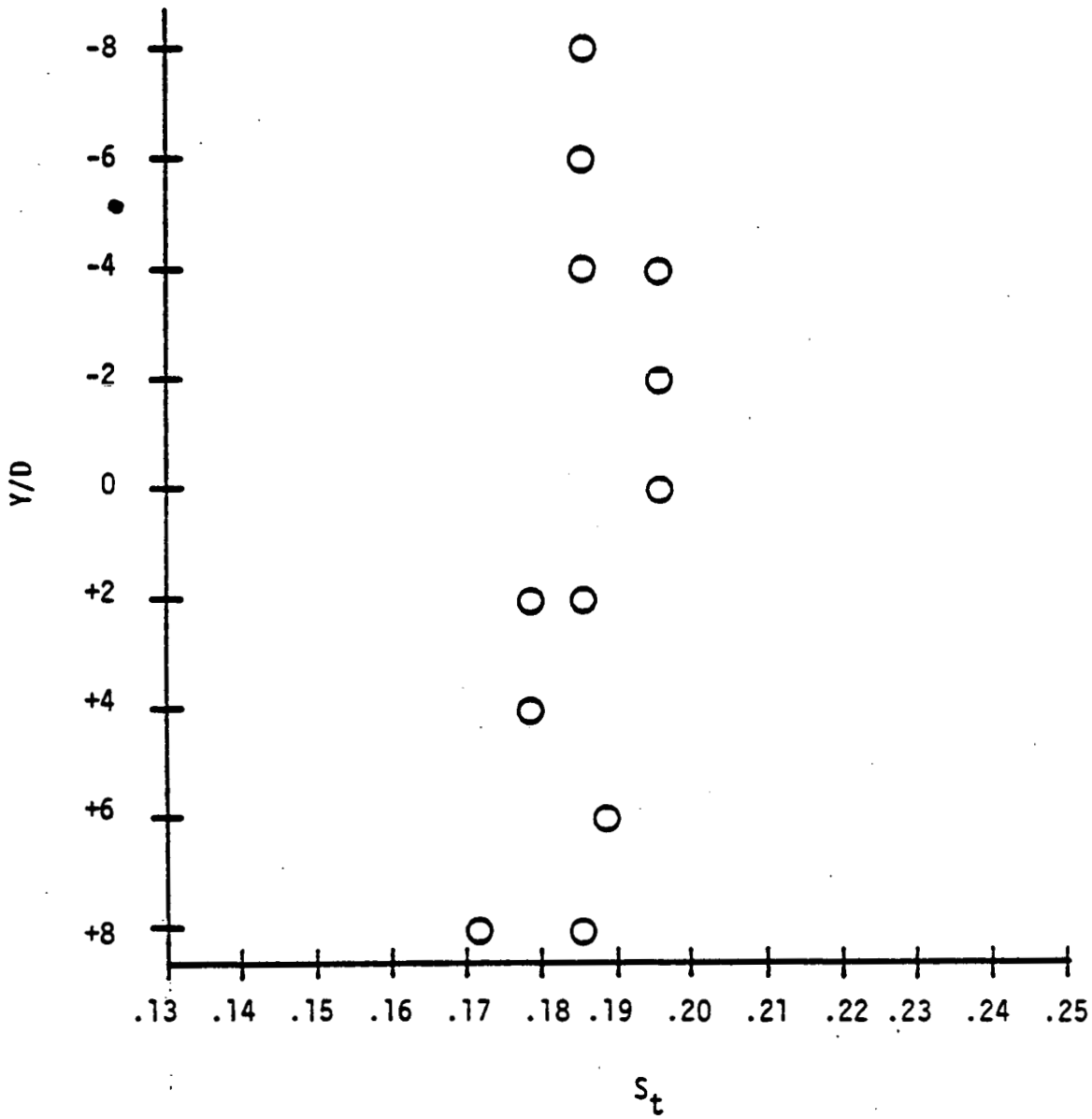


Fig. 35 Spanwise Variation of Centerline Strouhal Number ($Re = 1.6 \times 10^5$, $\beta = .007$, Rough Cylinder)

Re = $3.0 \times 10^5$. The spectra are graphed in Fig. 36.

(ii) Shear parameter, $\beta$ = .016

The doubling of the shear parameter produced a range of shedding frequencies, shown in Fig. 37, from 60 Hz at Y/D = -8.1 down to 48 Hz at Y/D = +8.1, for the smooth cylinder at Re = $1.6 \times 10^5$. This compares with a 7 Hz range for $\beta$ = .007, so the measured frequency range closely followed the relative shear level. Fig. 38 reveals that the Strouhal number range was from .204 to .161. However, it also reveals that the associated cell structure was still not very coherent. A four diameter long cell appeared at the high velocity end, but the mid-span near continuous variation of Strouhal number with Y/D closely paralleled the low shear results. An examination of the spectra in Fig. 37 shows that a number of the peaks were relatively broadband. Elaborating on the observation of Mair and Stansby on the fluctuations in cell boundaries, one may conclude that with a number of cells (at least three) a change in boundaries also changes the mean velocity of the cell, thereby changing the shedding frequency. In the averaged spectra this appears as a wide band of high energy frequencies, which gradually shifts with the mean velocity profile.

Raising the Reynolds number to $2.6 \times 10^5$ served again to clarify the cell structure, shown in Figs. 39 and 40. The peaks recorded at Y/D = -8.1 and Y/D = -6.1 at 105 Hz were very narrow, indicating a near sinusoidal shedding frequency. The mid-span section was characterized by weaker energy levels, before another strong signal at 85 Hz emerged at Y/D = 2.0 and was maintained up to the low velocity endplate. The spectrum at Y/D = 6.1 showed evidence of a second peak at the frequency of the weak mid-span cell. The Strouhal number range was from .205 to .169, again showing the shift upward with increasing Reynolds number.

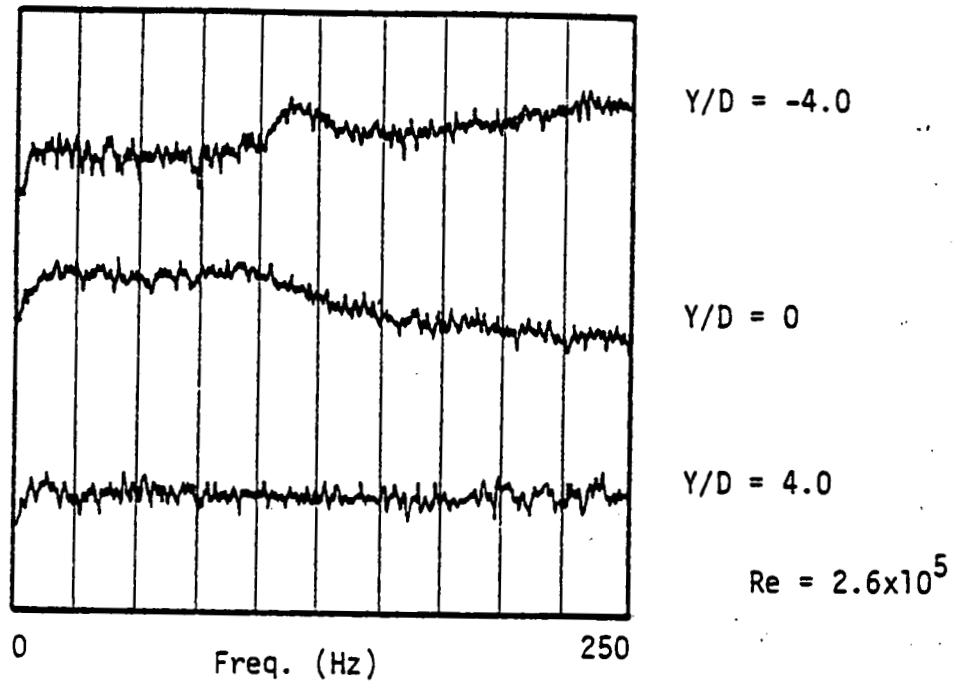


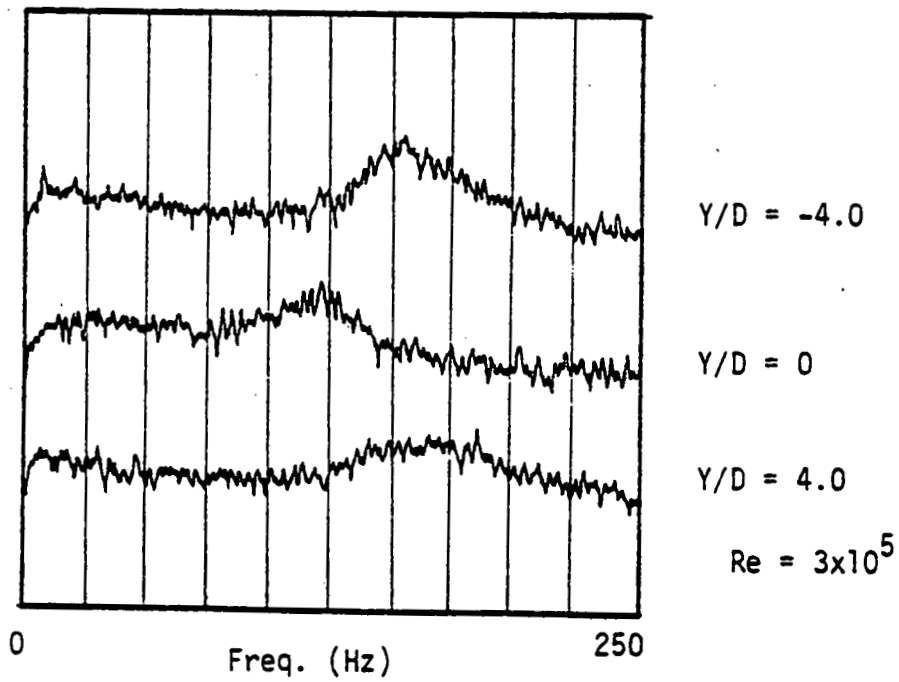


Fig. 36 Power Spectral Density of Eddy Shedding Frequency
($\beta$ = .007 Rough Cylinder)

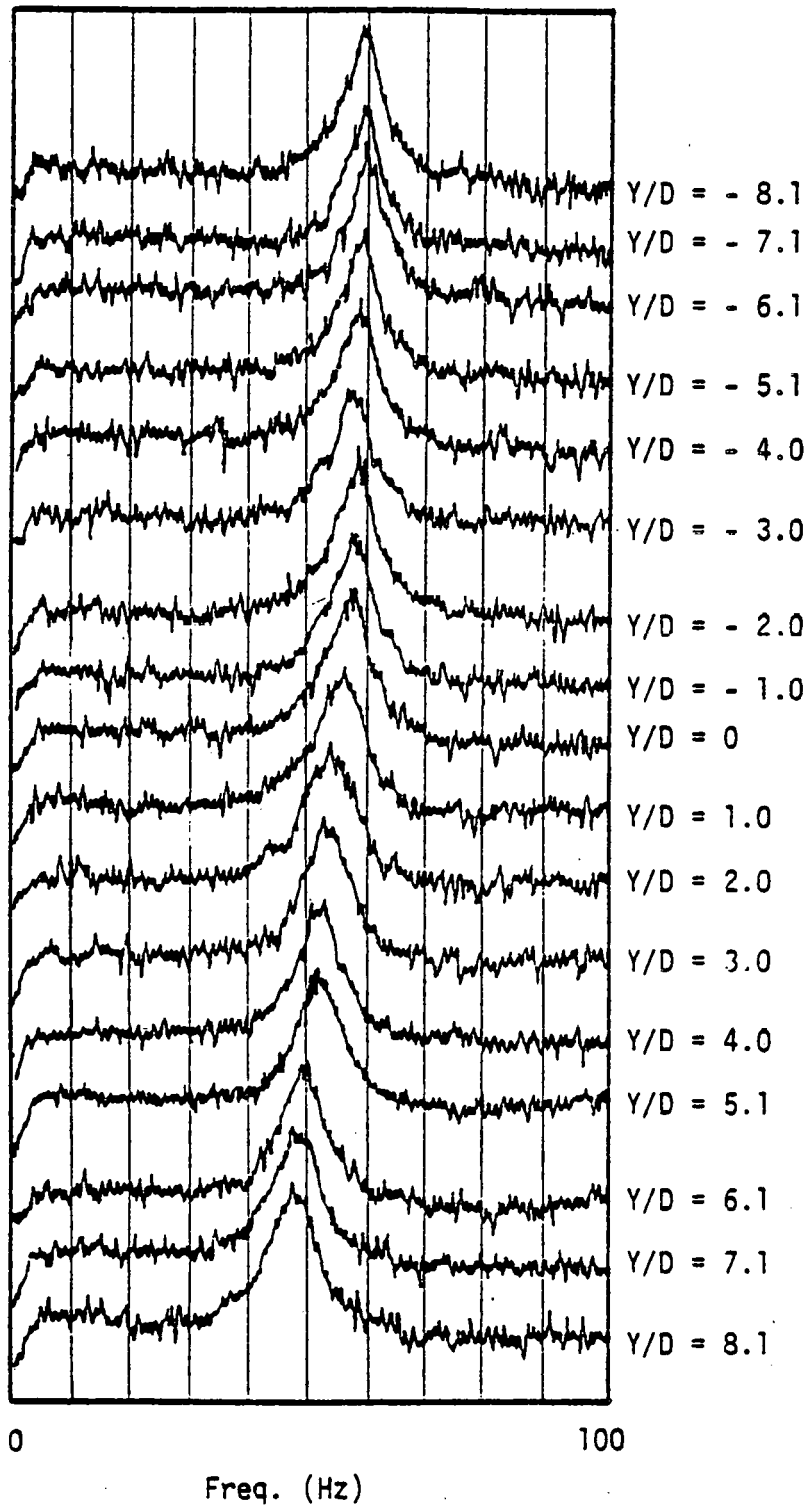


Fig. 37 Power Spectral Density of Eddy Shedding Frequency ($Re = 1.6 \times 10^5$, $\beta = .016$, Smooth Cylinder)

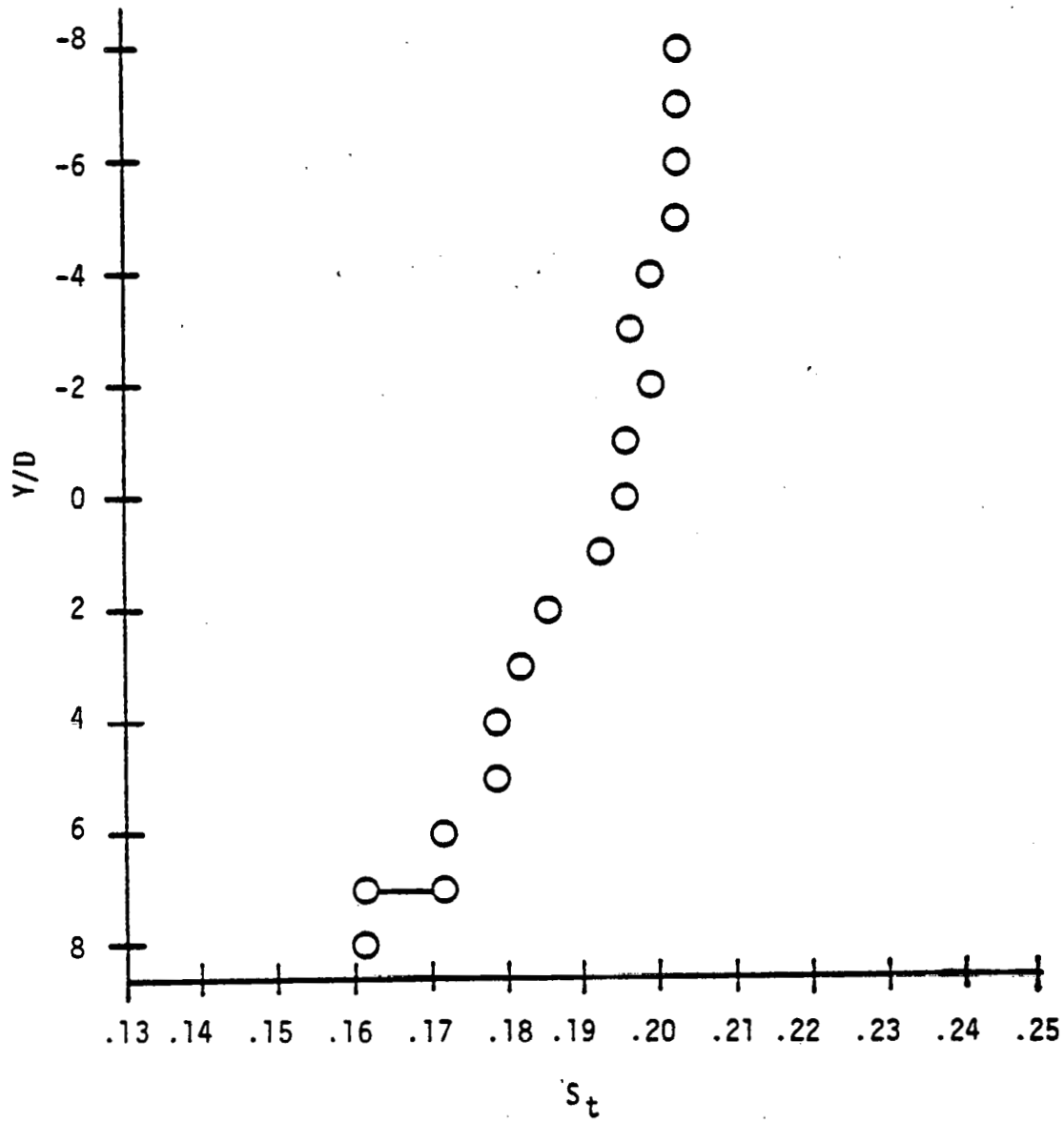


Fig. 38 Spanwise Variation of Centerline Strouhal Number
($Re = 1.6 \times 10^5$, $\beta = .016$, Smooth Cylinder)

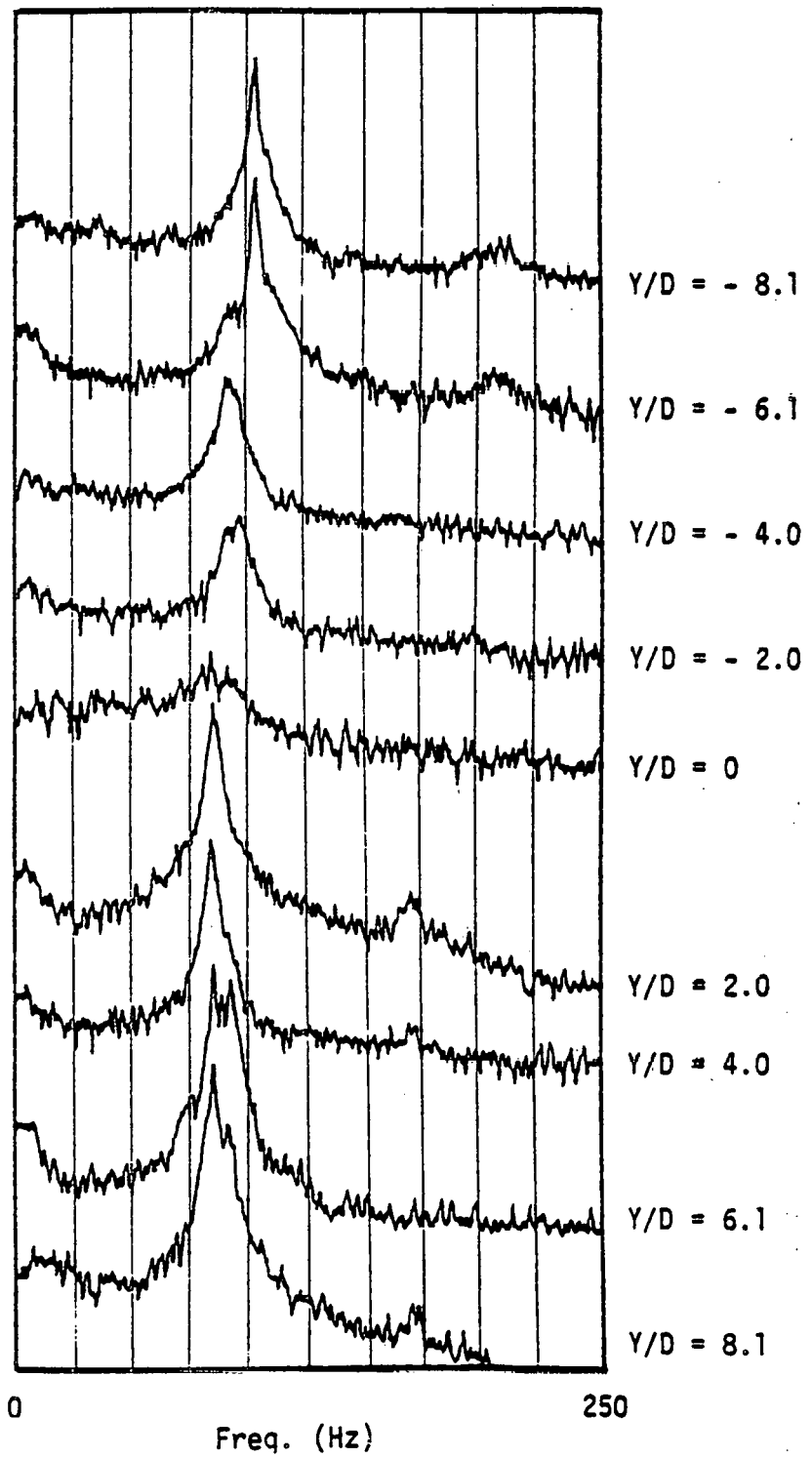


Fig. 39 Power Spectral Density of Eddy Shedding Frequency
($Re = 2.6 \times 10^5$, $\beta = .016$, Smooth Cylinder)

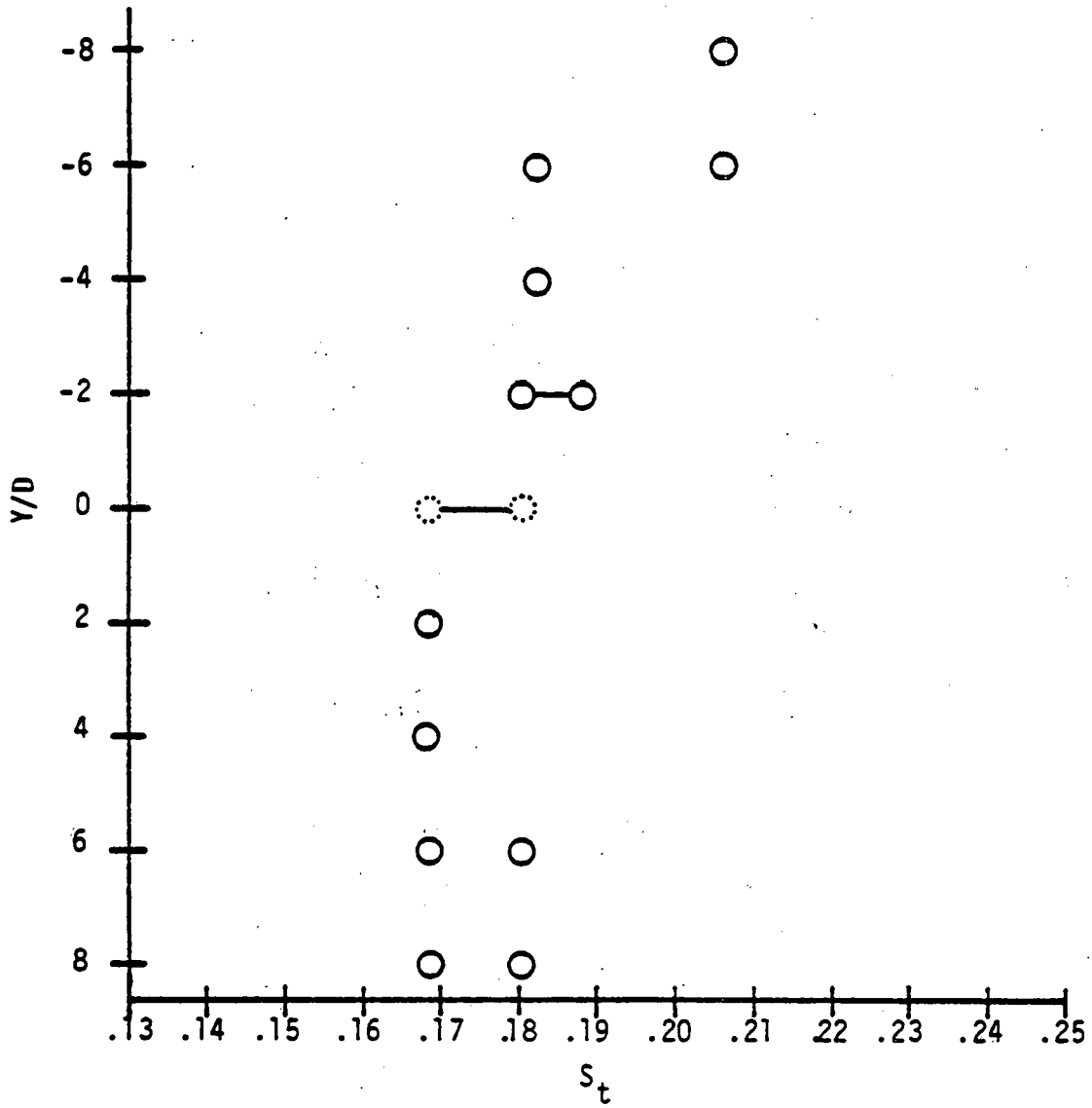


Fig. 40 Spanwise Variation of Centerline Strouhal Number (Re = 2.6 x $10^5$, $\beta$ = .016, Smooth Cylinder)

At Re = $3.0 \times 10^5$ the two end peaks were better consolidated, as can be seen from Figs. 41 and 42. Some of the mid-span diffuseness may have been the result of premature tripping of a critical wake by the very slight roughness associated with the center seam in the model. This possibility was discussed in Section IV C. No secondary peaks were measured at either of the two end cells, but the spanwise range of Strouhal numbers (.207 to .166) was only slightly different from those of the two lower Reynolds number cases.

A perplexing phenomenon associated primarily with the lower shear rough cylinder results was most pronounced at $\beta$ = .016 and Re = $1.6 \times 10^5$. At the high velocity end, from Y/D = -8.1 to Y/D = -4.0, the dominant frequency of the shed vortices was 54 Hz. The second cell, as can be seen in Fig. 43, was at a significantly higher (58 Hz) frequency, even though the mean velocity at the center of the second cell was about 3% lower than in the first. No irregularities in the mean and fluctuating velocity profiles (Fig. 6) existed on the high velocity side of the cylinder. Also, blockage effects could not have been responsible since no such reverse cell was documented in the corresponding smooth cylinder results. (One anomalous smooth cylinder example which appeared to exhibit the same phenomenon will be discussed in the next subsection.) It has been postulated that an endplate effect was the cause, even though the actual endplate boundary layer thickness was much smaller than one inch. Two important differences from the smooth cylinder flowfield which would tend to magnify the endplate effect on a rough cylinder must be taken into account: (a) the surface roughness promoted a more homogeneous cylinder boundary layer which could permit further penetration of endplate boundary layer effects, and (b) the rough cylinder flowfield was much closer to critical conditions than the smooth cylinder flowfield, and therefore may have been much more sensitive to small scale effects of the order of the endplate boundary layer.

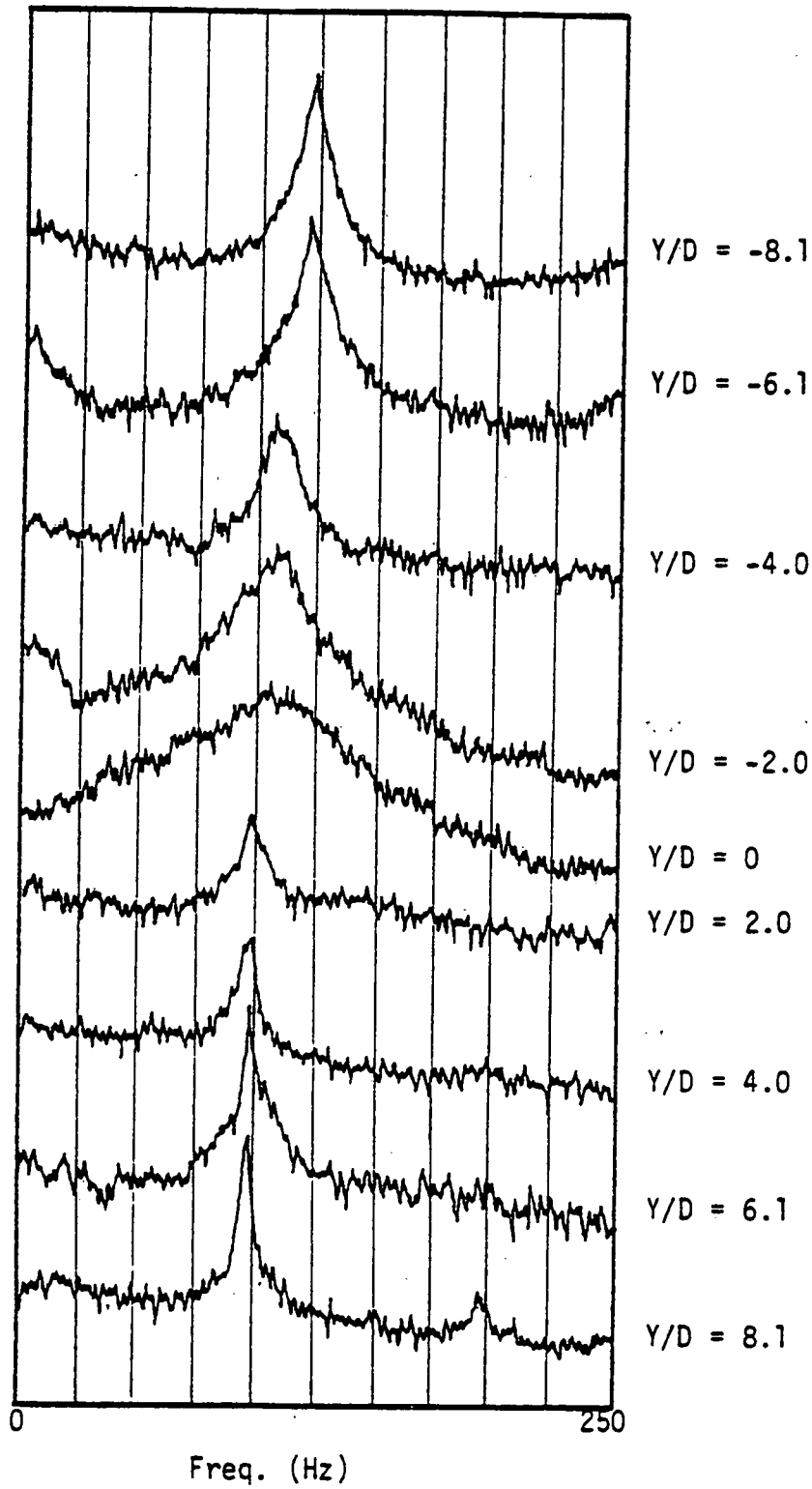


Fig. 41 Power Spectral Density of Eddy Shedding Frequency ($Re = 3.0 \times 10^5$, $\beta = .016$, Smooth Cylinder)

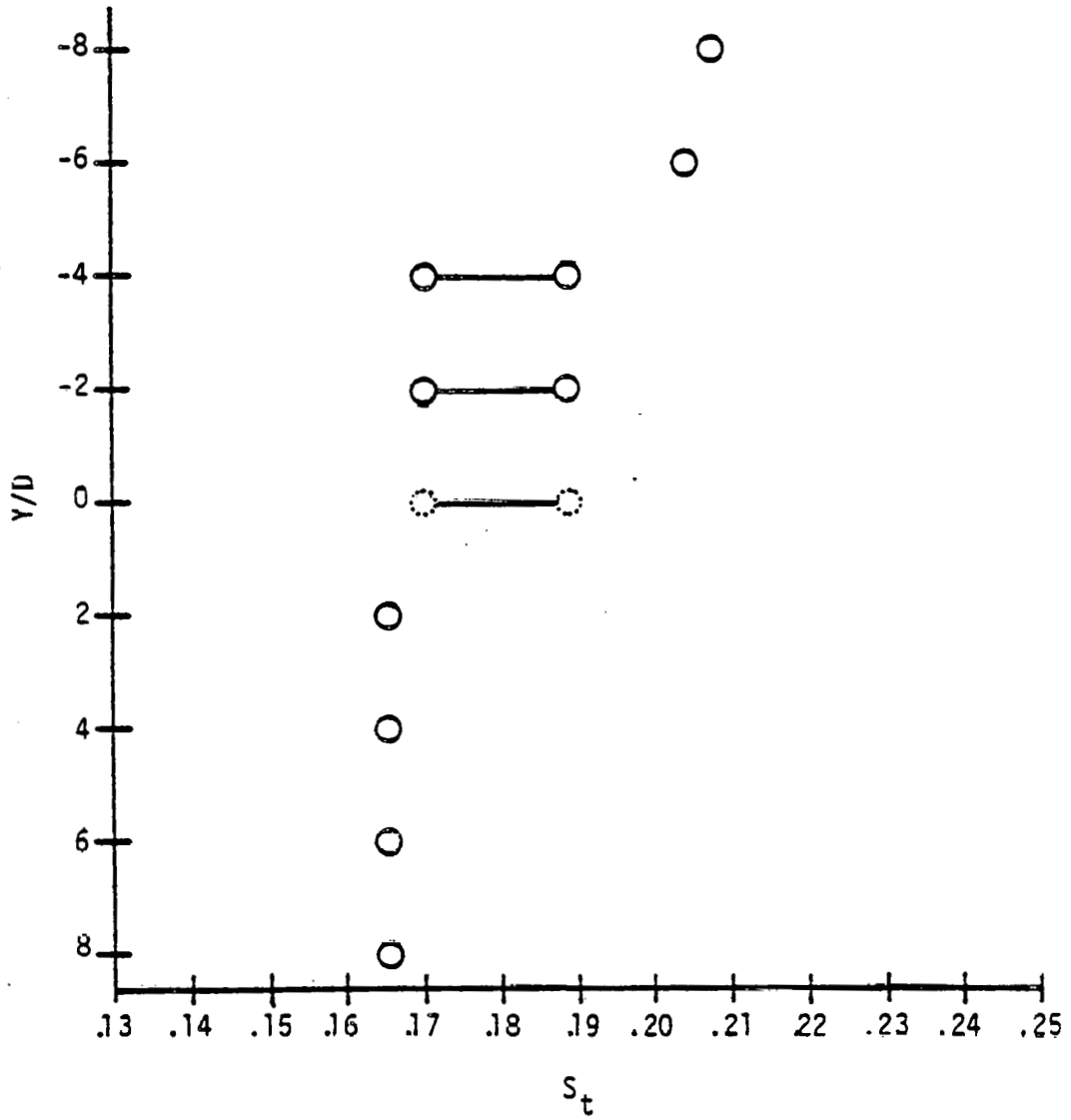


Fig. 42 Spanwise Variation of Centerline Strouhal Number (Re = 3 x $10^5$, $\beta$ = .016, Smooth Cylinder)

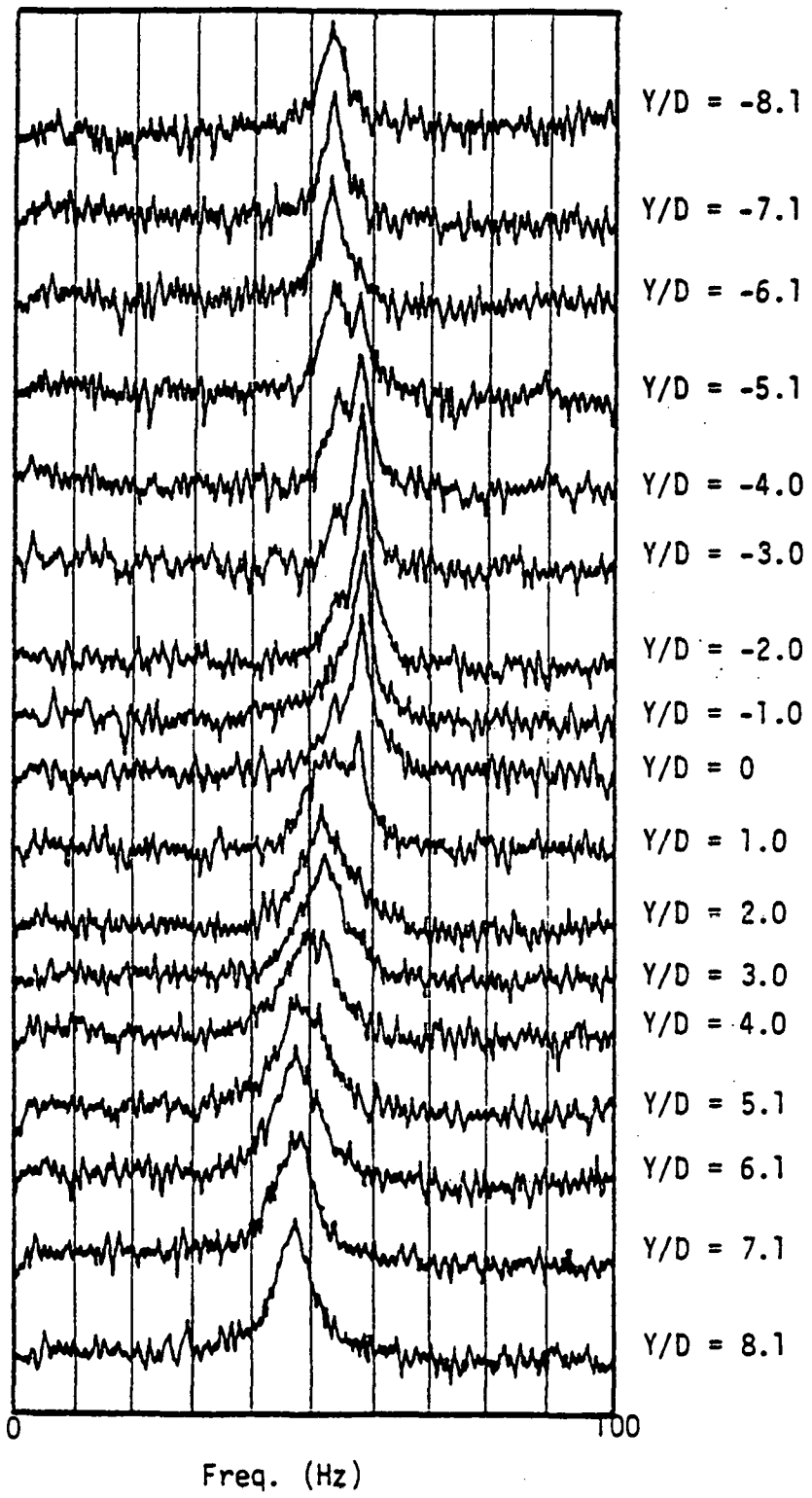


Fig. 43 Power Spectral Density of Eddy Shedding Frequency ($Re = 1.6 \times 10^5$, $\beta = .016$, Rough Cylinder)

In addition to the endplate cell, three other groupings emerge from the Strouhal number plot in Fig. 44. The range from maximum to minimum Strouhal number was .199 to .161, which represented a 1 Hz decrease from the range observed for the complementary smooth cylinder case. Nevertheless, the cell structure was more clearly defined than that shown in Fig. 38.

The spectra for the two higher Reynolds number cases presented in Fig. 45 are virtually identical to the rough cylinder results for $\beta = .007$. The one coherent peak at Y/D = -4.0 and Re = $3.0 \times 10^5$ again represented the emergence of a supercritical shedding pattern. It is somewhat better defined than in Fig. 36 because of the increase in local Reynolds number at the station for the higher shear case.

(iii) Shear parameter, $\beta = .021$

The addition of another screen to raise the shear parameter to .021 reduced the number of cases to two (Re = $1.6 \times 10^5$ and Re = $2.6 \times 10^5$).

The lower Reynolds number smooth cylinder results are plotted in Fig. 46 and 47. Although the peaks near the midspan again show a gradual shift because of unsteady cell boundaries, the Strouhal number plot of Fig. 47 reveals a tendency toward a four cell structure. The first cell, at 63 Hz, predominates from the high velocity end to Y/D = -5.1, a second weaker cell at 60 Hz spans the distance to Y/D = -1.0, a third ill-defined cell at 53 Hz is present down to Y/D = +5.1, before yielding to a stronger endplate cell at 48 Hz. The total frequency spread is therefore 15 Hz, or in Strouhal numbers, from .216 down to .165.

Figs. 48 and 49 illustrate the single smooth cylinder case for which endplate effects masked the true nature of the cellular shedding pattern. It appears from the two figures that the shedding occurred in a single cell at a

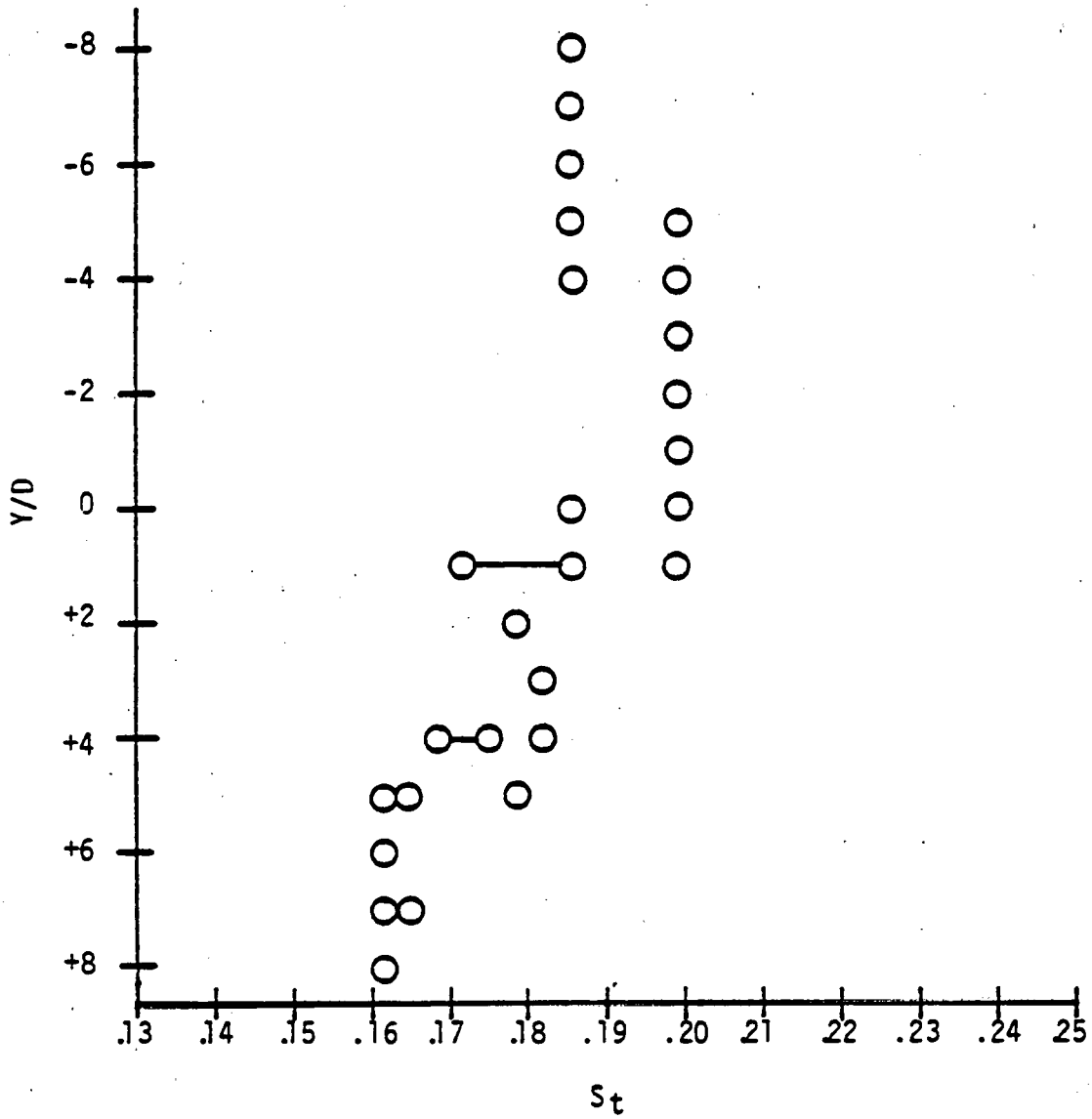


Fig. 44 Spanwise Variation of Centerline Strouhal Number ($Re = 1.6 \times 10^5$, $\beta = .016$, Rough Cylinder)

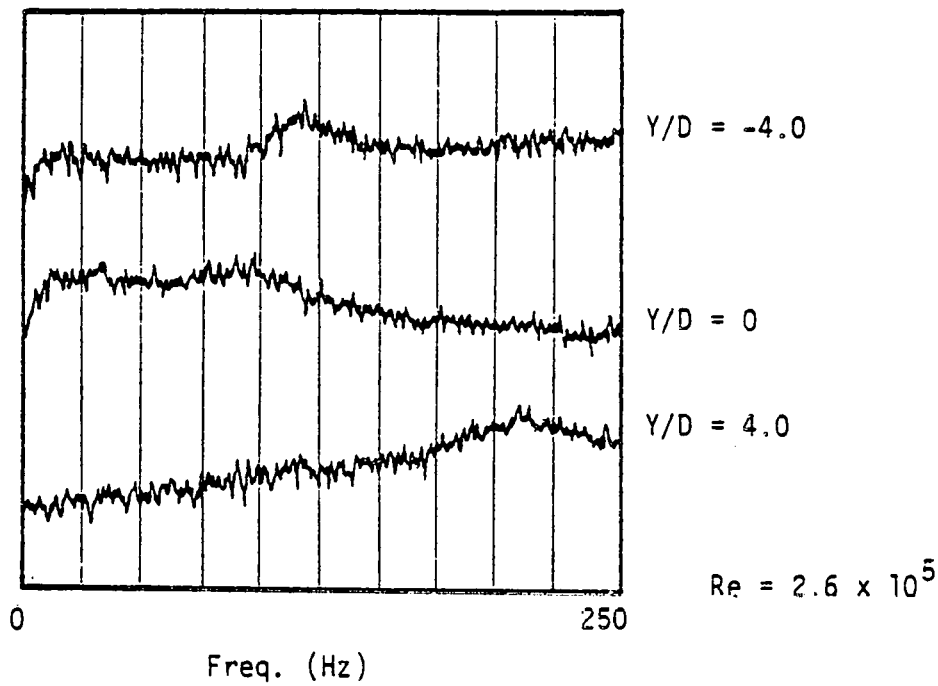


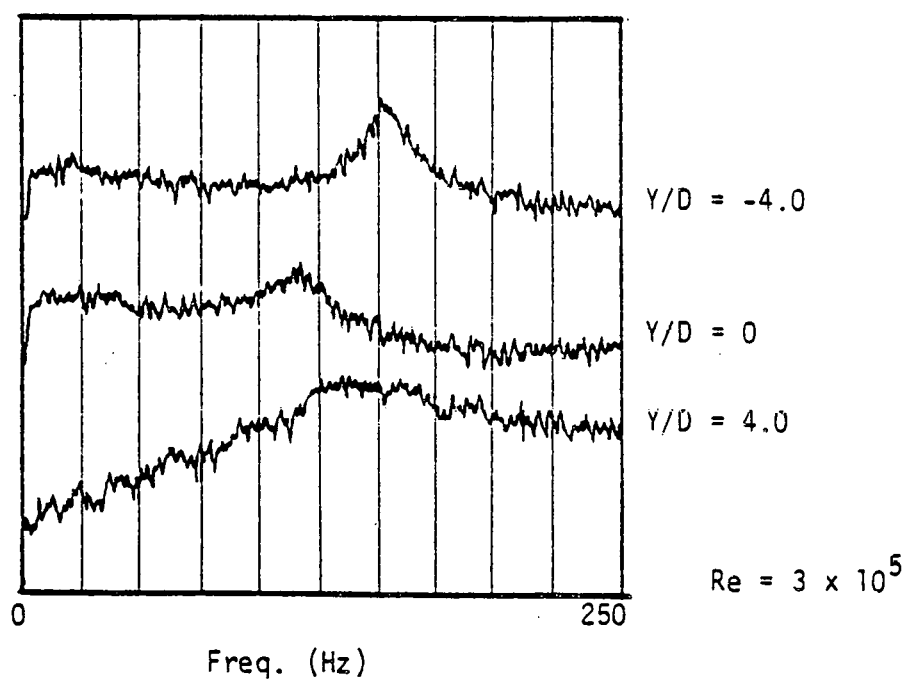


Fig. 45 Power Spectral Density of Eddy Shedding Frequency ($\beta$ = .016, Rough Cylinder)

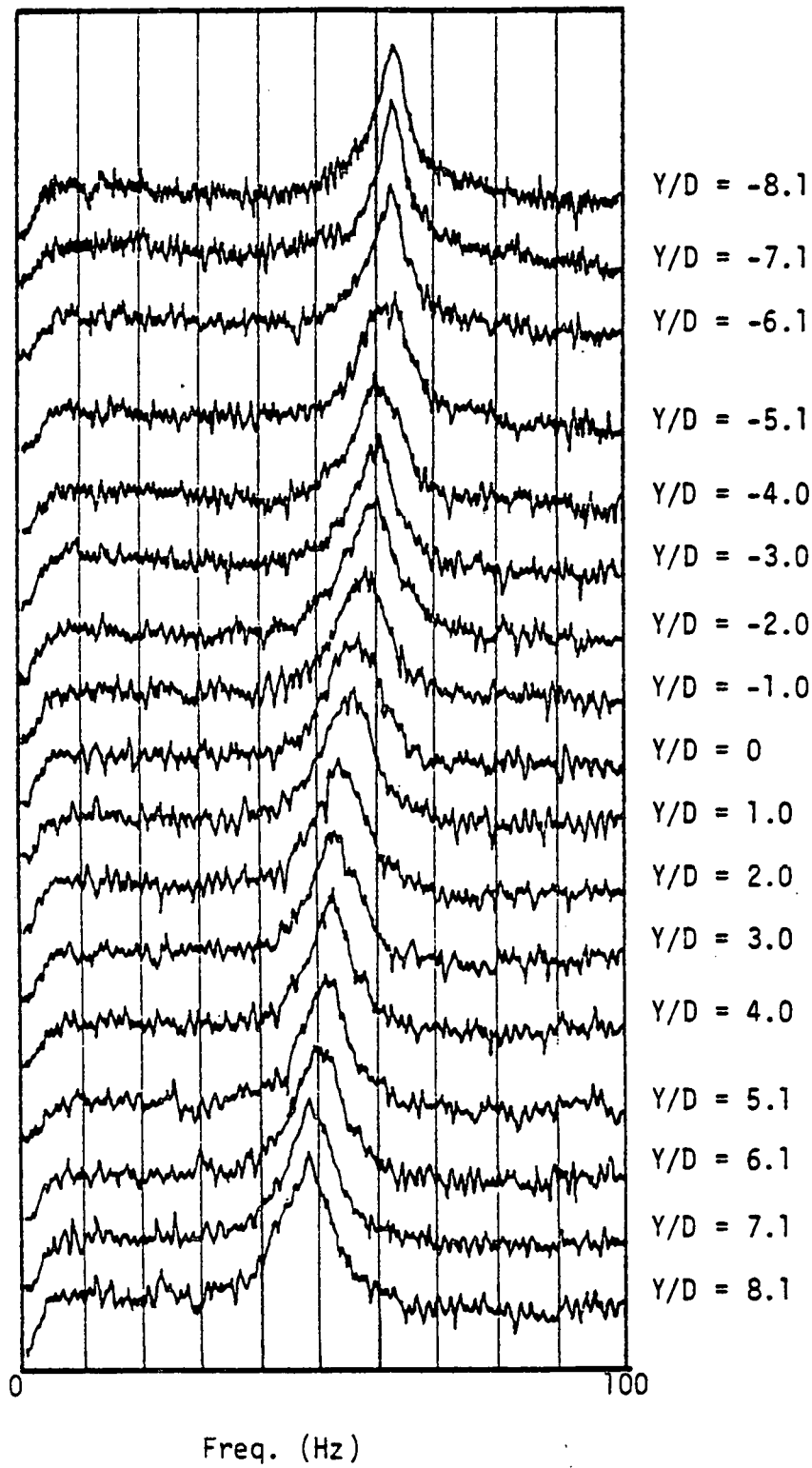


Fig. 46 Power Spectral Density of Eddy Shedding Frequency ($Re = 1.6 \times 10^5$, $\beta = .021$, Smooth Cylinder)

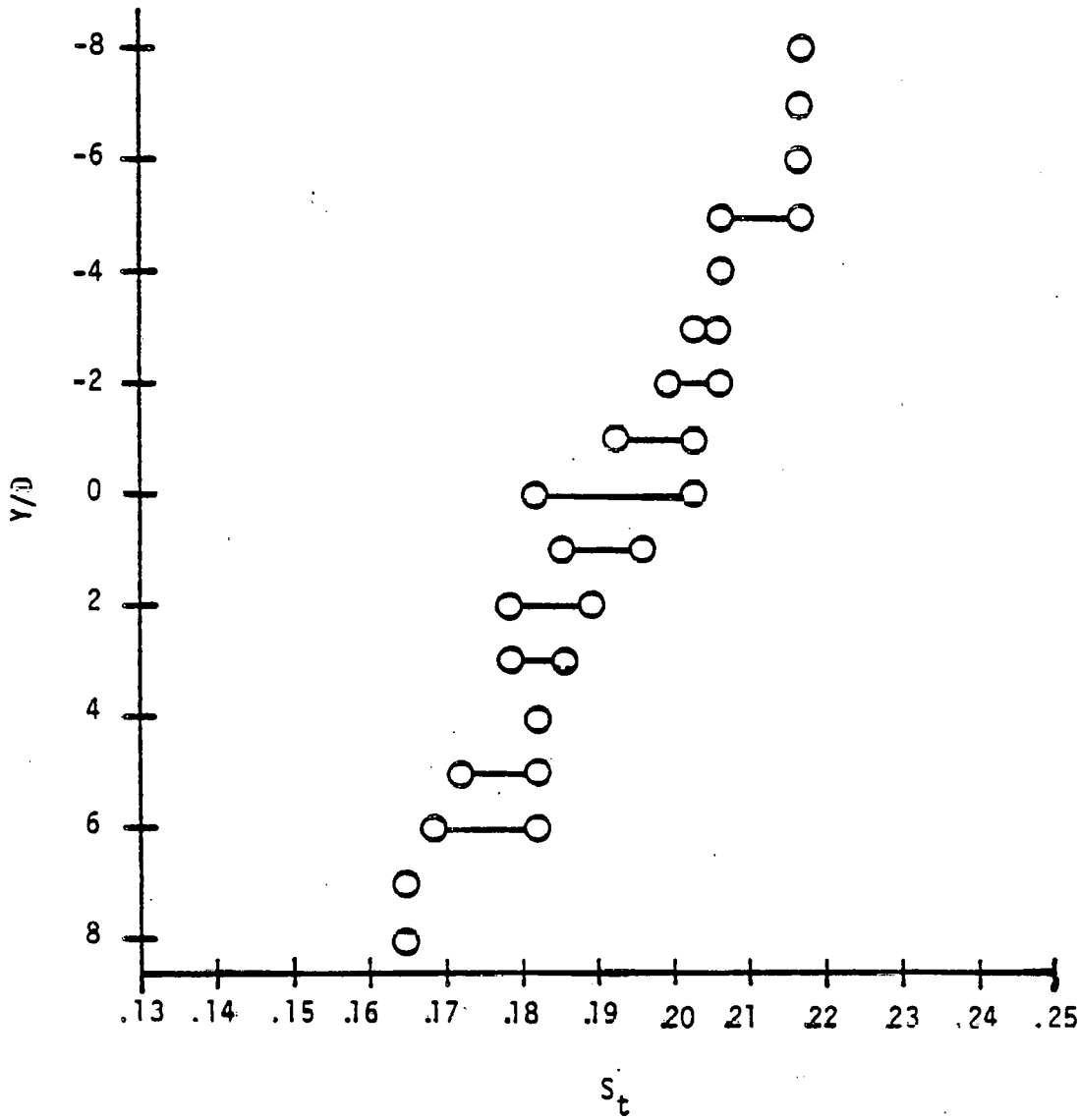


Fig. 47 Spanwise Variation of Centerline Strouhal Number (Re=1.6 x $10^5$, $\beta$ = .021, Smooth Cylinder)

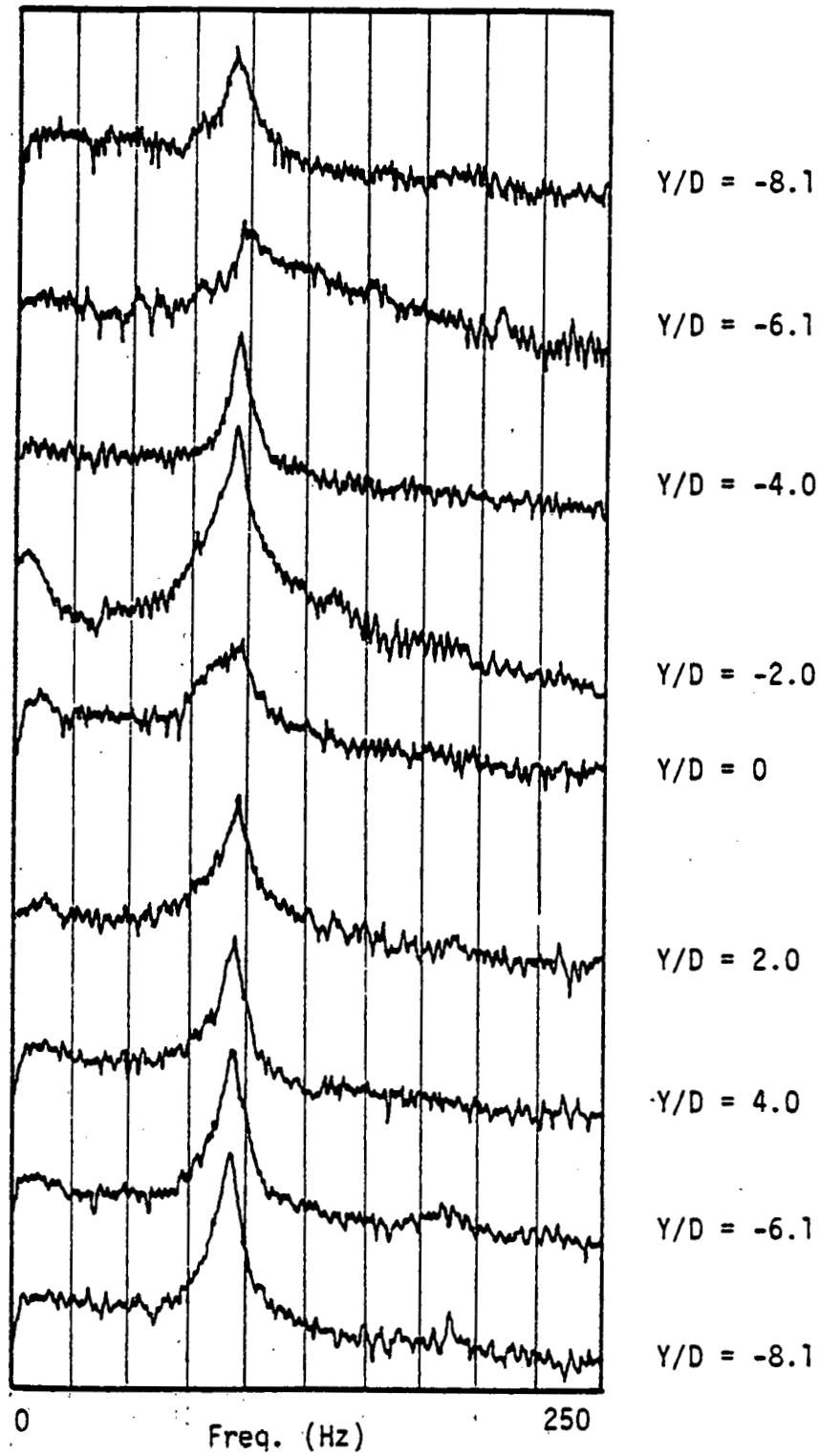


Fig. 48 Power Spectral Density of Eddy Shedding Frequency
($Re = 2.6 \times 10^5$, $\beta = .021$, Smooth Cylinder)

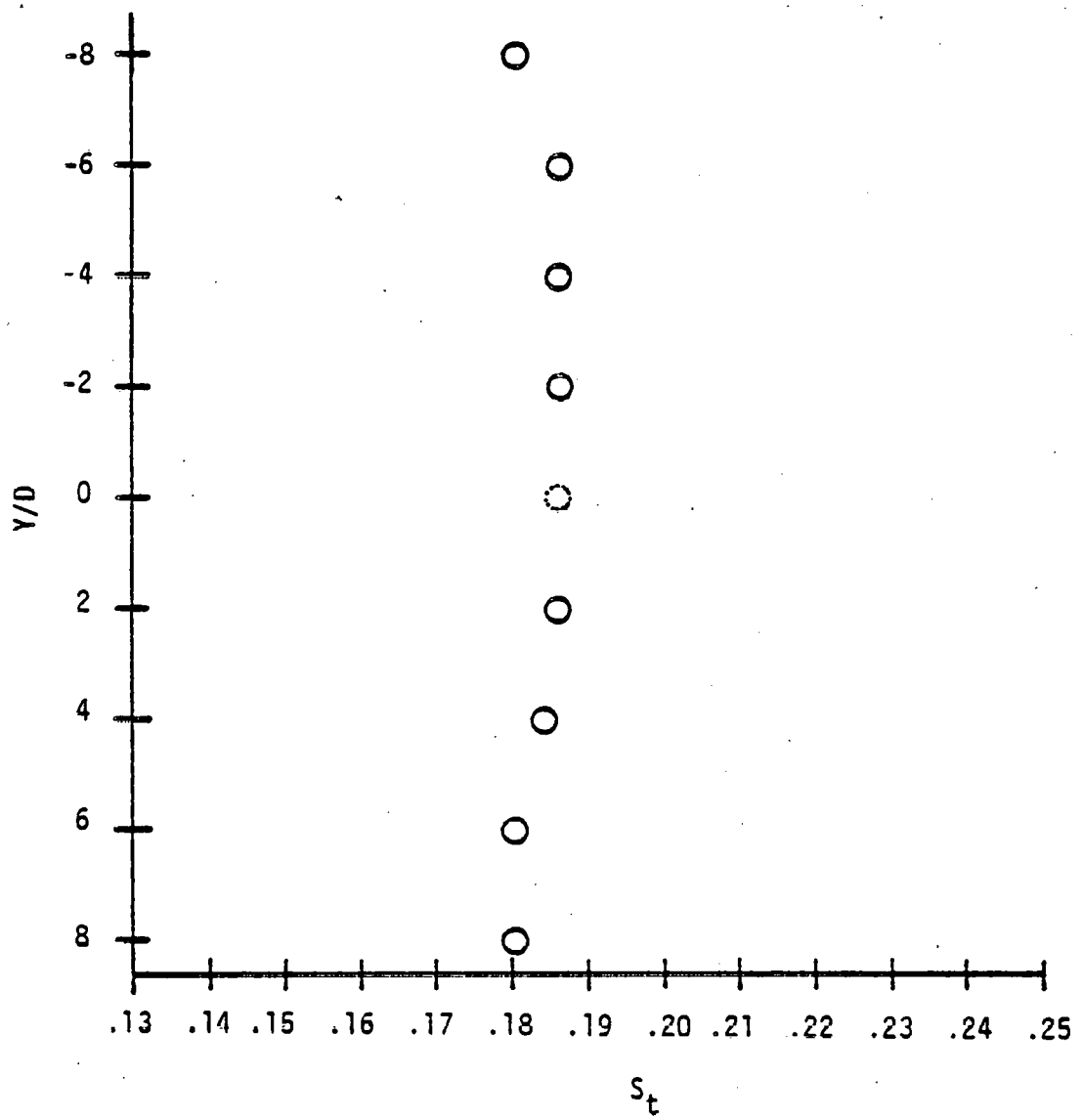


Fig. 49 Spanwise Variation of Centerline Strouhal Number
($Re = 2.6 \times 10^5$, $\beta = .021$, Smooth Cylinder)

Strouhal number of about .185. However, by referring back to Fig. 24, where the uniform flow shedding frequency is plotted as a function of Reynolds number, it is clear that in an unsheared flow the peak occurred at 101 Hz. The peaks graphed in Fig. 48 are all around 95 Hz, which strongly suggests that at the high velocity endplate, a retarding influence penetrated well along the cylinder. It is also apparent from comparing Fig. 48 with Fig. 39, the equivalent case for $\beta$ = .016, that the energy levels of the peaks were much lower in Fig. 48 at Y/D = -8.1 and Y/D = -6.1. Therefore it is reasonable to suppose that the same endplate effect which produced lower frequency end peaks in a number of rough cylinder cases at Re = $1.6 \times 10^5$ was also at work in this smooth cylinder test at Re = $2.6 \times 10^5$.

Figs. 50 and 51 reveal a strong cellular grouping for the rough cylinder at Re = $1.6 \times 10^5$, but the increase in upstream shear did not eliminate the low peak at the high velocity endplate. It did, however, reduce the difference in frequency between that peak and the adjacent one from 4 Hz at $\beta$ = .016 (see Fig. 43) to approximately 2 Hz. The overall range in frequencies was about 11 Hz, which translated to a Strouhal range of .214 down to .172, counting the single mid-span peak at 50 Hz. Once again, therefore, the range for the rough cylinder was decidedly narrower than for the smooth cylinder with the same upstream velocity profile. As in previous cases, the rough cylinder showed no sign of vortex shedding at Re = $2.6 \times 10^5$, as demonstrated in Fig. 52.

(iv) Shear parameter, $\beta$ = .033

It was noted earlier that the screen configuration producing $\beta$ = .033 also generated the highest freestream turbulence levels, which may have been partly responsible for the width of the individual peaks displayed in Fig. 53. A greater factor, however, was the very wide range of frequencies required by the added shear. The first, and only organized, cell was shedding at 64 Hz,

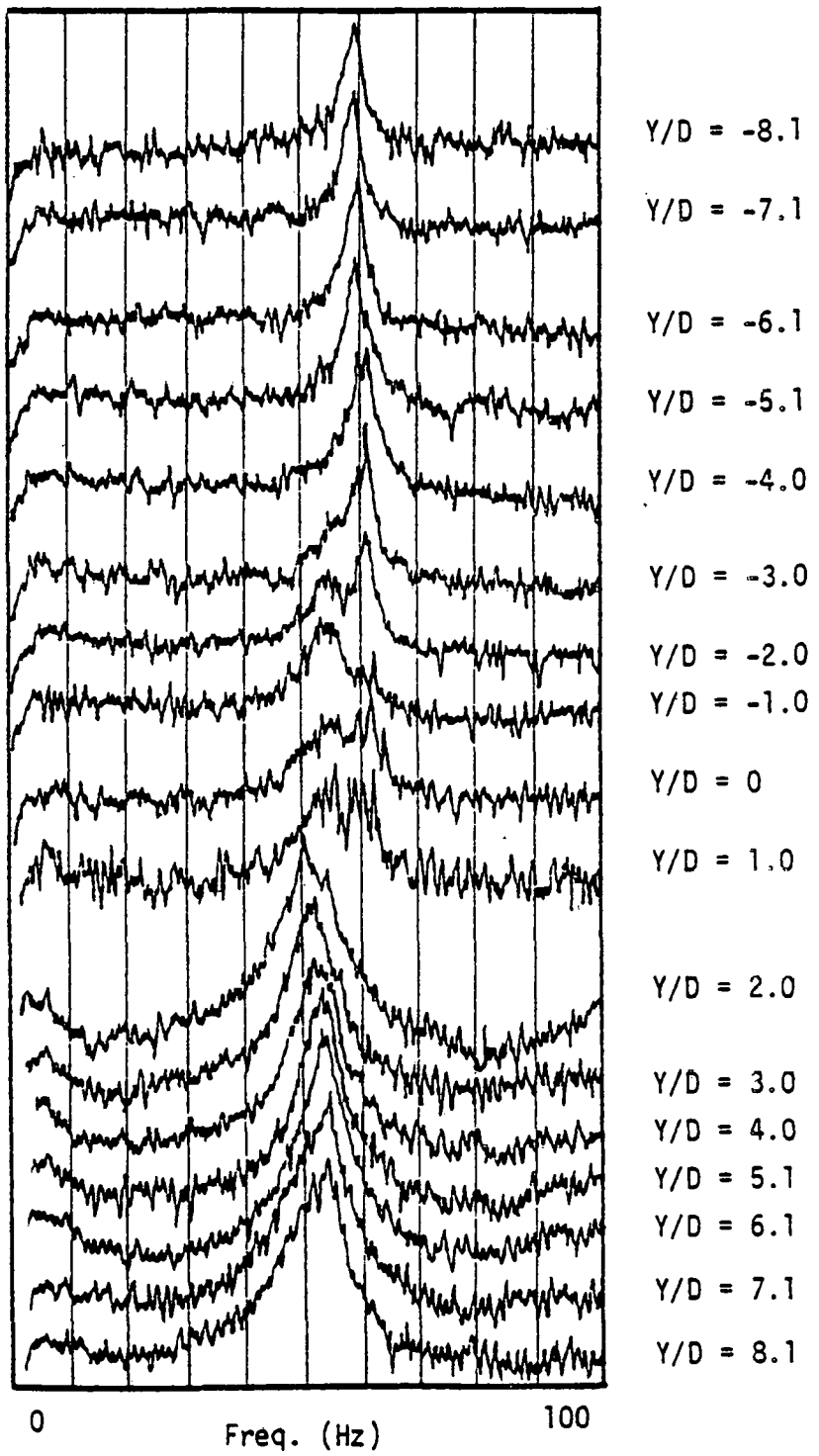


Fig. 50 Power Spectral Density of Eddy Shedding Frequency
($Re = 1.6 \times 10^5$, $\beta = .021$, Rough Cylinder)

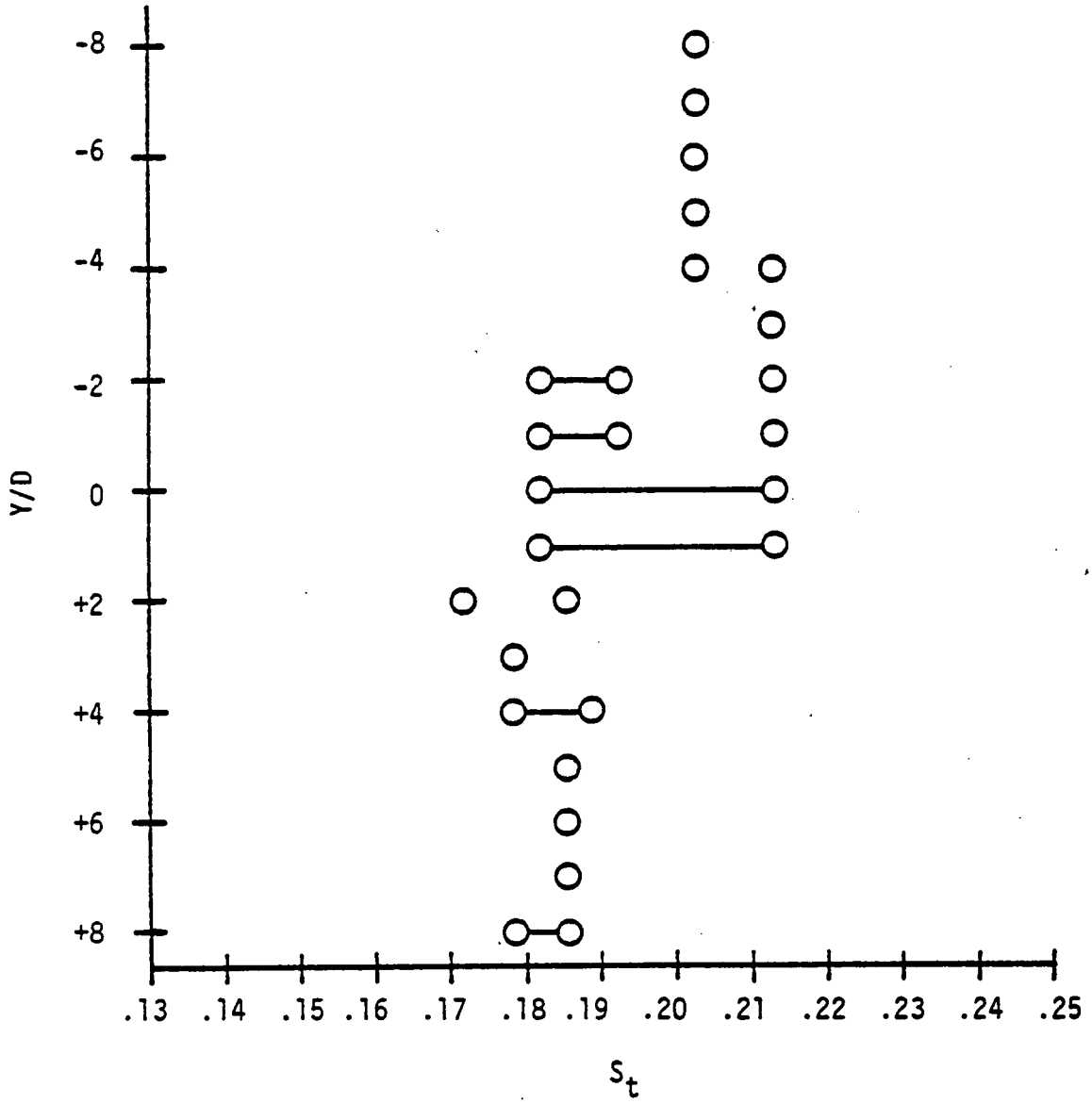


Fig. 51 Spanwise Variation of Centerline Strouhal Number
($Re = 1.6 \times 10^5$, $\beta = .021$, Rough Cylinder)

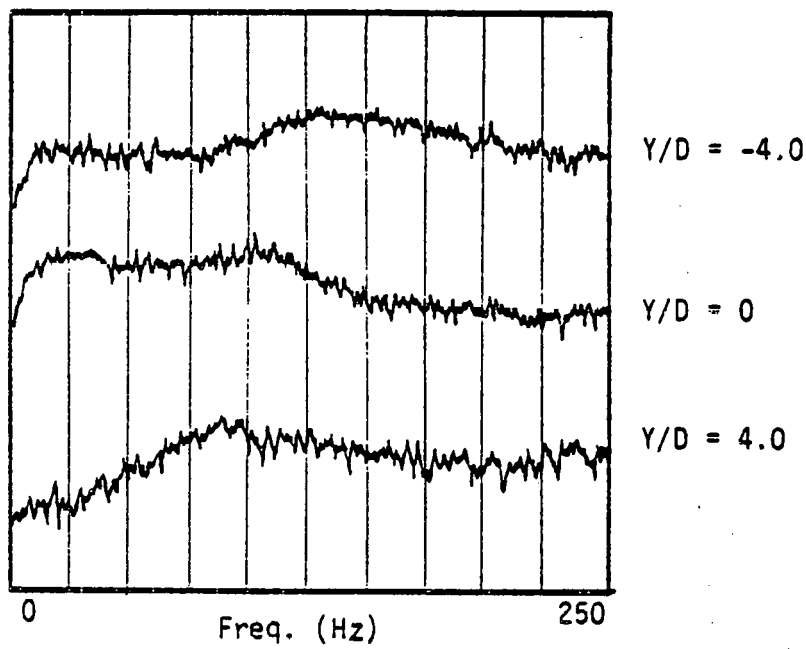


Fig. 52 Power Spectral Density of Eddy Shedding Frequency
($Re = 2.6 \times 10^5$, $\beta = .021$, Rough Cylinder)

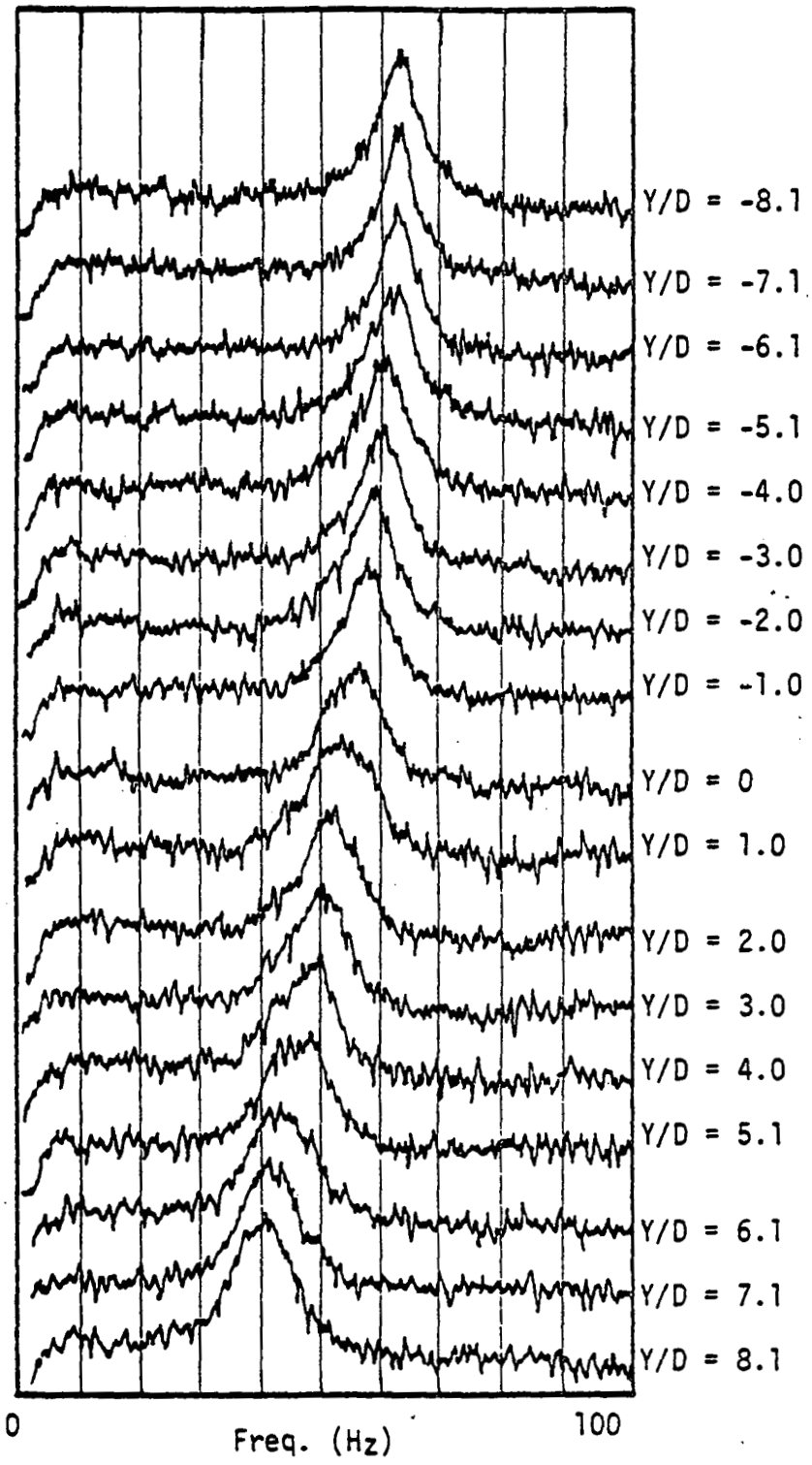


Fig. 53 Power Spectral Density of Eddy Shedding Frequency ($Re = 1.6 \times 10^5$, $\beta = .033$, Smooth Cylinder)

while at the low velocity end, the last two spectral peaks were centered around 41 Hz. This set of spectra revealed the least tendency toward developed cell structure of any of the cases examined. Apparently the boundaries between cells were rapidly varying, and the high shear therefore caused the time-averaged spectra to be very broadbanded. The variation in Strouhal frequencies, given in Fig. 54, was from .218 to .128, proportionately greater than was exhibited in Fig. 47 for $\beta$ = .021.

When the Reynolds number was raised to $2.6 \times 10^5$, however, a much more stable cell structure developed. The first peak, shown in Fig. 55, was at 110 Hz, and spanned about two cylinder diameters. It was then replaced with a cell at 98 Hz, which was extremely well defined, and persisted beyond the midspan of the cylinder. The third, and final cell started at Y/D = 2.0, and is noteworthy for the very significant change in shedding frequency (down to about 80 Hz) over a single cylinder diameter. It was maintained down to the low velocity endplate. The Strouhal number graph of Fig. 56 again testifies to the sharp cell boundaries. The Strouhal range, .206 down to .150, is much lower than the range exhibited in the lower Reynolds number case. The reason is that the lowest frequency cell, which spanned the distance from Y/D = 2.0 to Y/D = 8.1, was fed by a higher relative mean velocity than the unsteady smaller cells of Fig. 54.

The rough cylinder results (Figs. 57 and 58) displayed two extremely sharp peaks and a third weak cell at Re = $1.6 \times 10^5$. The high velocity end cell at 56 Hz persisted down to Y/D = 0, where it broadened and then was abruptly replaced by the second peak at 48 Hz. The low velocity end cell appeared around Y/D = 5.1, but was very broadband. Following the pattern of previous cases, the frequency range, 56 Hz down to 40 Hz, was narrower than for the smooth cylinder. The bandwidth of the individual rough cylinder

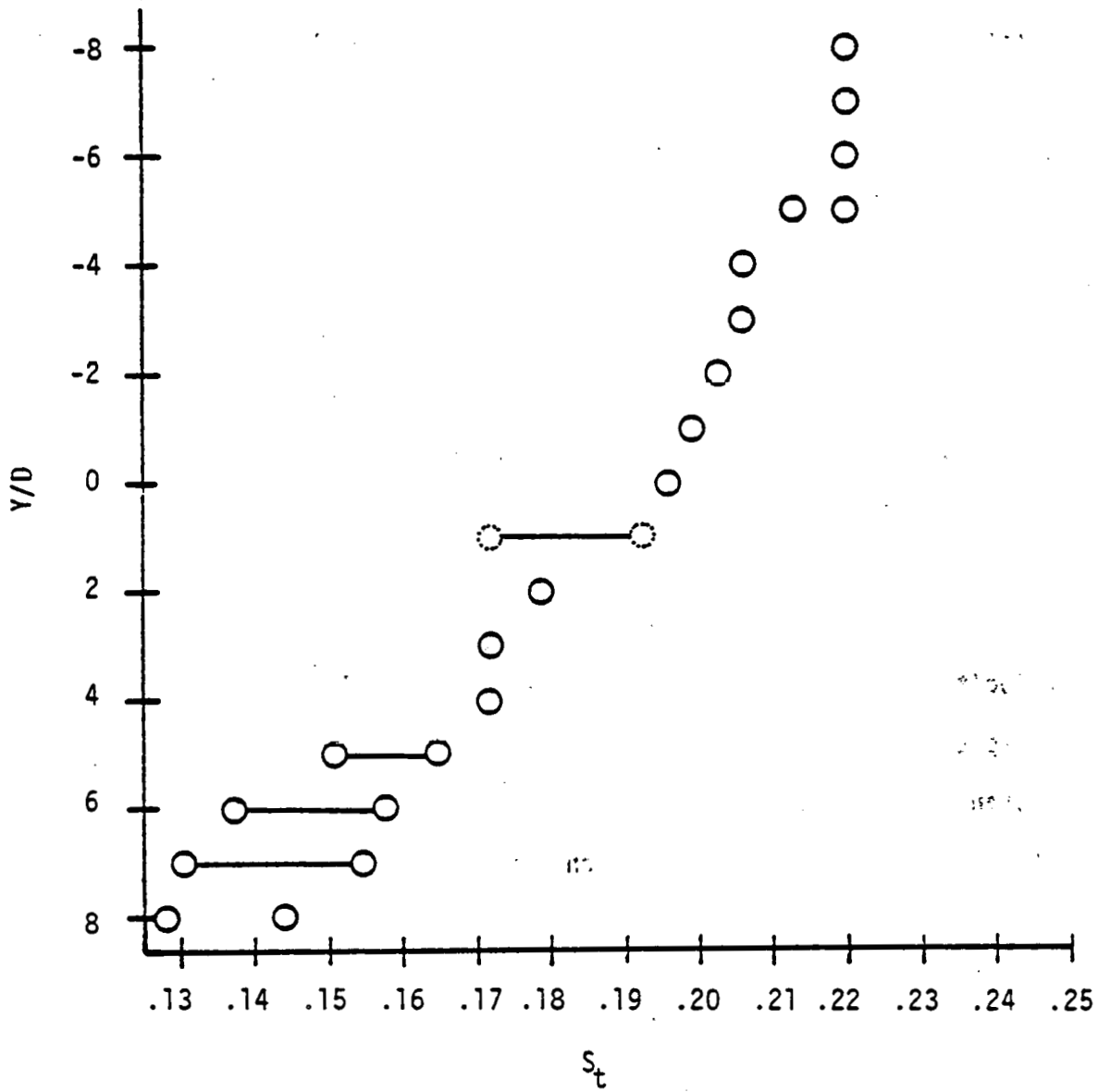


Fig. 54 Spanwise Variation of Centerline Strouhal Number
($Re = 1.6 \times 10^5$, $\beta = .033$, Smooth Cylinder)

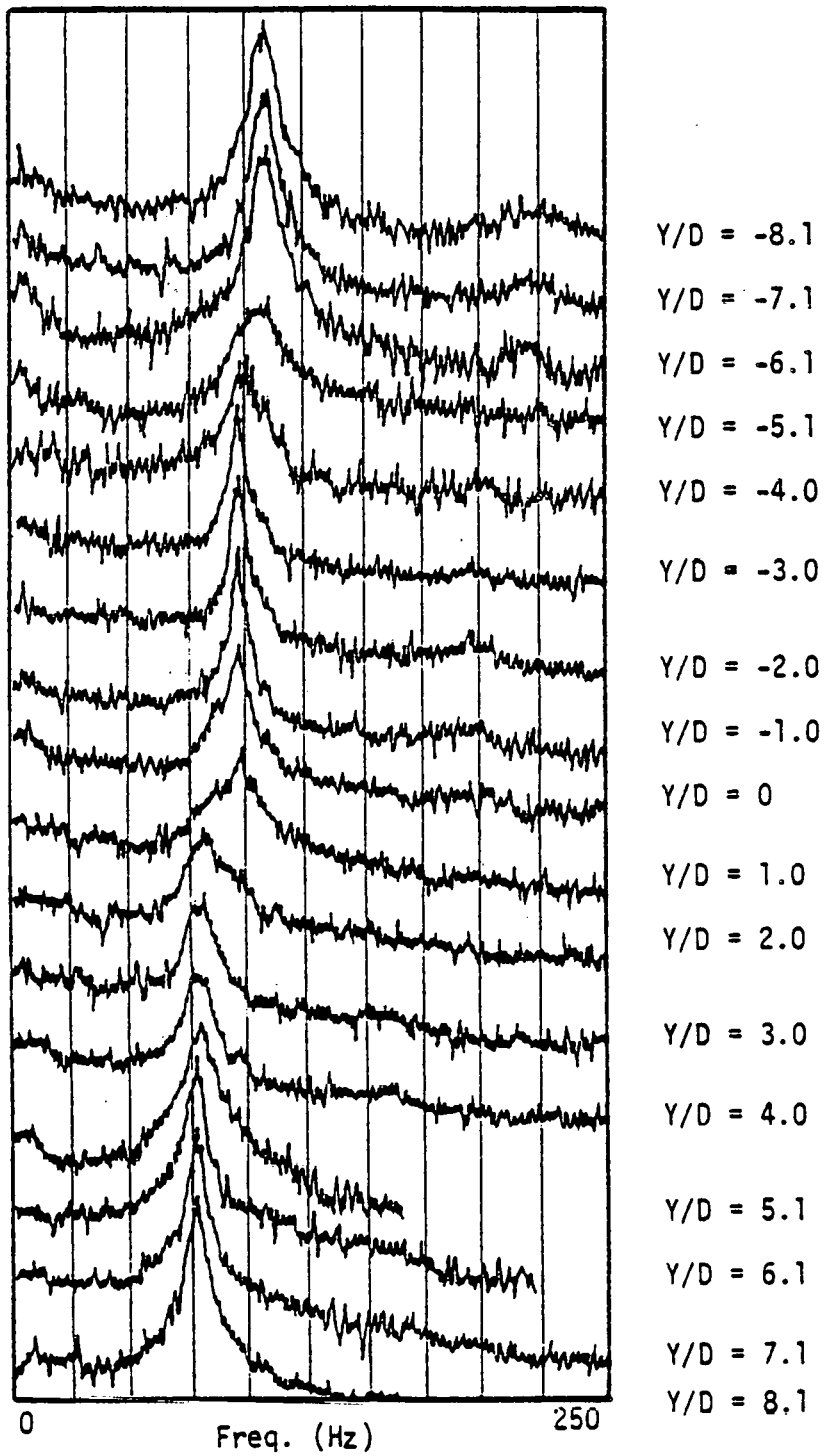


Fig. 55 Power Spectral Density of Eddy Shedding Frequency
($Re = 2.6 \times 10^5$, $\beta = .033$, Smooth Cylinder)

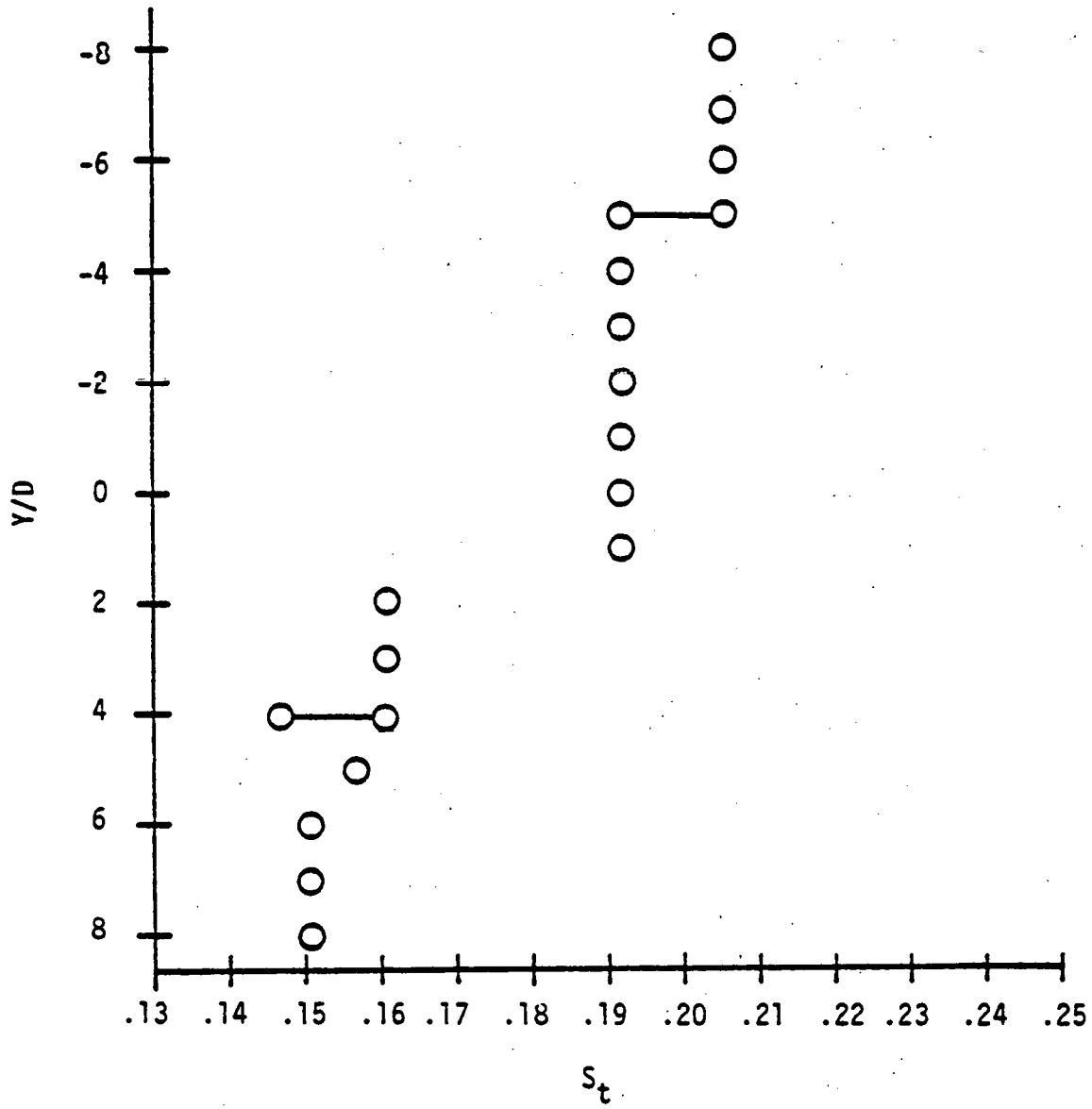


Fig. 56 Spanwise Variation of Centerline Strouhal Number
($Re = 2.6 \times 10^5$, $\beta = .033$, Smooth Cylinder)

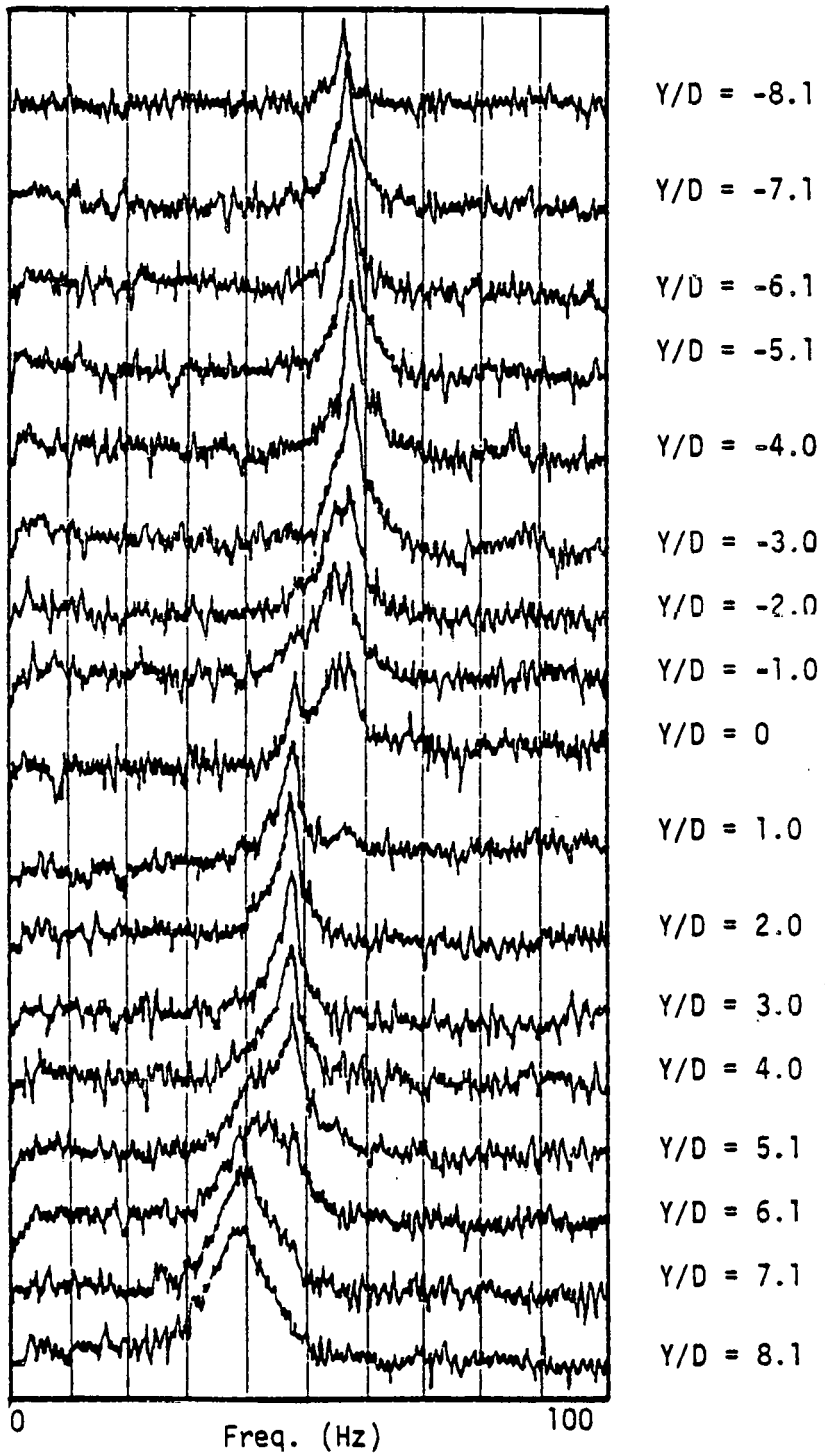


Fig. 57 Power Spectral Density of Eddy Shedding Frequency
($Re = 1.6 \times 10^5$, $\beta = .033$, Rough Cylinder)

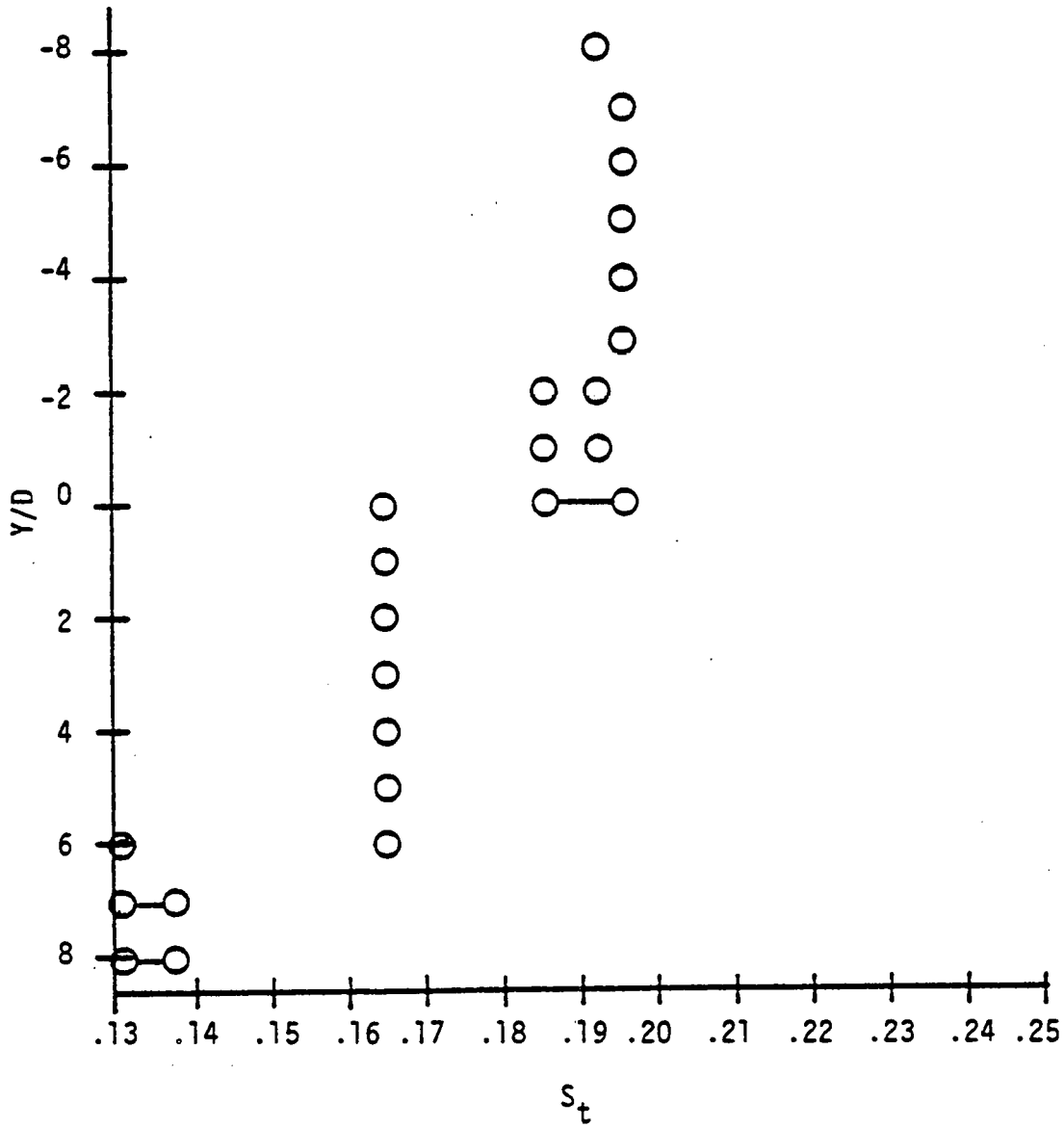


Fig. 58 Spanwise Variation of Centerline Strouhal Number
(Re = $1.6 \times 10^5$, $\beta$ = .033, Rough Cylinder)

peaks was also narrower than in Fig. 53, which again fit a trend apparent in the other shear cases.

The spectra for Re = $2.6 \times 10^5$, shown in Fig. 59, revealed no measureable shedding.

(v) Shear parameter, $\beta$ = .041

The final series of cases, run under the highest shear conditions attainable in the wind tunnel, demonstrated the clearest pattern of multiple cellular shedding.

The smooth cylinder at Re = $1.6 \times 10^5$, shown in Fig. 60, exhibited broad-band peaks but significant changes in their frequencies occurred over short length scales, so cells were well defined. The high velocity endplate cell shed at 72 Hz. At Y/D = -5.1, an equally prominent peak at 66 and 67 Hz appeared, but quickly gave way to a peak centered around 60 Hz. It is difficult to determine whether one or two cells were present in the length from Y/D = -5.1 to Y/D = 0. A peak at 53 Hz and 52 Hz formed the next cell down to Y/D = 4.0, and finally an endplate peak centered around 43 Hz formed the fourth (or fifth) cell. The range in Strouhal numbers, graphed in Fig. 61, was .244 down to .144, and each cell boundary was marked by a jump in Strouhal number of about .20.

At the higher Reynolds number, Re = $2.2 \times 10^5$, the relative lengths of the four major cells, easily identifiable in Fig. 62, was virtually unchanged. The uniform flow shedding frequency for this case, shown in Fig. 24, was 80 Hz. With $\beta$ = .041, the high velocity end cell shed at 98 Hz, and was followed successively by peaks at 85 Hz to 90 Hz, 80 Hz, 68 Hz, and 62 Hz. The spanwise spread in Strouhal numbers, plotted in Fig. 63, was from .236 down to .149, a slight decrease from the previous case, but the low velocity end cell was much more coherent and therefore centered at a higher mean velocity.

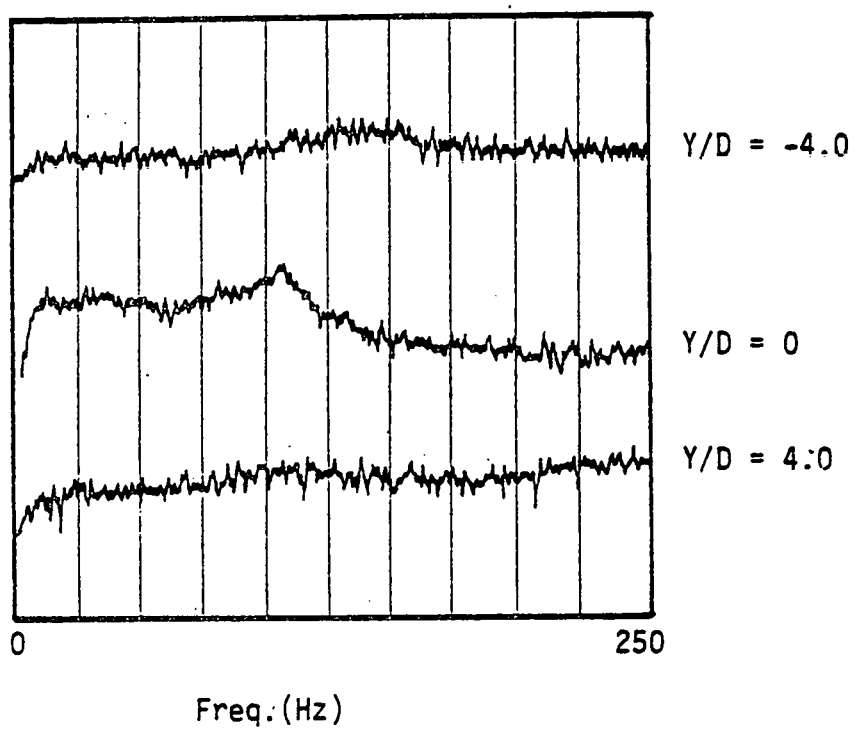


Fig. 59 Power Spectral Density of Eddy Shedding Frequency
($Re = 2.6 \times 10^5$, $\beta = .033$, Rough Cylinder)

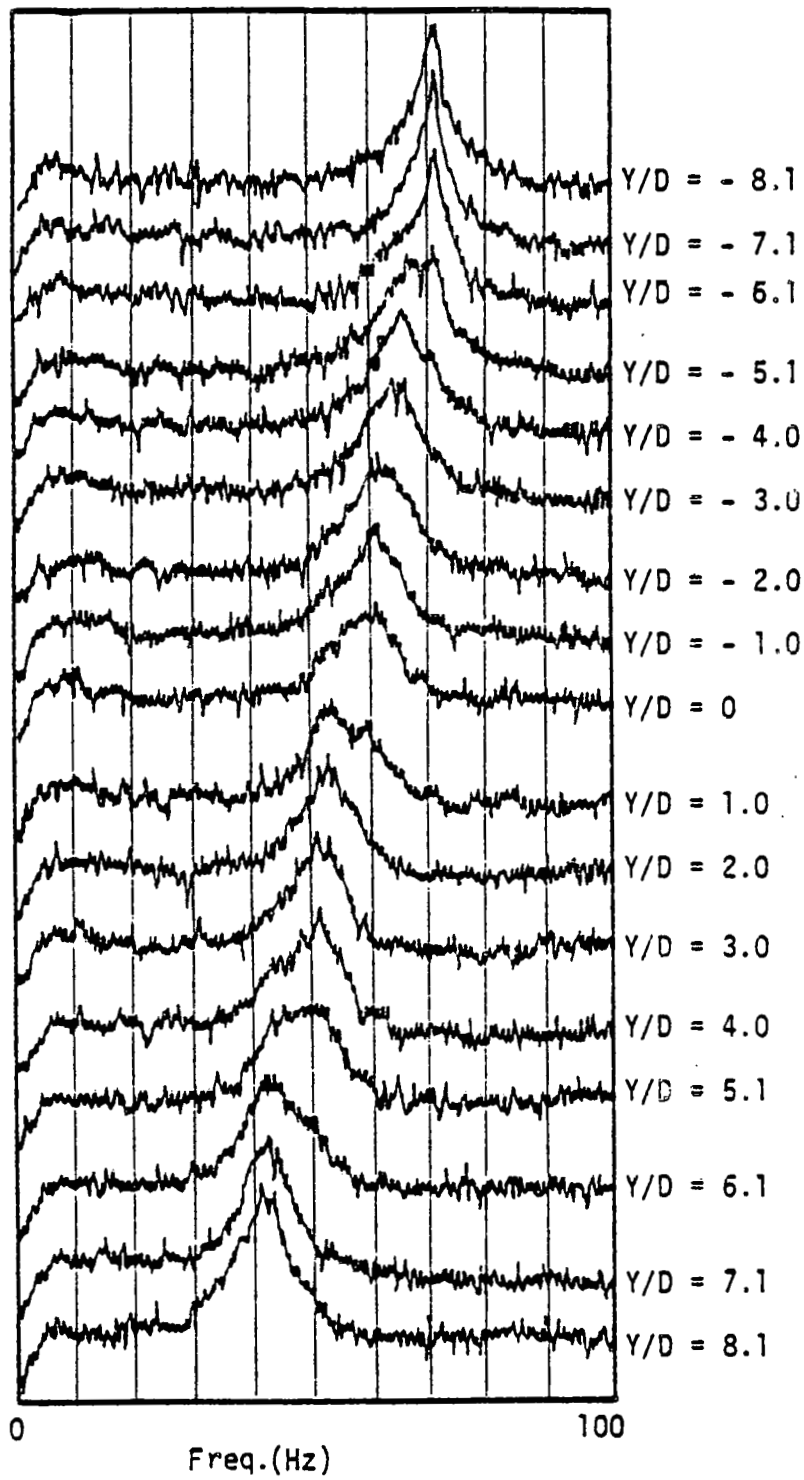


Fig. 60 Power Spectral Density of Eddy Shedding Frequency
($Re = 1.6 \times 10^5$, $\beta = .041$, Smooth Cylinder)

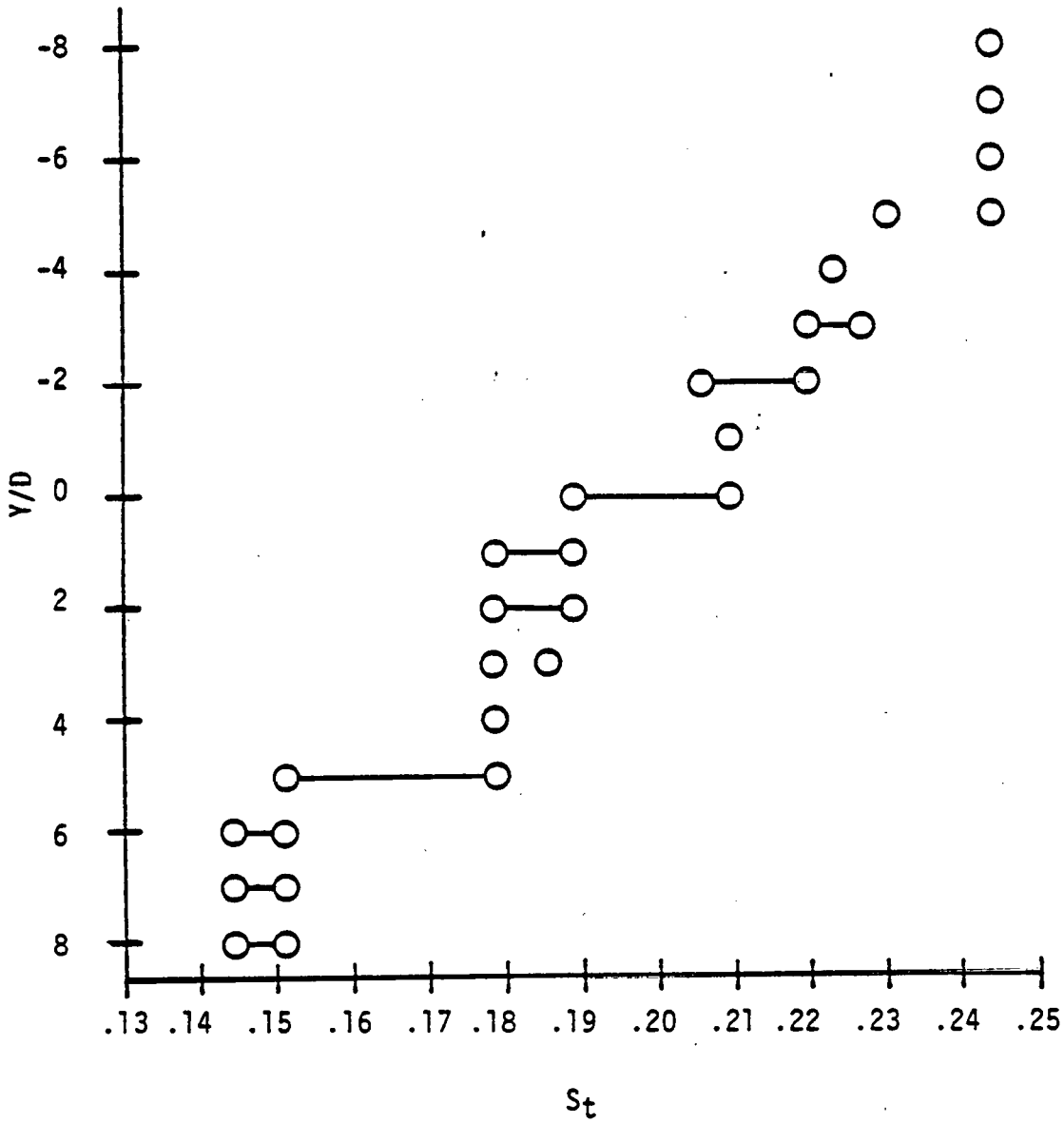


Fig. 61 Spanwise Variation of Centerline Strouhal Number
($Re = 1.6 \times 10^5$, $\beta = .041$, Smooth Cylinder)

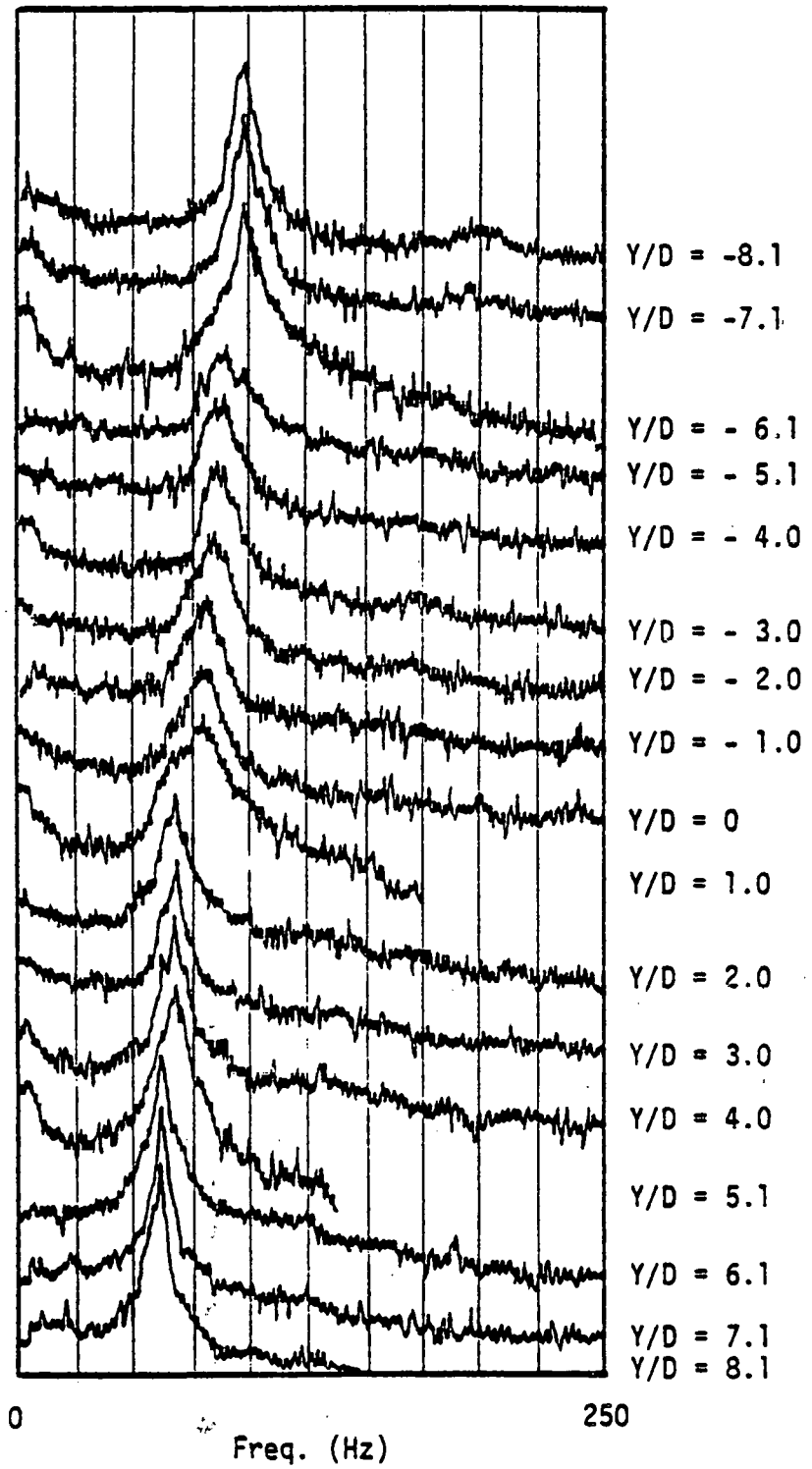


Fig. 62 Power Spectral Density of Eddy Shedding Frequency ($Re = 2.2 \times 10^5$, $\beta = .041$, Smooth Cylinder)

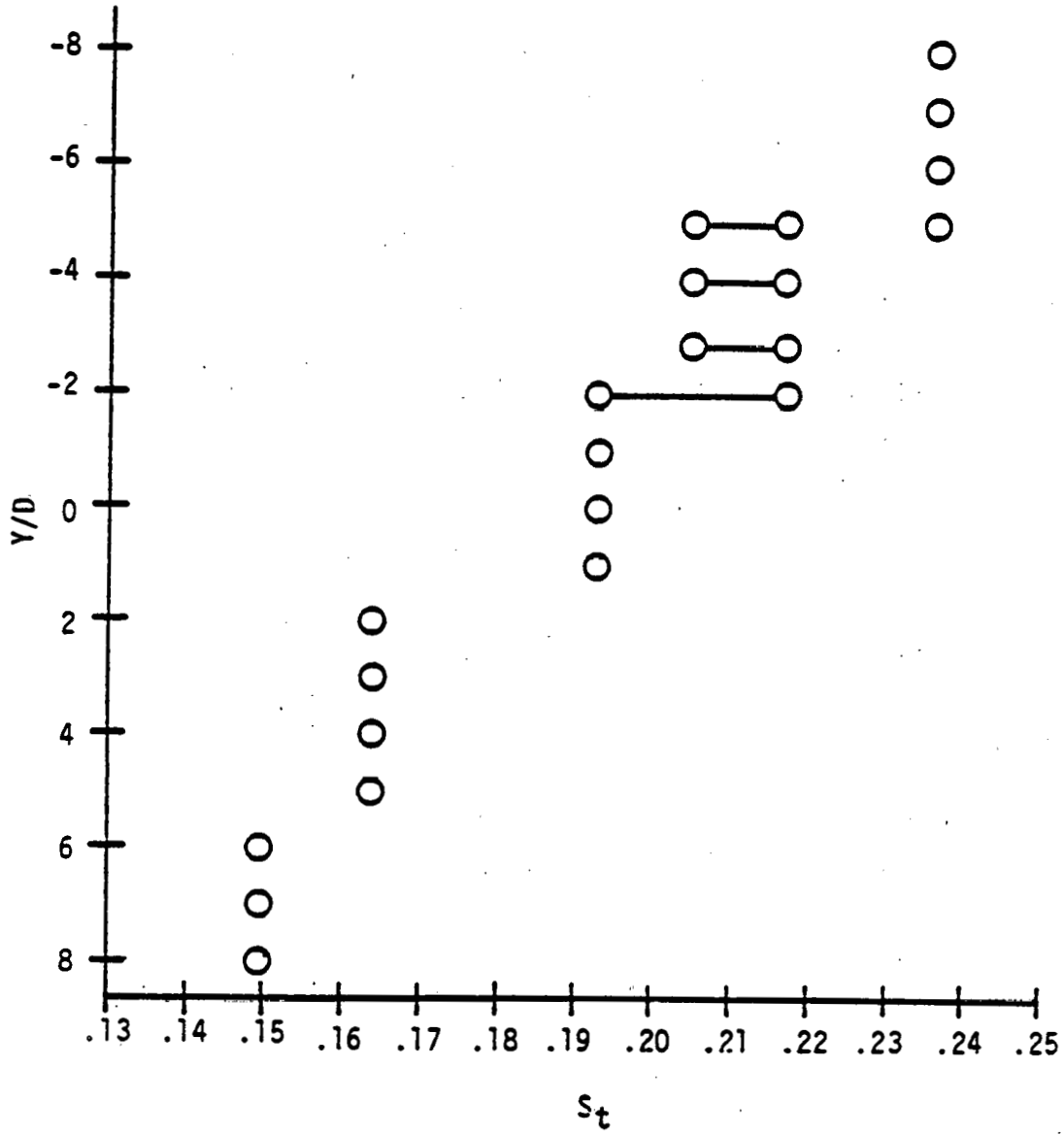


Fig. 63 Spanwise Variation of Centerline Strouhal Number
($Re = 2.2 \times 10^5$, $\beta = .041$, Smooth Cylinder)

Again the cell boundaries were marked by very large discontinuities in Strouhal number.

The rough cylinder exhibited a well-defined four cell structure at $Re = 1.6x10^5$, as indicated by Figs. 64 and 65. The relative lengths and amplitudes of the peaks were somewhat different than in the corresponding smooth cylinder case. The highest frequency cell shed at 66 Hz, extended almost half the cylinder length, and was extremely well-defined. A second peak at 60 Hz gave way to another sharply defined cell at 52 Hz, and the final cell was centered at 41 Hz. The range in Strouhal numbers was .226 down to .144, again corroborating the previously noted tendency toward smaller spanwise variation in rough cylinder tests, as opposed to smooth cylinder tests. A physical explanation of this phenomenon is in order. It is evident from a comparison of the results at $\beta = .033$ and $\beta = .041$ that the high velocity end peak in the rough cylinder tests penetrates much further down the cylinder than it does on the smooth one. Therefore the peak is centered at a lower mean velocity, hence the smaller shedding frequency. The rough surface probably acts to homogenize flow conditions over a larger area, permitting a wider coherence in the shedding pattern. The average cell size would then be expected to be larger for a rough cylinder. An attempt will be made in the next section to examine that conclusion more thoroughly based on the results of the entire set of test runs.

The final graphs of spectra and Strouhal numbers, Figs. 66 and 67, display the shedding pattern on the rough cylinder at $Re = 2.2x10^5$. These graphs are unique in the series in that they represent a case where the flow regime was actually changing over the length of the cylinder. It has previously been established, both from an analysis of surface pressure distributions and from shedding patterns in uniform flow, that $Re = 2.2x10^5$ represents the

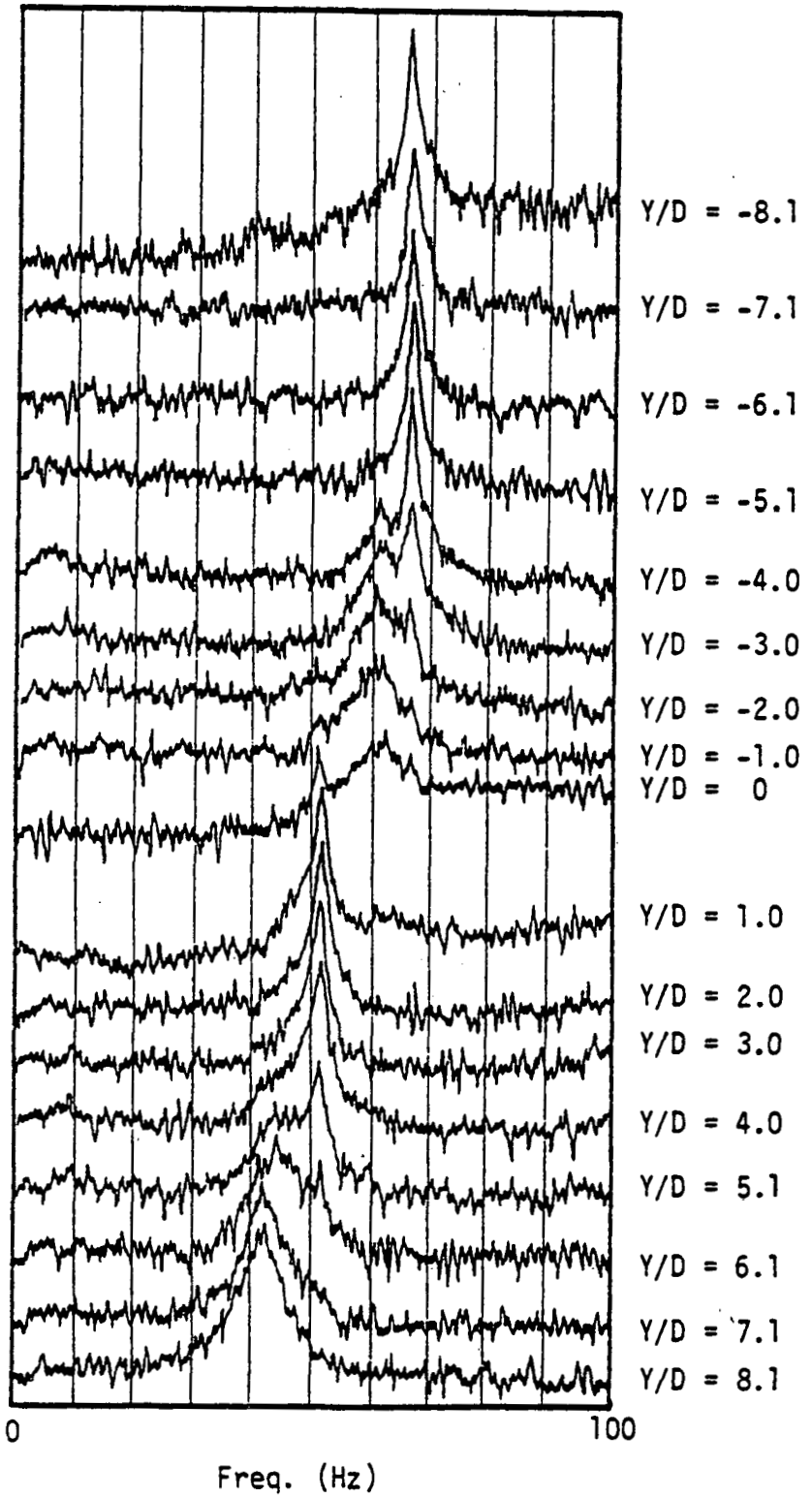


Fig. 64 Power Spectral Density of Eddy Shedding
(Frequency (Re = $1.6 \times 10^5$, $\beta$ = .041, Rough Cylinder)

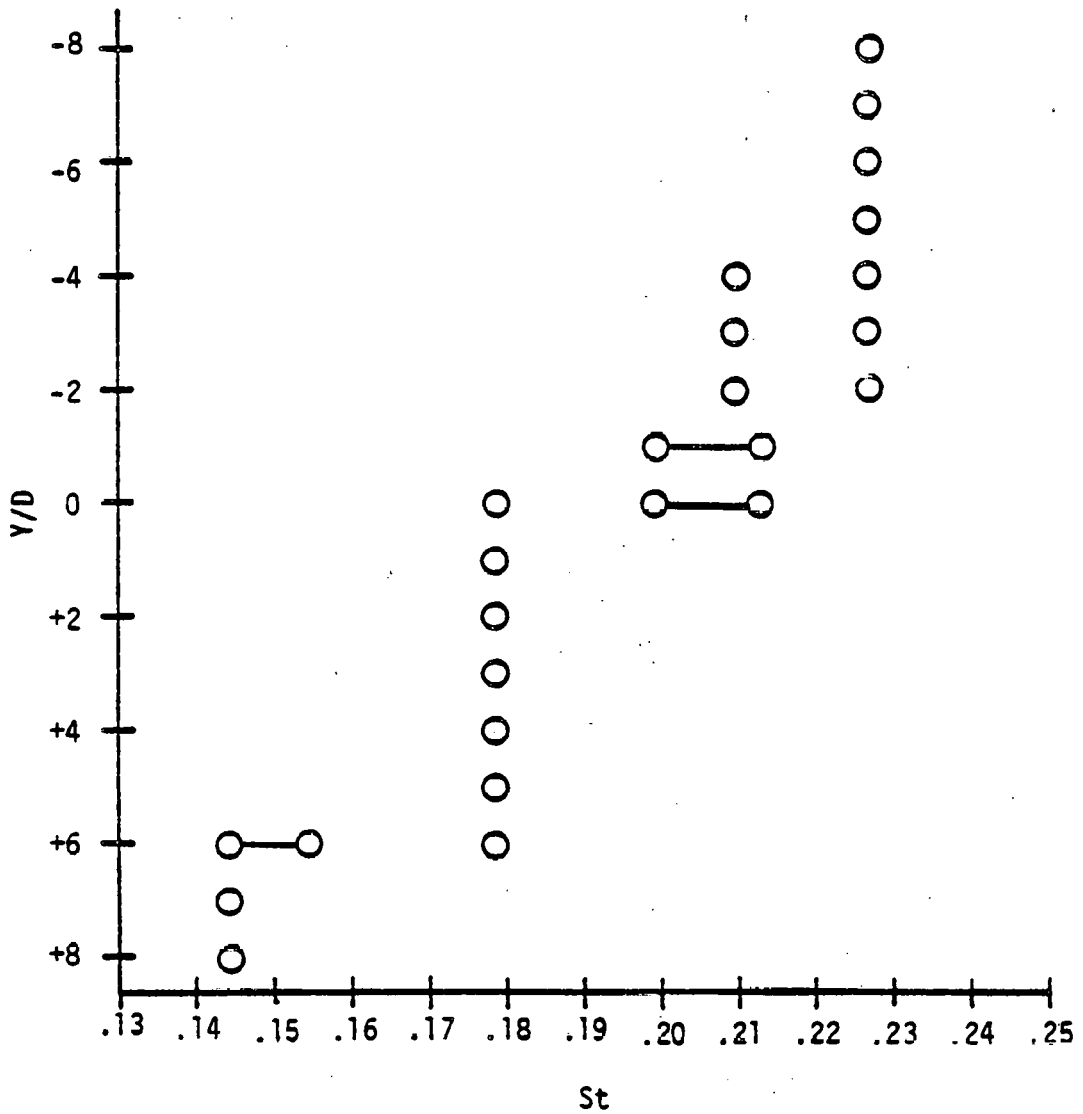


Fig. 65 Spanwise Variation of Centerline Strouhal Number (Re = $1.6 \times 10^5$, $\beta$ = .041, Rough Cylinder)

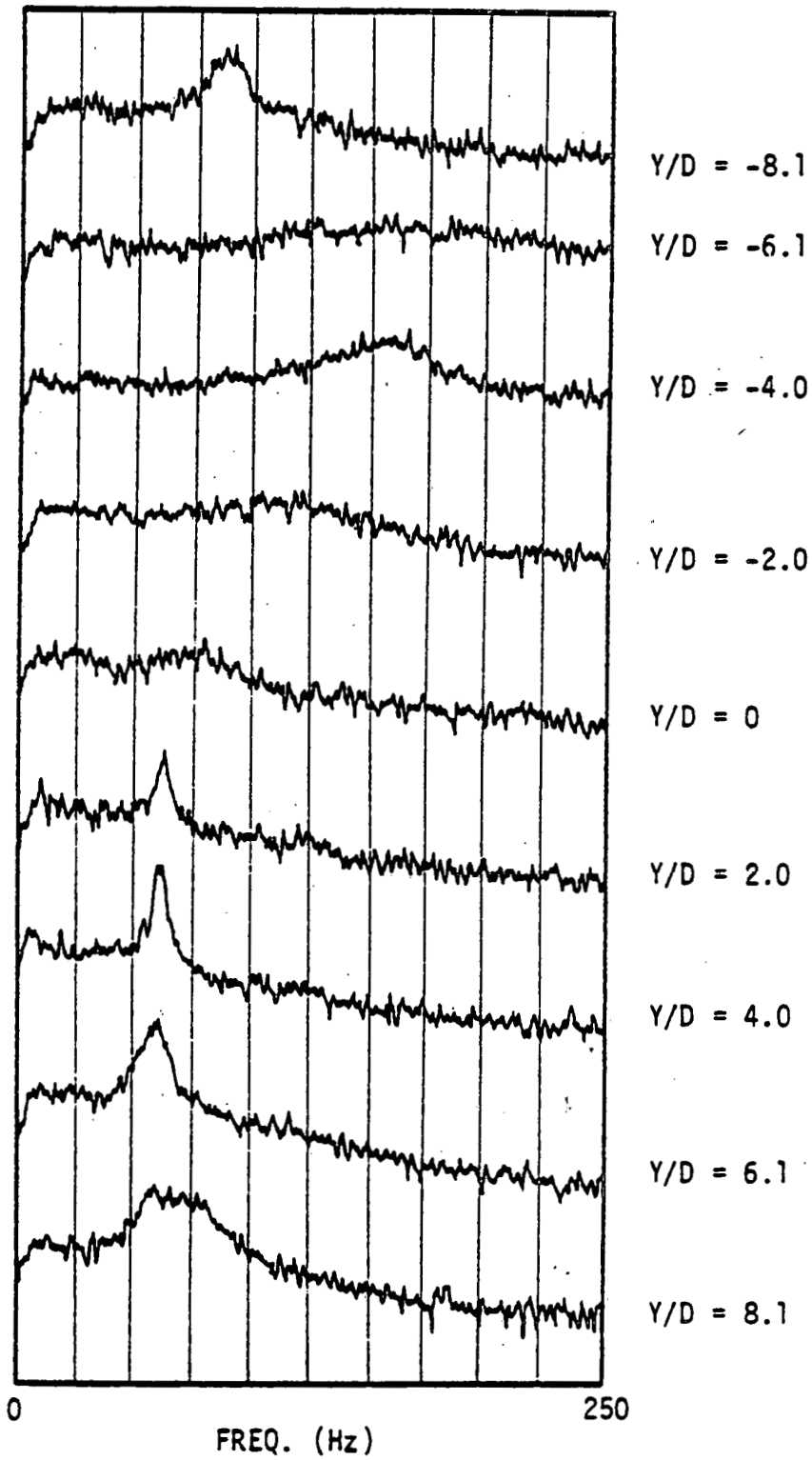


Fig. 66 Power Spectral Density of Eddy Shedding Frequency ($Re = 2.2 \times 10^5$, $\beta = 0.041$, Rough Cylinder)

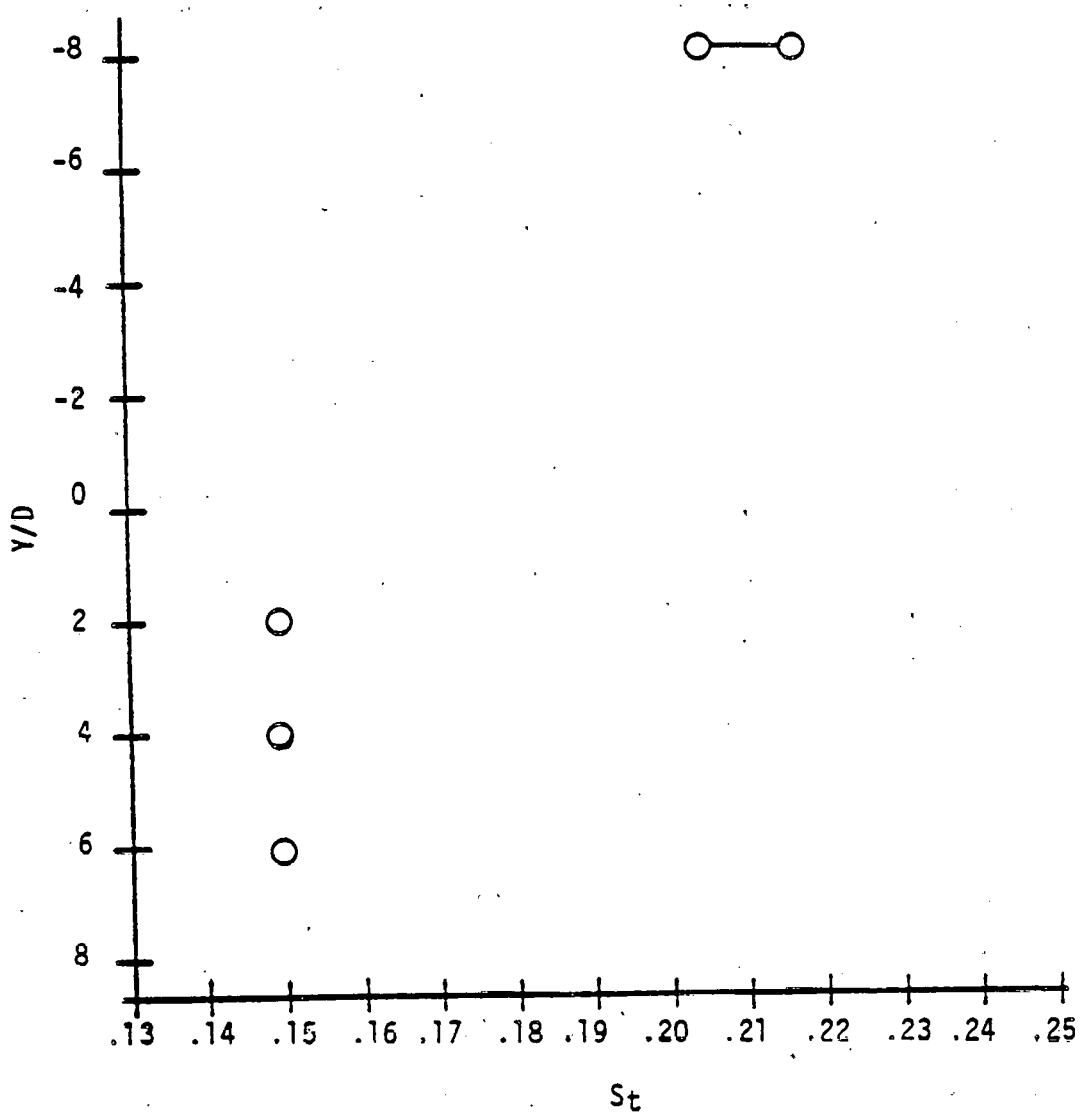


Fig. 67 Spanwise Variation of Centerline Strouhal Number ($Re = 2.2 \times 10^5$, $\beta = .041$, Rough Cylinder)

beginning of the transition from subcritical to critical conditions on the rough cylinder. For $\beta$ = .041, the local Reynolds number from Y/D = 0 to Y/D = 8.1 was significantly less than $2.2 \times 10^5$, so the fairly well-defined peaks measured around 62 Hz, with a Strouhal number of .150, were to be expected. For the high velocity side, the wake pattern was definitely critical, and so, no shedding was measured. The weak broadband peak at Y/D = -8.1 probably was caused by the endplate effect which was evident in previous rough cylinder cases.

## E. Effect of Shear on Cell Length

An attempt was made to determine whether a definite correlation between upstream shear level and size of cells of constant shedding frequency could be extracted from the data plotted and analyzed in the preceding section.

The result is the graph in Fig. 68, plotting cell length as a function of $\beta$. Before drawing any conclusions from the graph, one must bear in mind two physical limitations which make the process of identifying cells quite difficult. The first is the unsteadiness of many cell boundaries, which can even obscure the existence of a cell, let alone its length. The second is the effect of the endplates. It has been observed that the endplates contaminated the rough cylinder results up to $\beta$ = .021 by imposing a lower velocity cell over some spanwise distance down from Y/D = -8.1.

Nevertheless, two trends are apparent in Fig. 68. The first is that an increase in $\beta$ generally resulted in a decreased cell size, where each point graphed represents the average cell size for a particular case tested. The one noteworthy exception is the single point at $\beta$ = .021, which has already been observed to have been affected by the endplate.

The second trend which developed (above $\beta$ = .021) is the tendency for the rough cylinder to generate longer cells than the smooth cylinder. The

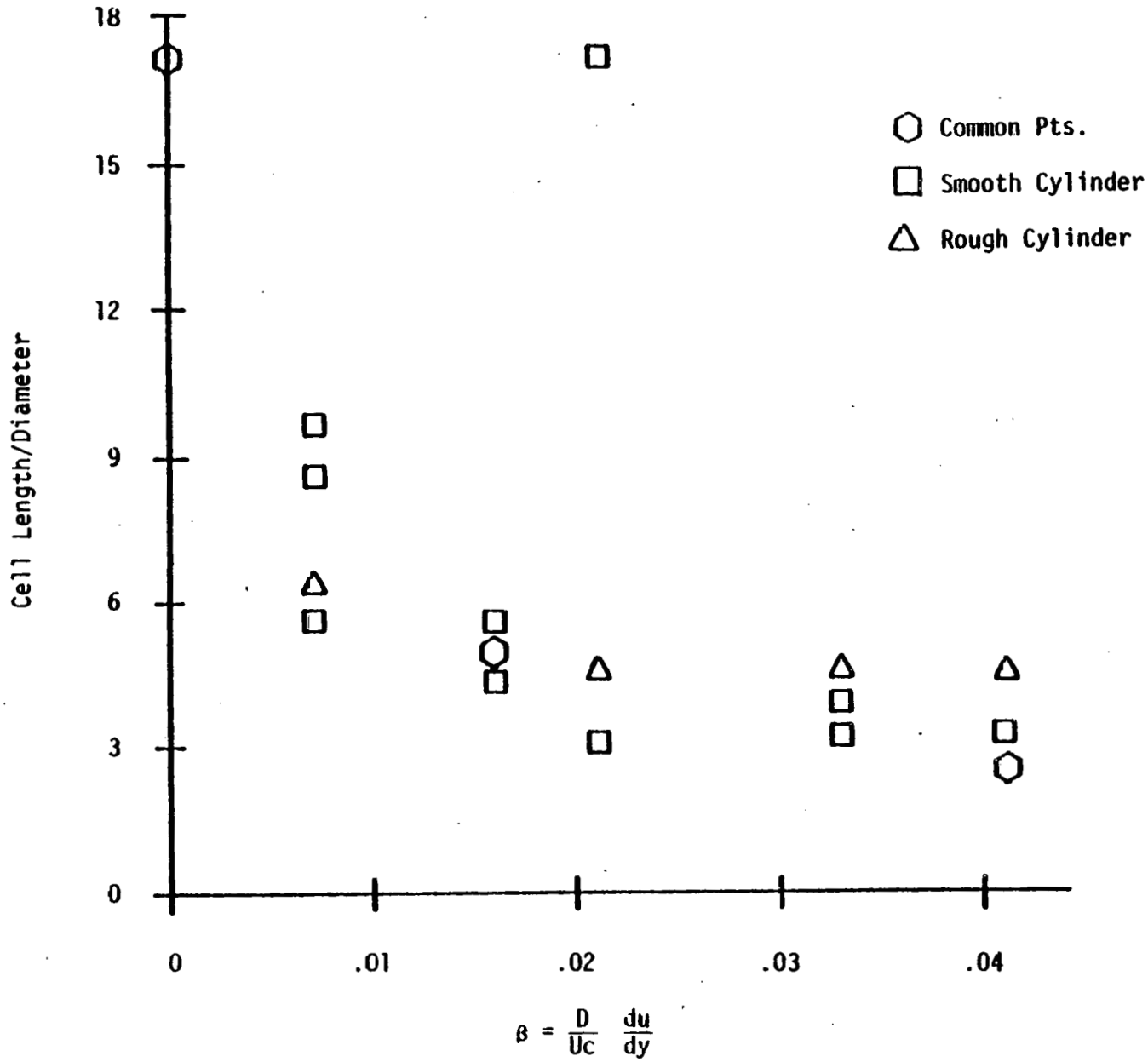


Fig. 68 Variation of Cell Length as a Function of Shear Parameter

increased homogeneity in wake structure caused by roughness elements is hypothesized to spread the influence of a single cell, diminishing the number of cells, and producing the narrower range in shedding frequencies which was documented in the rough cylinder results.

## V. CONCLUSIONS

The test program discussed in the report revealed a number of significant results, some confirming previously documented phenomena, and others which are being illuminated for the first time.

Among the conclusions which are in accord with already established findings are:

(a) An increase in freestream turbulence reduces the critical Reynolds number, even for very low turbulence levels.

(b) The peak suction on a rough cylinder is greatest at the critical Reynolds number, and decreases as the flow becomes supercritical.

(c) Pressure measurements on a rough cylinder verify that critical flow conditions are preceded by an asymmetric separation bubble. On the rough cylinder tested, this phenomenon occurred at $Re = 2.2 \times 10^5$.

A rather wide range of values of supercritical Strouhal numbers has been observed. The present study indicates that in uniform flow on the rough cylinder, shedding took place at a frequency yielding a Strouhal number of approximately .240.

The phenomena associated with shear flow vortex shedding which are newly documented are the following:

(a) Any linear shear, however slight, in the upstream velocity profile, triggers a cellular vortex shedding pattern.

(b) At a given subcritical Reynolds number, the range in shedding frequencies is greater on a smooth cylinder than on a rough cylinder.

(c) The average cell length for a rough cylinder is greater than for a smooth cylinder in tests for which endplates effects are not predominant.

(d) A general trend toward decreasing cell length with increasing shear

has been documented, but was partially obscured by unsteady cell boundaries in some tests.

## VI. RECOMMENDATIONS

A wide range of follow-on studies are suggested by the findings of the present study.

An exhaustive analysis of the effect of roughness on supercritical Reynolds number vortex shedding needs to be performed in order to explain the discrepancy between the results of Bearman and Szechenyi. Likewise, the effect of roughness on pressure fluctuations around a cylinder should be more thoroughly examined.

As a corollary to the plots of shedding frequency as a function of spanwise distance along a cylinder, a series of graphs of wake width versus spanwise length would permit further validation of some universal Strouhal number theories.

The influence of yaw angle on vortex shedding cell patterns in a sheared flow should be of interest to designers of mooring cables, which are often placed at an angle to the vertically sheared incident flow.

Much research still needs to be done on the interaction of vortex shedding phenomena with flexible cylinders of very large aspect ratio which are free to vibrate at natural frequencies. Such tests must, of necessity, be performed at subcritical Reynolds numbers in wind tunnels. Again, the effect of shear on shedding cells, as well as the variation in wake width, deserve close examination for such unconstrained cylinders.

## VII. REFERENCES


1. Batham, J. P., "Pressure distributions on circular cylinders at critical Reynolds numbers," Journal of Fluid Mechanics, vol. 57, 1973, pp. 209-228.

2. Bearman, P. W., "On vortex shedding from a circular cylinder in the critical Reynolds number regime", Journal of Fluid Mechanics, vol. 37, 1969, pp. 577-585.

3. Davies, M. E., "The effects of turbulent shear flow on the critical Reynolds number of a circular cylinder," National Physical Laboratory ( U.K. ) NPL Report Mar Sci R 151, January 1976.

4. Mair, W. A., and Stansby, P. K., "Vortex wakes of bluff cylinders in a shear flow," SIAM Journal of Applied Mathematics, vol. 28, 1975, pp. 519-540.

5. Maull, D. J., and Young, R. A., "Vortex shedding from bluff bodies in a shear flow," Journal of Fluid Mechanics, vol. 60, 1973, pp. 401-409.

6. Rooney, D. M., and Peltzer, R. D., "The effects of shear on vortex shedding patterns in high Reynolds number flow: an experimental study," Proceedings of Sixth OTEC Conference, Washington, D.C., June 19-22, 1979, (in print).

7. Stansby, P. K., "The locking-on of vortex shedding due to the cross-stream vibration of circular cylinders in uniform and shear flows," Journal of Fluid Mechanics, vol. 74, 1976, pp. 641-667.

8. Szechenyi, E., "Supercritical Reynolds number simulation for two dimensional flow over circular cylinders," Journal of Fluid Mechanics, vol. 70, 1975, pp. 529-542.

# APPENDIX

The successful execution of the test program outlined in the report depended entirely on the reliability and accuracy of the instrumentation which was assembled to measure and analyze the data. Therefore, a brief discussion of instrumentation error ranges, along with some examples of data verification by use of multiple measuring techniques, is presented in the following paragraphs.

## A. General Experimental Set-Up

The entire test apparatus (including the cylinder, plates, traverse, and sensing devices) was dismantled and reassembled during the course of the test program, since the two weeks of allocated wind tunnel time were separated by a two month period. The equivalence of rough and smooth cylinder results depended on exact reproducibility of test conditions. Therefore, before examining specific pieces of equipment, this question needs to be addressed.

Either cylinder could be positioned such that the front stagnation points were within $\pm$ 0.25° of the oncoming flow, a range which produces a negligible error in surface pressure readings. In addition, the spanwise centering of the cylinder in the tunnel could be reproduced to within $\pm$ 0.25 cm. The traverse was connected to the cylinder endplates, assuring an exact correspondence of traverse positions for each set of tests. Finally, the traverse position was set by a precision motor drive which guaranteed accuracy to within $\pm$ 0.10 cm.

## B. Accuracy of Velocity Profile Measurements

The freestream volocity profiles could be measured by either of two methods: total head tube readings (without the cylinder in place), as described in Section IIIA; or by measuring the stagnation pressures along

the span of the cylinder. The first method was employed to obtain the profiles, and consequently to characterize the shear parameters for the test cases. However, only a comparison with the data obtained from the stagnation port pressures can resolve the question of the influence of tunnel blockage in altering the profiles.

Fig. 69 presents a plot of the velocity profiles corresponding to the maximum shear case attainable, as measured by both methods. In addition, the least squares line for the total head tube profile is superposed over the data points. The slope of the line yields $\beta = .041$. It is apparent that both profiles are virtually identical, except in the range $+ 5.3 < Y/D < + 8.1$, for which the total head tube gave slightly higher values. The centerline velocity for both tests was 82 ft/sec., and the standard error of estimate of the total head readings from the least squares line was $\pm$ 1.52 ft/sec., while for the stagnation point profile, the error was $\pm$ 2.02 ft/sec. based on the same least squares line. If a least squares line were fitted to the stagnation point data, the resulting value of the shear parameter would be $\beta = .040$, a negligible difference from the value used.

C. Accuracy of Turbulent Intensity Profiles

Two methods were also available to measure the freestream turbulent intensities, although both relied on hot-wire anemometry for the raw voltage signal. The method employed for the present series of tests involved routing the non-linearized d.c. and a.c. signals to the data acquisition system as described in Section II. A computer program determined the polynomial relating mean volocity to d.c. voltage, while recording the operating temperature and pressure. The a.c. output was filtered and fed to an rms unit, and then sent to the data acquisition system. The program read 20 values and averaged them to produce the final rms velocity as a percentage of the

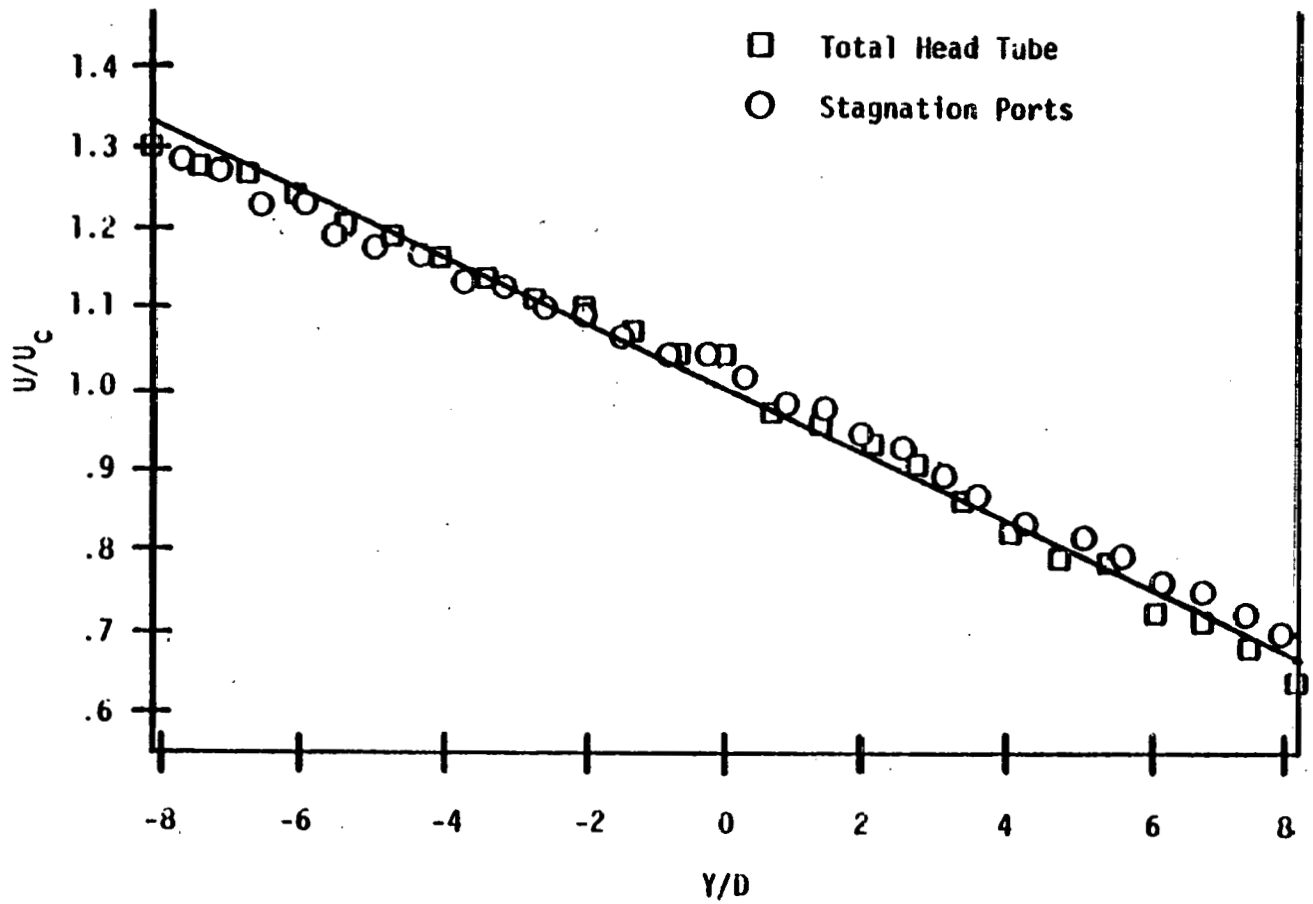


Fig. 69 Spanwise Velocity Profile ($\beta$ = .041)

mean velocity.

The technique utilized in previous test programs involved linearizing the d.c. output through a unit on the anemometer, and reading the rms voltages directly from the rms meter, a decidedly less efficient procedure. Linearizing the anemometer was a relatively time-consuming procedure, so the internal coefficients were left untampered through a wide range of operating temperatures and pressures.

Fig. 70 presents the results of two surveys across the tunnel for the shear case $\beta = 0.21$. The linearized anemometer results were obtained in March 1979, and the computer program results were obtained in July. The equivalence of the profiles is surprisingly good, particularly since the first technique relied on eye averaging of the rms output. Some discrepancy at a few points may be the result of the loosening or tightening of some of the screen wires between the two test periods.

D. Accuracy of Pressure Transducer Output

The transducer employed in the scanivalue pressure sensing unit is composed of a thin, stretched stainless steel diaphragm welded to a stainless steel case, forming a variable capacitance with an insulating electrode located close to the diaphragm. Its natural frequency is 5 KHz and it is virtually hysteresis-free.

The recommended range of the transducer is ± 0.25 psig, with a maximum overrange in the positive direction of 100 psig and, in the negative direction, 1.25 psig. Three calibration points on the transducer specification sheet reflect the relation between voltage and pressure:

+0.25 psig = +2.501 volts

0.00 psig = -0.012 volts

-0.25 psig = -2.537 volts

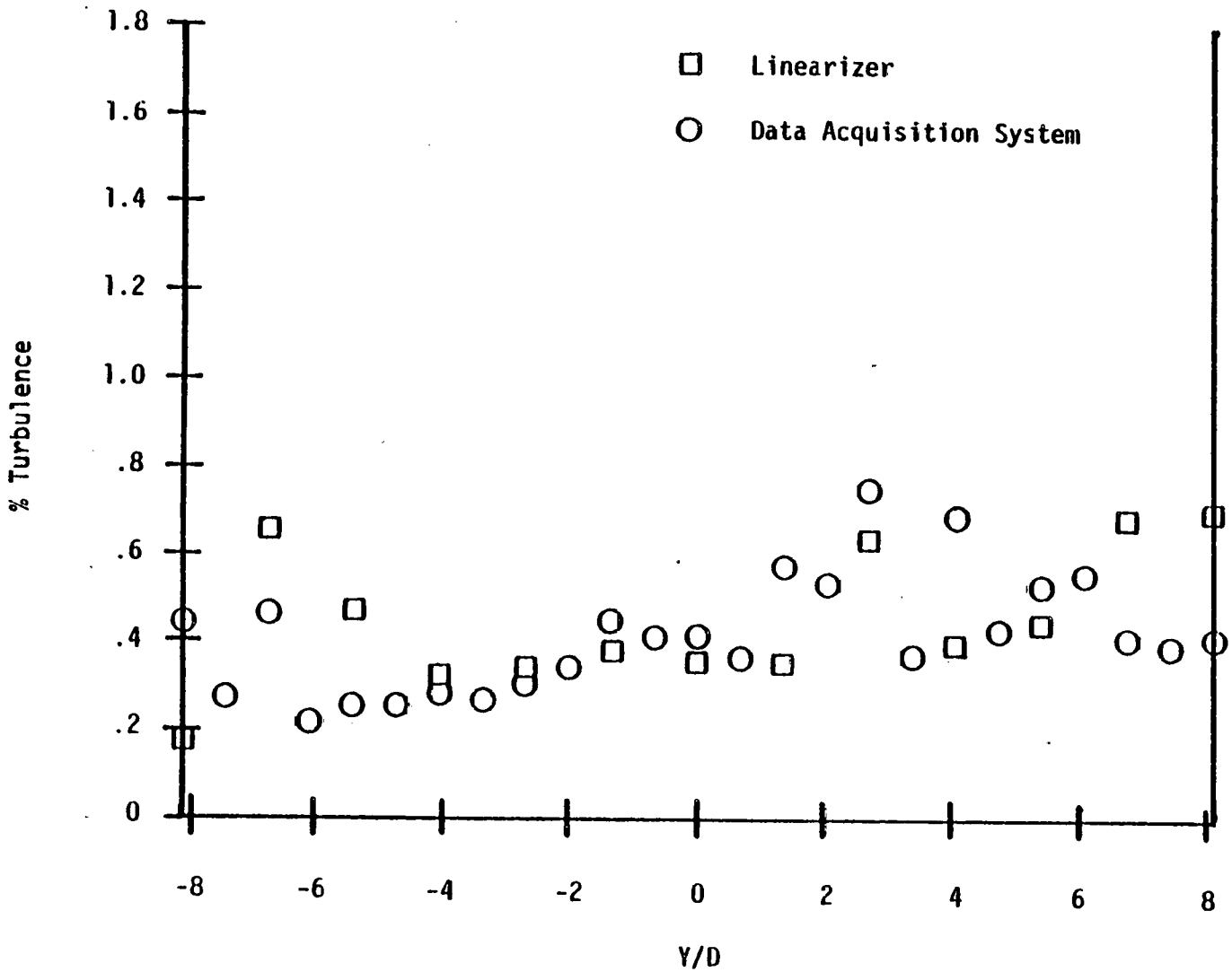


Fig. 70 Spanwise Turbulence Profile ($\beta$ = .021)

The specified linearity of the transducer is ± 0.25% at full scale. During test runs it occasionally recorded pressures of -0.50 psig, twice the normal negative limit, but still only 40% of the overrange value. The non-linearity induced by the extreme value was most likely still significantly below ± 1%, while the calibration error was probably less than 2%.

The output from the transducer was fed into a voltmeter and to a strip-chart recorder. Centerline tunnel velocities were set by reading the voltage output from a port 2.54 cm from the center of the cylinder, as indicated on the voltmeter. This arrangement was considered accurate to ± 2% in reproducing the centerline flow conditions.

The circumferential pressure distributions were plotted on the strip-chart recorder, which damped out any high frequency fluctuations. The maximum frequency to which the stripchart pen can respond is about 10 $H_Z$. Nevertheless, significant fluctuations about the mean values were recorded at a number of angles, particularly for the smooth cylinder, as will be brought out below. The mean value was determined visually from the stripchart data, and was in most cases fairly obvious.

Figs. 71 and 72 give an indication of the spread in the instantaneous pressure values about the mean, as recorded on the stripchart, for two test cases. It should be emphasized that the limits, represented by the bars, do not correspond exactly to the full range in instantaneous values, but only to the range of the damped lower frequency components which could be registered on the stripchart. Even so, a very marked trend can be noted.

Fig. 71 indicates that the fluctuations about the mean for the smooth cylinder case of $\beta$ = .033 and Re = $2.6 \times 10^5$ were substantial in the range of suction pressures. By contrast, Fig. 72 reveals that the rough cylinder under identical flow conditions experienced a much smaller range of fluctuations.

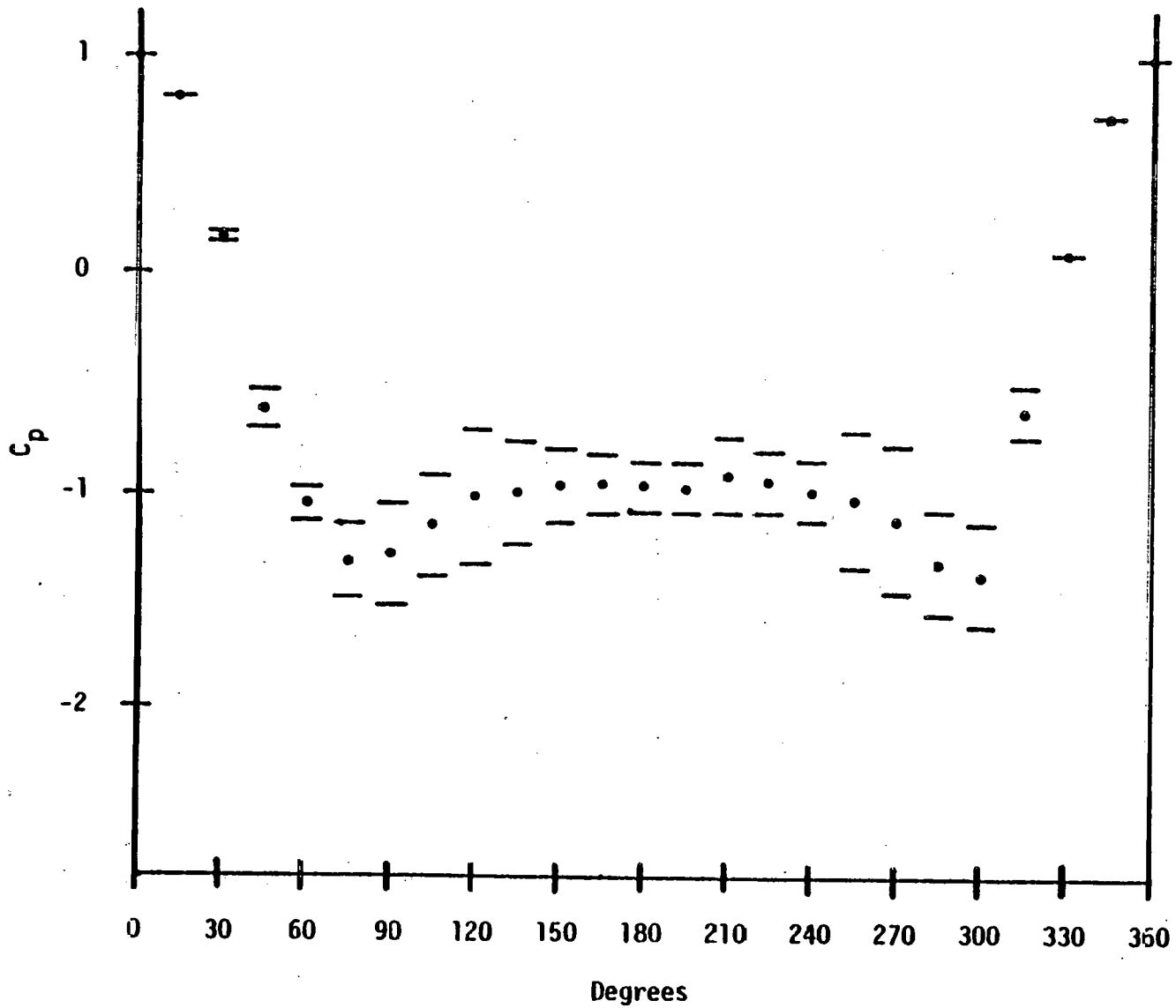


Fig. 71 Fluctuations in Circumferential Pressure Distribution ($\beta$ = .033, Smooth Cylinder, Re = $2.6 \times 10^5$)

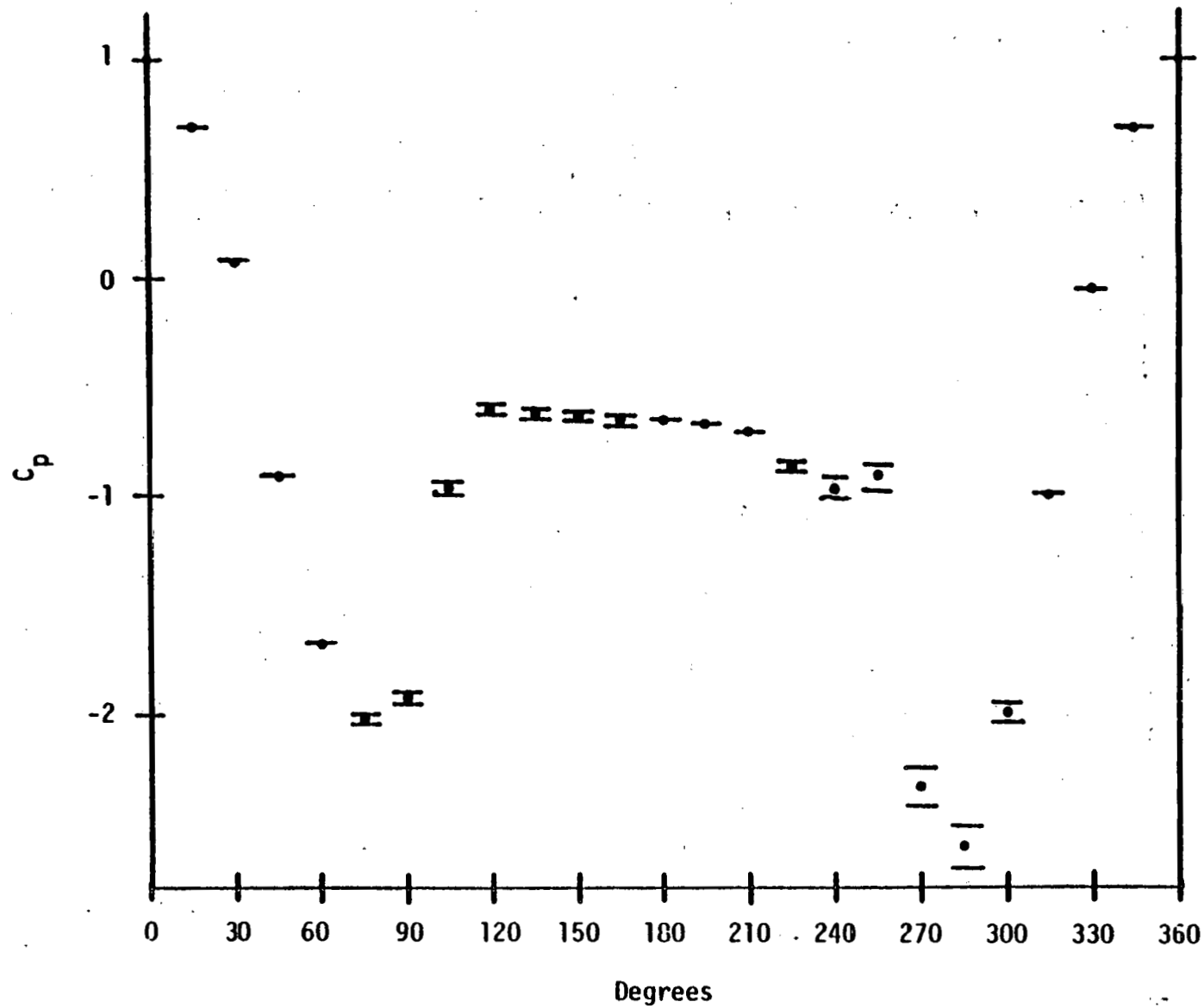


Fig. 72 Fluctuations in Circumferential Pressure Distribution
($\beta$ = .033, Rough Cylinder, Re = $2.6 \times 10^5$)

The primary purpose behind including the graphs was to demonstrate the reliability of the method of choosing the mean pressure values. However, it can also be concluded that they point to a damping effect of roughness on the pressure distribution, a factor which could be significant in computing the instantaneous loading on a given structural member.

E. Accuracy of Spectral Analysis Methods

The hotwire output was filtered to exclude signals with frequencies less than 0.3 Hz and greater than 300 Hz before being sent to the FFF Processor. Therefore, since the output from the processor was in the 0 to 100 Hz or 0 to 250 Hz range, a certain amount of Nyquist folding occurred. The effect on the output was negligible, however, since only one high energy signal (at the eddy shedding frequency) was being measured, so the folding only impressed a uniformly distributed small amplitude signal over the region of interest.

It is worthwhile to note the bandwidth of the displayed spectra to determine the capability of the analyzer to resolve the frequency components. For the 0 to 100 Hz plots with a sampling rate of 1024 points, the bandwidth is 0.2 Hz, while for the 0 to 250 Hz plots, again with a sampling rate of 1024 points per spectrum, the bandwidth is 0.5 Hz. The most significant factor affecting the resolution of the spectra was the number of averages obtained. The trade-off involved in the selection of an appropriate number was duscussed in Section III C. The high energy level at the shedding frequency reduced the need for strong resolution, which would only have served to smooth out the signal of the low energy frequency contributions.

It can therefore be concluded that the spectral averaging technique employed was particularly well adapted to analyzing the signals to reveal the necessary information.



☆U.S. GOVERNMENT PRINTING OFFICE. 1980-640-258/267